ELECTRICAL CONDUCTION AND THERMOELECTRIC POWER IN ThO$_2$— CaO ELECTROLYTES

By

HIMADRISEKHAR MAITI

DEPARTMENT OF METALLURGICAL ENGINEERING

INDIAN INSTITUTE OF TECHNOLOGY KANPUR

JANUARY, 1975

ELECTRICAL CONDUCTION AND THERMOELECTRIC POWER IN ThO_2 — CaO ELECTROLYTES

A Thesis Submitted
In Partial Fulfilment of the Requirements
for the Degree of
DOCTOR OF PHILOSOPHY

By
HIMADRISEKHAR MAITI

to the

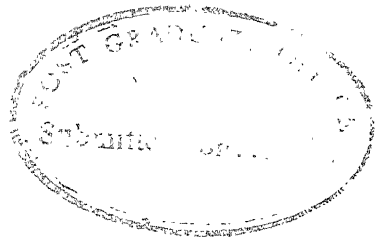DEPARTMENT OF METALLURGICAL ENGINEERING
INDIAN INSTITUTE OF TECHNOLOGY KANPUR
JANUARY, 1975

ME-1975-D-MAI-ELE
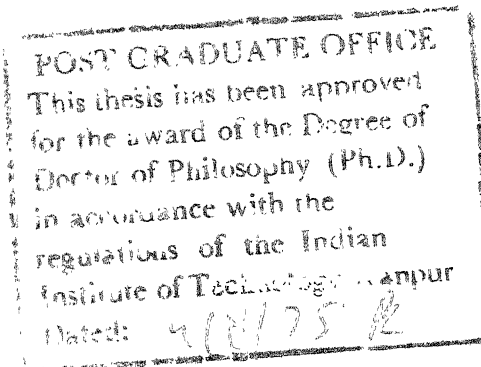
CERTIFICATE

Certified that this work on "Electrical Conduction and Thermoelectric Power in ThO_2-CaO Electrolytes" has been carried out under my supervision and that it has not been submitted elsewhere for a degree.

(E.C. Subbarao)
Professor
Department of Metallurgical Engineer
Indian Institute of Technology
Kanpur-208016.

ACKNOWLEDGEMENTS

I am indebted to Professor E.C. Subbarao for his
guidance and encouragement throughout the course of this
research.

I am grateful to Mr. C.B. Choudhary for his
co-operation, suggestions and the discussions I had with
at different stages of the work.

I am thankful to Mr. B. Sharma, Mr. R.K. Prasad,
Mr. K.P. Mukherjee, Mr. K.R. Sharma and Mr. V.P. Gupta fo
their assistance in various ways during the progress of t
research.

I am also thankful to Mr. V.K. Gupta for his hel
in the computational work. I wish to thank Dr. S.K. Ray
Mr. S. Mazumdar, Mr. A.K. Ray, Mr. A.N. Tiwari and my oth
friends for their cooperation which has contributed towar
the completion of this work.

I wish to express my deep appreciation towards
Dr. (Miss) Kamal Singh, Mr. G.V.S. Sastry and C.S. Vitla
for their timely help in preparing the manuscript of the
thesis within a very short time.

I wish to thank Mr. R.S. Misra for his constant
co-operation at various stages of the work.

I am thankful to Mr. R.N. Srivastava, Mr. Vishwan Singh and Mr. A. Ganguli for their prompt and timely help getting the thesis in the printed form.

Finally, I like to acknowledge the co-operation which I received from the Material Science Centre, I.I.T. Kharagpur-721302 where I am presently employed.

Kanpur
January, 1975   HIMADRISEKHAR MAITI

CONTENTS

LIST OF TABLES

LIST OF FIGURES

CHAPTER I

REVIEW OF LITERATURE

I-1. INTRODUCTION

The electrical conductivity of a solid compound is a consequence of the presence of mobile electronic as well as ionic charge carriers. In a solid, several kinds of charge carriers may be present simultaneously and therefore it is important to know their relative contributions to the total conductivity. The transference number (t_i) of the ith carrier is defined as

$$t_i = \frac{\sigma_i}{\sigma_T} \qquad (I-1)$$

where σ_i is the conductivity due to the ith specie only and σ_T is the total conductivity which may be expressed as

$$\sigma_T = \sum_i n_i(z_i e)\mu_i \qquad (I-2)$$

where n_i, z_i and μ_i are respectively the concentration, valency and the mobility of the ith charge carrier and e is the charge of the electron.

Wagner [1] has considered the transport of ions and electrons in a binary compound $M_{z_X} X_{z_M}$ and has shown theoretically that the electromotive force (E) of a galvanic cell containing the binary compound as the solid electrolyte may be expressed as

$$E = -\frac{1}{F} \int_{\mu_X''}^{\mu_X'} (t_{ion}) \frac{d\mu_X}{|z_X|} = -\frac{1}{F} \int_{\mu_M'}^{\mu_M''} (t_{ion}) \frac{d\mu_M}{|z_M|} \qquad ...(I-3)$$

where t_{ion} is the sum of the cationic and anionic transference numbers, μ_X' and μ_X'' are the chemical potentials of the nonmetal at the two electrolyte-electrode interfaces with $\mu_X' < \mu_X''$; similarly μ_M' and μ_M'' are the chemical potentials of the metallic component at the same interfaces with $\mu_M' > \mu_M''$. F is the Faraday's constant and z_M and z_X are the valencies of the metal and the nonmetal respectively. The compounds which are of practical importance as solid electrolytes in galvanic cells are those which are predominantly ionic conductors i.e. for which $t_{ion} \simeq 1$. A large number of crystalline compounds, which are mainly ionic in character, including alkali halides, calcium fluoride, silver-, copper-, lead-, barium-and strontium halides and pure and mixed oxide solid solutions have been shown to exhibit exclusive ionic conductivity and may be considered as good solid electrolytes. In general, the oxide electrolytes are useful in the high temperature range $(600-1600^{o}C)$, although several of them (e.g. β-aluminas) may be used at lower temperatures. The alkali halides may be considered as the low temperature counterpart of the high melting oxide electrolytes and act as prototypes for these materials. The theory and the experiments on the alkali

halides have been thoroughly reviewed by Lidiard and his co-workers [2,3] and also by Supitz and Teltow [4].

Wagner and his co-workers [5-18] have correlated the equilibrium concentrations of the ionic and electronic defects in an ionic compound to the deviation from the exact stoichiometric composition and have pointed out that the movement of these charged defects is responsible for the electrical conduction in these solids. Applying the mass action law and assuming an infinitely small defect concentration and the concentration independent mobilities, they have been able to explain the predominant electronic conductivities in a number of binary oxides like CuO, ZnO, CdO, NiO, FeO etc. These oxides, due to their nonstoichiometric character, are not useful as solid electrolytes but may be considered as oxide semiconductors.

Among the oxide electrolytes, the major attention has been paid to zirconia and thoria base solid solutions due to their predominant ionic conduction over a wide range of oxygen potential and temperature. After preliminary electrical conductivity measurements, Kiukkola and Wagner [19] were the first to introduce these oxide electrolytes (ZrO_2-CaO solid solutions), having cubic CaF_2 type crystal structure, for the determination of standard free energies of formation of a number of binary oxides by forming galvanic cells with metal metal oxide electrodes. This was followed by Peters et al.[20,21

who carried out similar experiments with $ThO_2-La_2O_3$ and $ZrO_2-Y_2O_3$ electrolytes.

For an oxygen concentration cell the equation (I-3) may be modified as

$$E = -\frac{1}{4F} \int_{\mu'_{O_2}}^{\mu''_{O_2}} (t_{ion}) d(\mu_{O_2}) \qquad (I-3a)$$

where $\mu''_{O_2} > \mu'_{O_2}$

For an exclusive oxygen ion conductor for which $t_{ion} = 1$,

$$E = \frac{RT}{4F} \ln \frac{P''_{O_2}}{P'_{O_2}} \qquad (I-3b)$$

where R is the universal gas constant and T is absolute temperature. Schmalzried [22,23] has derived an expression for P_{O_2} dependence of t_{ion} which allows the integration of equation (I-3a) in the mixed conduction region.

The simultaneous electrical conductivity and O^{18} oxygen exchange measurements made by Kingery et al. [24] have demonstrated that the conductivity in ZrO_2-15 m/o CaO solid solution is solely due to the movement of oxygen ions and the conductivity values may be related to the diffusion coefficient through Nernst-Einstein relation. They have also confirmed that the transport of oxygen ions in these electrolytes takes place through a vacancy mechanism. The details of the defect structure and the electrical properties of common oxide electrolytes have been reviewed by several authors [25-27].

Based on these observations, the oxide electrolytes have been put to numerous scientific and technical applications e.g. high temperature fuel cells [28], numerous thermodynamic and kinetic measurements in metallic and nonmetallic systems, an excellent account of which is given by Rapp and Shores [29], control and measurement of oxygen activity in the solid, liquid and gaseous systems [30-45],for resistance and induction heating purposes [46,47] and electrochemical thermometry [48].

The required characteristics of the solid electrolyte vary with the intended application and therefore the type of the solid electrolyte should be chosen accordingly. For most purposes the solid electrolyte should have a very high electrical conductivity and the ionic transference number should be very close to unity ($t_{ion} > 0.99$). The predominant ionic conductivity in a solid electrolyte is always limited to a definite range of the chemical potential of the metal or the nonmetal component and therefore to the metal or the nonmetal activity in the surrounding atmosphere which controls the extent of nonstoichiometry in the electrolyte.

Initial investigations [23,49] showed that the predominant ionic conductivity in $Zr_{0.85}Ca_{0.15}O_{1.85}$ occurs at oxygen partial pressures greater than that of the coexistence of Fe-FeO at $1000^{\circ}C$. However later measurements by Tretjakow and Schmalzried [50] and Patterson et al. [51] have proved that the calcia stabilized zirconia electrolyte exhibits

predominant ionic conductivity upto an oxygen partial
pressure as low as 10^{-22} atm., the equilibrium pressure for
$Cr-Cr_2O_3$ coexistence at $1000^{\circ}C$. At lower pressures this
electrolyte becomes n-type semiconductor and can not be used
as a solid electrolyte. Contrary to this, thoria base
electrolytes exhibit ionic conduction down to a much lower
oxygen partial pressure ($\sim 10^{-35}$ atm. at $1000^{\circ}C$) [51,52]
and becomes p-type semiconductor [52-54] at oxygen partial
pressures greater than 10^{-6} atm. at $1000^{\circ}C$.

The fact that the solid oxide electrolytes contain
mobile ionic defects means that there will be thermoelectric
effects associated with the motion of these charged defects.
The ionic charge carriers redistribute themselves under a
temperature gradient in a way analogous to that of the
electronic charge carriers in a semiconductor. One of the
important thermodynamic properties which can be determined by
measuring thermoelectric power of ionic crystals is the
'heat of transport' of different charge carriers. However,
the successful interpretation of the experimental results
needs a knowledge of the defect structure and the transference
numbers of each of the carriers. The pioneering work to
develop the theory of thermoelectric power of an ionic compound
of the type MX was made by de Groot [55] and Holtan et al.
[56-57]. The theory has been later developed for specific
type of defect models and has been successfully applied to a

number of ionic crystals, chiefly pure and impurity doped
alkali halides, Ag- and Cu-halides [58-66] to determine the
heat of transport of cationic and anionic defects. A
detailed account of the theory and experiments with different
kinds of thermocells has been recently put forth by Wagner [67].
The theory of thermoelectric power has been extended to
purely oxygen ion conductors like calcia stabilized zirconia
by Ruka et al. [68] and Pizzini and his co-workers [69] and
also to pure ThO_2 by Tallan and Bransky [70].

In the following sections an attempt has been made
to review the theories of electrical conduction and thermo-
electric power of ionic conductors and the results obtained
by earlier investigators on ThO_2 base electrolytes are
presented.

I-2 ATOMIC ARRANGEMENT

Most of the important oxide electrolytes exhibit
either cubic fluorite (CaF_2) or related crystal structures.
A unit cell of the CaF_2 lattice is shown in Fig. 1.1. It may
be considered either as an f.c.c. cation lattice with an
interpenetrating simple cube of anions or as a simple cubic
anion lattice with the cations at the centres of the alternate
cubes.   The square at the centre of Fig. 1.1 indicates the
interstitial position.   There are equivalent sites at the edge
centres. The structure is an open one and contains empty

Ca

F
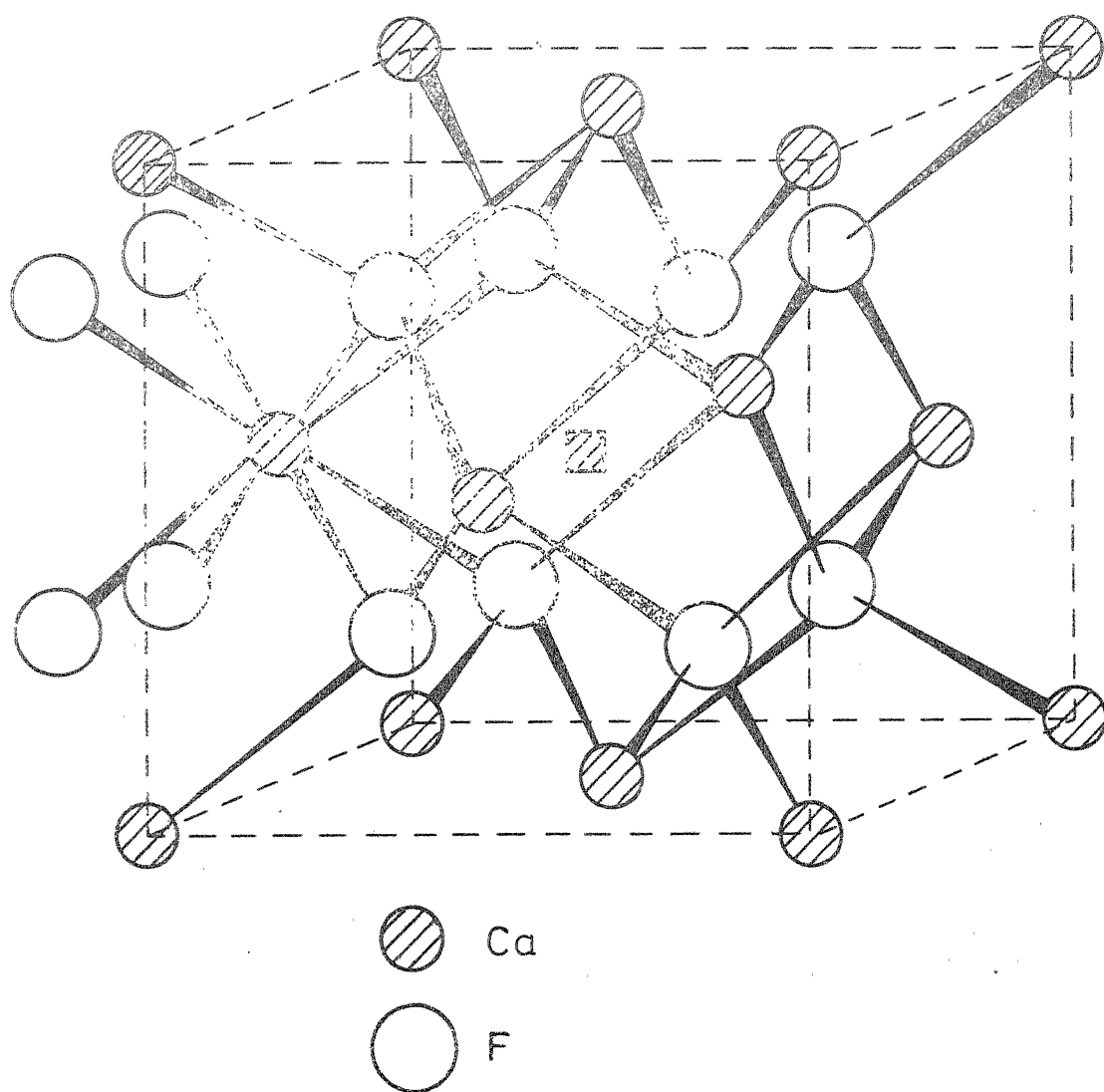
FIG.1.1   CRYSTAL STRUCTURE OF CaF$_2$

spaces through which the conducting ion can move freely. Although at room temperature, pure ZrO_2 has a monoclinic crystal structure, it forms a distorted fluorite type solid solution when doped with sufficient quantity of CaO or MgO. However, both pure ThO_2 and its solid solutions with a number of other oxides such as Y_2O_3, La_2O_3, CaO etc. have CaF_2 type structures.

Assuming a hard sphere model for the ions, Möbius [71] has separately calculated the normalized free radii (R) available for the movement of anions and the cations in a CaF_2 lattice. For the migration of an anion out of its neighbouring cation tetrahedra the normalized radius of the free space, R_{anion}, may be expressed as

$$R_{anion} = \frac{r_{hole}}{r_{anion}} = 0.943 - 0.57 \left[\frac{r_{cation}}{r_{anion}}\right] \qquad (I-4)$$

Similarly

$$R_{cation} = \frac{r_{hole}}{r_{cation}} = 0.816 - 0.184 \left[\frac{r_{anion}}{r_{cation}}\right] \qquad (I-5)$$

In a ThO_2 lattice having CaF_2 structure, Möbius [72] has given that $r_{Th^{4+}} = 1.15$ A$^\circ$ and $r_{O^{2-}} = 1.27$ A$^\circ$. Using these values, the following values may be obtained.

$$R_{O^{2-}} = 0.89$$

and

$$R_{Th^{4+}} = 0.61$$

Since $R_{O^{2-}} > R_{Th^{4+}}$, the oxygen ions can move more easily than the thorium ions.

I-3. POINT DEFECTS

Crystalline solids contain point defects at temperatures higher than $0^{\circ}K$. Under the intrinsic condition, these defects are produced as a result of thermal disorder within the crystal. On the other hand, extrinsic defects are produced due to the presence of impurities.

In a crystal the following types of atomic disorders may be present.

i) Vacancies are the sites where an atom is missing from a normally occupied position.

ii) Interstitials are those where an atom is found in a normally unoccupied position.

iii) Misplaced atoms are those which are found at a site normally occupied by another.

iv) Impurity atoms may occupy either an interstitial position or may substitute an atom in the normal site.

If the crystal is ionic in character these defects may be present in different states of ionization, and are termed as 'ionic defects'. Referring to oxides, the oxygen vacancies or interstitials may be present in either neutral, singly ionized or doubly ionized states. Ionic

defects may be considered as fully ionized atomic defects. Under stoichiometric condition, to maintain the over all electrical neutrality in the solid, the ionic defects carrying either positive or negative charges are formed in several combinations, the most common of which are Schottky and Frenkel pairs. Schottky disorder consists of a pair of cation vacancy and anion vacancy while a Frenkel pair is formed by a cation vacancy and cation interstitial. An anti-Frenkel defect consists of vacancy and interstitial in the anion sublattice. Besides the ionic defects, crystals contain electronic defects, like excess electronsor electron holes especially under a nonstoichiometric condition developed as a result of equilibrium with the surrounding atmosphere containing vapours of either metal or the nonmetal of the compound. Therefore in a solid, several kinds of ionic or electronic defects are possible. However, it has often been observed that only one kind of defect becomes energetically more favourable than the others.

Based on the calculations presented in the earlier section (Section I-2) Möbius [71] has predicted the predominance of anion defects in CaF_2 type lattices. The presence of anti-Frenkel pairs i.e. anion vacancies and anion interstitials in fluorite lattices have been experimentally verified using different techniques like X-ray diffraction, density and electrical conductivity measurement and the results have been reviewed by several authors [73-76].

I-4. DEFECT CONCENTRATION AND ELECTRICAL CONDUCTIVITY

I-4.1 Pressure Variation

The notable feature of the point defects is that
they are in thermal equilibrium within the solid and may be
treated as chemical species in terms of equilibrium constant
and mass action law. To determine the effect of nonmetal
activity of the surrounding atmosphere on the concentration
of different type of defects, Kröger and Vink [77] considered
the various combinations of defects in a compound MX and
applying the mass action law, made detailed calculation to
find out the variation of the concentration of individual
defects as a function of nonmetal activity of the surroundings
under an isothermal condition. As has been shown later, the
concentration of the defects changes in a different manner
in the different ranges of nonmetal activity with various
combinations of defects. Since the conductivity is directly
proportional to the concentration of the defect (equation
I-2), the variation of the electrical conductivity with the
nonmetal activity indicates the behaviour of the predominant
defect and has often been used to predict the defect
structure of ionic solids, especially that of oxide electrolytes
by comparing the experimental results with the theoretically
calculated slopes of conductivity vs nonmetal activity plots.
In case of pure ZrO_2 such slopes have been calculated by

Vest et al. [78] for the various combinations of ionic and electronic defects. The results obtained are summarised in Table 1.1.

As has been mentioned earlier, the oxides of the general formula MO_2 and having CaF_2 type crystal structure are known to have anti-Frenkel pair i.e. oxygen vacancies and oxygen interstitials, as their predominant defect. Both the defects are assumed to be in the fully ionised state, carrying two negative and positive charges respectively. The defect equilibrium in such an oxide under the exact stoichiometric condition may be described by

$$O_o \rightleftharpoons O_i'' + V_O^{\cdot\cdot} \qquad (I-6)$$

$$\text{and} \quad e_V \rightleftharpoons e' + h^{\cdot} \qquad (I-7)$$
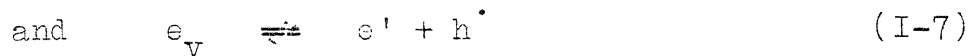
where the notations used are those given by Kröger and Vink [77]. O_o represents an oxygen ion in its normal site. O_i and V_O are the oxygen interstitial and oxygen vacancy respectively. e and h are the excess electron and electron hole respectively. e_V is a valence electron. The primes designate negative charges while the dots represent positive charges.

As the oxide is brought into equilibrium with the surrounding atmosphere of either higher or lower oxygen partial pressure (P_{O_2}) compared to that of the stoichiometric condition, changes in the composition take place, following

Table 1.1

Pressure Dependence of Defect Concentration in ZrO_2

for Various Possible Defects

	Oxidation-reduction predominates	Thermal disorder predominates	
Predominant defects	x	Predominant defects	x
V_O^{m+} , e'	$-1/4$, $-1/6$	V_O^{n+}	$-1/2$, $-1/4$
Zr_i^{n+} , e'	$-1/2$, $-1/3$, $-1/4$, $-1/5$	Zr_i^{n+}	-1, $-1/2$, $-1/3$, $-1/4$
V_{Zr}^{p-} , h·	$1/2$, $1/3$, $1/4$, $1/5$	V_{Zr}^{p-}	1, $1/2$, $1/3$, $1/4$
O_i^{q-} , h·	$1/4$, $1/6$	O_i^{q-}	$1/2$, $1/4$

m, n, p, q are the degrees of ionization of defects

m and q = 0, 1, 2   n and p = 0, 1, 2, 3, 4

$[\ ] \propto P_{O_2}^x$

introduction of ionic defects like oxygen interstitials or
oxygen vacancies together with the compensating electronic
defects like electron holes or excess electrons respectively.
The reactions may be represented as

$$\tfrac{1}{2}O_2(g) \rightleftharpoons O_i'' + 2h^\cdot \tag{I-8}$$

$$(\text{At high } P_{O_2})$$

$$\text{and} \quad O_o \rightleftharpoons \tfrac{1}{2}O_2(g) + V_O^{\cdot\cdot} + 2e' \tag{I-9}$$

$$(\text{At low } P_{O_2})$$
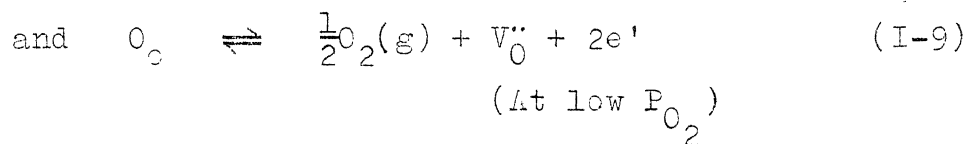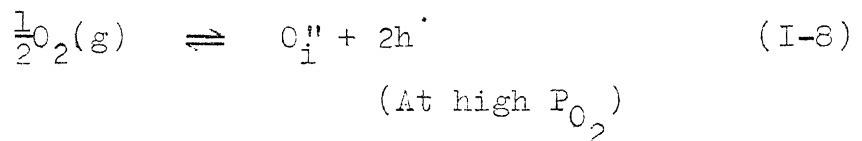
Therefore the overall defect equilibria in the oxide,
throughout the oxygen partial pressure range, may be described
by the equations (I-6) to (I-9). However only three of these
four equations may be considered independent and the fourth
one may be derived from the other three.

Assuming a dilute solution model where the
activities are equal to the concentrations, the application
of mass action law to the equations (I-6) to (I-9) gives rise
to

$$K_1 = [O_i''][V_O^{\cdot\cdot}] \tag{I-10}$$

$$K_2 = [e'][h^\cdot] \tag{I-11}$$

$$K_3 = [O_i''][h^\cdot]^2 \, P_{O_2}^{-1/2} \tag{I-12}$$

$$\text{and} \quad K_4 = [V_O^{\cdot\cdot}][e']^2 \, P_{O_2}^{1/2} \tag{I-13}$$

where K_1, K_2, K_3 and K_4 are the equilibrium constants for
the corresponding reactions, the brackets represent the
concentration of individual species and the concentration of
O_2 gas is given by its partial pressure. Equations (I-10)
through (I-13) are applicable throughout the partial pressure
range. To maintain electrical neutrality in the solid under
any condition, the following relation must be satisfied.

$$[h^{\cdot}] + 2[V_O^{\cdot\cdot}] = 2[O_i''] + [e']$$ (I-14)

Considering equations (I-6) to (I-14) the concentration of
individual defects may be expressed as a function of P_{O_2} under
three limiting cases.

Case I   Stoichiometric Composition

        Significant ionic transfer can take place in the
P_{O_2} range where the concentration of ionic defects far exceeds
that of the electronic defects and the equation (I-14) will
essentially reduce to

$$[V_O^{\cdot\cdot}] = [O_i'']$$ (I-15)

representing a stoichiometric condition.

        Therefore, from equation (I-10)

$$[O_i''] = [V_O^{\cdot\cdot}] = K_1^{1/2}$$ (I-16)

The ionic defect concentrations are independent of oxygen
partial pressure.

Following equations (I-12), (I-13), and (I-16), the concentrations of the electronic defects in this range may be expressed as

$$[h^{\cdot}] = K_3^{1/2} K_1^{-1/4} P_{O_2}^{1/4} \qquad (I-17$$

$$\text{and} \qquad [e'] = K_4^{1/2} K_1^{-1/4} P_{O_2}^{-1/4} \qquad (I-18$$

Case II Oxygen Deficient Region

At very low oxygen partial pressures, according to equation (I-9), the concentration of oxygen vacancies and electrons will be much greater than that of interstitials and holes so that

$$[V_O^{\cdot\cdot}] = \tfrac{1}{2}[e'] \gg [O_i''] \text{ or } \tfrac{1}{2}[h^{\cdot}] \qquad (I-19$$

and therefore

$$[V_O^{\cdot\cdot}] = (K_4/4)^{1/3} P_{O_2}^{-1/6} \qquad (I-20$$

$$[O_i''] = \frac{K_1}{[V_O^{\cdot\cdot}]} = K_1(K_4/4)^{-1/3} P_{O_2}^{1/6} \qquad (I-21$$

$$[e'] = (2K_4)^{1/3} P_{O_2}^{-1/6} \qquad (I-22$$

$$\text{and} \qquad [h^{\cdot}] = \frac{K_2}{[e']} = K_2(2K_4)^{-1/3} P_{O_2}^{1/6} \qquad (I-23$$

Case III   Excess Oxygen Region

In the high oxygen partial pressure range.

$$[O_i''] = \tfrac{1}{2}[h^{\cdot}] \gg [V_O^{\cdot\cdot}] \text{ or } \tfrac{1}{2}[e'] \qquad (I-24)$$

thus

$$[O_i''] = \tfrac{1}{2}[h^{\cdot}] = (\frac{K_3}{4})^{1/3} P_{O_2}^{1/6} \qquad (I-25)$$

$$\therefore [h^{\cdot}] = (2K_3)^{1/3} P_{O_2}^{1/6} \qquad (I-26)$$

Similarly

$$[V_O^{\cdot\cdot}] = \tfrac{1}{2}[e'] = (\frac{4K_1^{\,3}}{K_3})^{1/3} P_{O_2}^{-1/6} \qquad (I-27)$$

$$\therefore [e'] = 2(\frac{4K_1^{\,3}}{K_3})^{1/3} P_{O_2}^{-1/6} \qquad (I-28)$$

The variation of the concentration of individual defects with P_{O_2} may be represented graphically following Kröger and Vink type of diagram and is shown in Fig. 1.2a. The electrical conductivity of the system is chiefly determined by the concentration of the predominant defects and may be derived from Fig. 1.2a by applying equation (I-2) with the assumption that the mobility of the defects is independent of concentration. This is particularly true at a lower defect concentration and sufficiently high temperature. The calculated electrical conductivity in an oxide MO_2 is shown in Fig. 1.2b. The mobilities of the electronic defects are in general
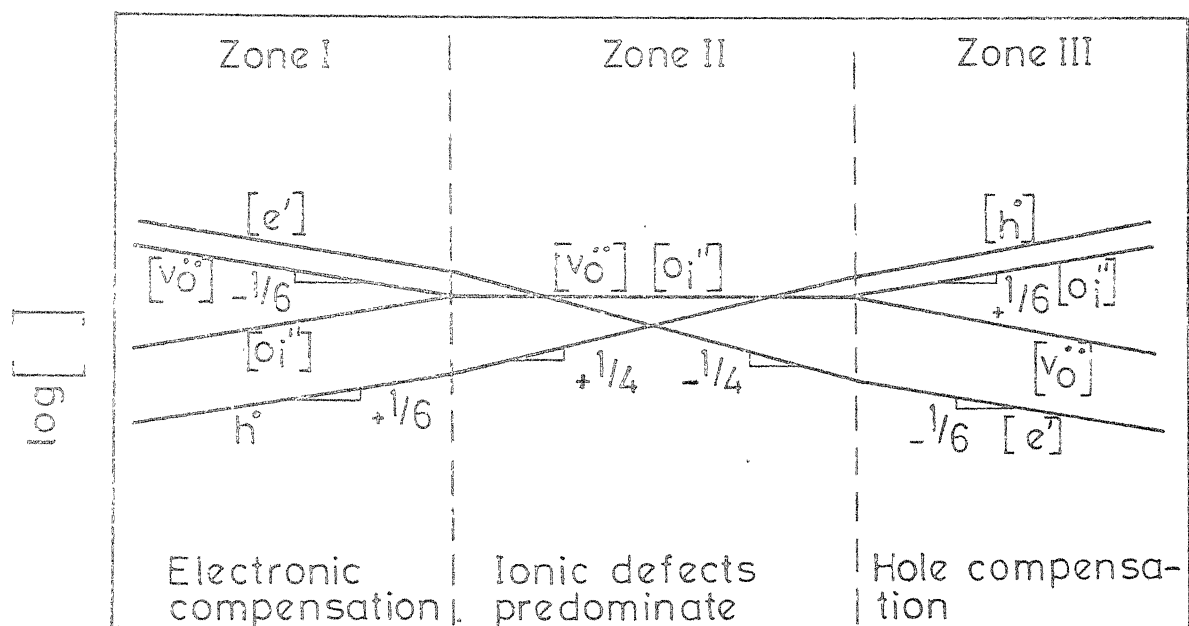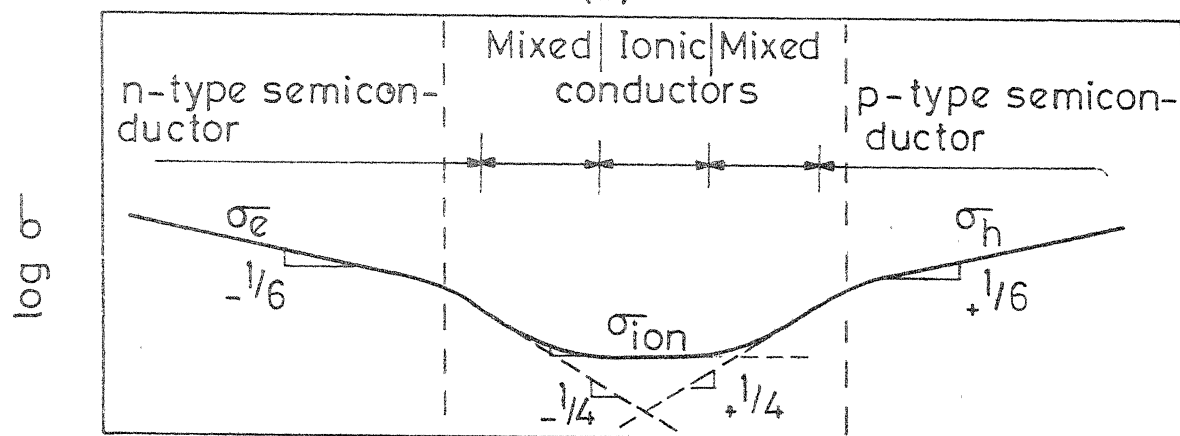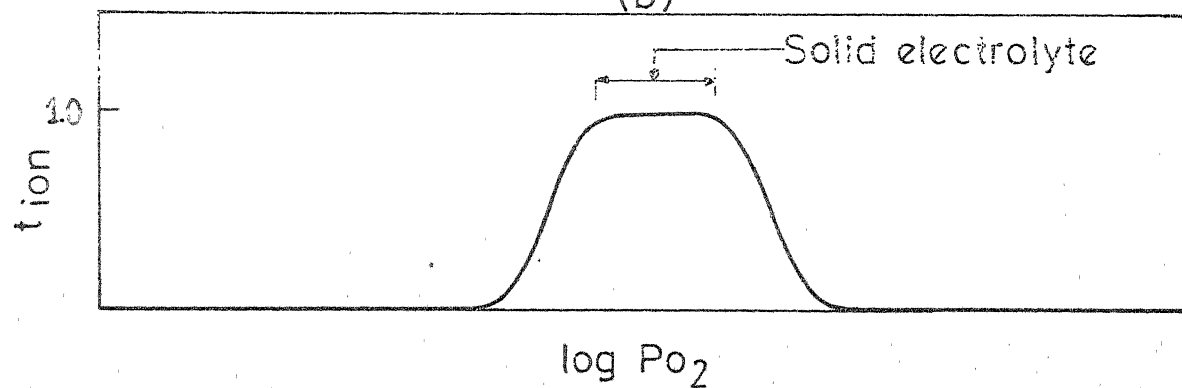
FIG.1-2 SCHEMATIC REPRESENTATION OF (a) DEFECT CONCENTRA-
TION (b) ELECTRICAL CONDUCTIVITY AND (c) IONIC TRANS
FERENCE NUMBER AS A FUNCTION P_{O_2} FOR AN OXIDE
MO_2 CONTAINING ANTIFRENKEL DEFECT. [29]

100-1000 times greater than that of ionic defects and therefore predominant ionic conduction takes place in the P_{O_2} range where the concentration of ionic defects greatly exceeds that of the electronic defects. As a result, the oxygen partial pressure range of exclusive ionic conductivity is shorter than that corresponding to the predominant ionic defects. According to the assumption made by Lasker and Rapp [52], the ionic contribution in the mixed conduction region may be represented by the P_{O_2} independent conductivity plateau in the intermediate partial pressure range (Fig. 1.2b while the P_{O_2} dependent conductivity above this plateau represents the electronic or electron hole contribution. Following this assumption the ionic transference number as a function of P_{O_2} may be derived from Fig. 1.2b by using equation (I-1). The results are schematically represented in Fig. 1.2c. The oxide may be considered as a solid electrolyte in the P_{O_2} range where t_{ion} is almost equal to unity.

Pure oxides are not of major importance as solid electrolytes because the exclusive ionic conductivity extends over a limited range of oxygen partial pressure. If the oxid is doped with an aliovalent cation like trivalent yttrium or divalent calcium, the concentration of the predominant ionic defect is drastically increased along with the P_{O_2} range of ionic conductivity. Lasker and Rapp [52] have developed a

dilute solution model for Y_2O_3 doped ThO_2 electrolytes to predict the partial ionic and electronic conductivities and also the ionic transference number as a function of P_{O_2} and dopant concentration.

In thoria doped with Y_2O_3, a part of the tetravalent thorium ions are substituted by trivalent yttrium ions and to maintain the electrical neutrality, oxygen vacancies are formed as the compensating defects, the concentration of which depends upon the Y_2O_3 content.

$$[V_O^{\cdot\cdot}] \;=\; \tfrac{1}{2}[YO_{1.5}] \tag{I-29}$$

Even with a small amount of Y_2O_3, the concentration of oxygen vacancies will far exceed that of the intrinsic defects and therefore

$$[V_O^{\cdot\cdot}] \;=\; \tfrac{1}{2}[YO_{1.5}] \gg [O_i^{\prime\prime}] \tag{I-30}$$

and the ionic conductivity in the intermediate oxygen partial pressure range may be given by

$$\sigma_{ion} \;=\; |e|\,\mu_V\,[YO_{1.5}] \tag{I-31}$$

where μ_V is the mobility of the oxygen vacancies. Following an analysis similar to that for MO_2 given above and taking μ_e and μ_h as the mobilities of electrons and electron holes respectively, the electronic conductivity of Y_2O_3 doped ThO_2 in the low P_{O_2} range may be expressed from the equations (I-13) and (I-29) as

$$\sigma_e \;=\; |e|\,\mu_e(2K_4)^{1/2}\,(P_{O_2})^{-1/4}\,[YO_{1.5}]^{-1/2} \tag{I-32}$$

Similarly, at high P_{O_2} range, the hole conductivity (σ_h) may be obtained from equation (I-10), (I-12) and (I-29) as

$$\sigma_h = |e|\mu_h \left(\frac{K_3}{2}\right)^{1/2} K_1^{-1/2} P_{O_2}^{1/4} [YO_{1.5}]^{1/2} \qquad (I-33)$$

The results of the above analysis are schematically represented in Fig. 1.3 which shows that, with increasing amount of Y_2O_3 content, the predominant ionic conduction takes place over a wider range of partial pressure extended towards both higher and lower values. The general expression for the ionic transference number for this electrolyte may be obtained from equations (I-31), (I-32) and (I-33) as

$$t_{ion} = \frac{\sigma_{ion}}{\sigma_{ion} + \sigma_e + \sigma_h}$$

$$= \frac{1}{1 + 2^{\frac{1}{2}} K_4^{\frac{1}{2}} \beta_e P_{O_2}^{-1/4} [YO_{1.5}]^{-3/2} + K_3^{\frac{1}{2}} (2K_1)^{-\frac{1}{2}} \beta_h P_{O_2}^{1/4} [YO_{1.5}]^{-\frac{1}{2}}}$$

$$\dots(I-34)$$

where $\quad \beta_e = \frac{\mu_e}{\mu_v} \quad$ and $\quad \beta_h = \frac{\mu_h}{\mu_v} \qquad (I-35)$

The equation (I-34) illustrates the effect of $YO_{1.5}$ content on the ionic transference number in Y_2O_3 doped ThO_2 electrolytes.

I-4.2 Temperature Variation

Under thermal equilibrium the concentration of the Schottky pairs in a crystal is given by
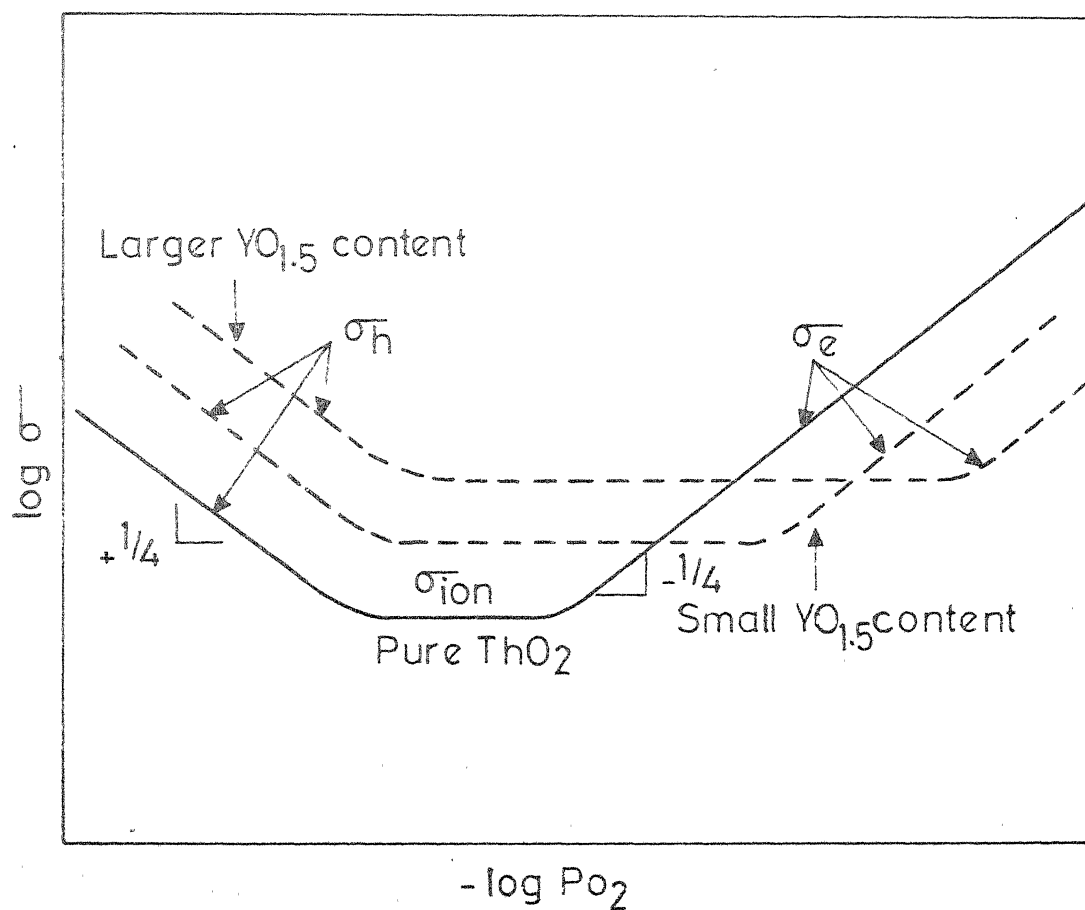
FIG. 1·3 SCHEMATIC ILLUSTRATION OF THE EFFECT OF
YO$_{1.5}$ CONTENT ON THE CONDUCTIVITY OF ThO$_2$ -YO$_{1.5}$
ELECTROLYTES. [25]

$$n_S/N = \exp(\Delta S_{th}/2k - \Delta H_S/2kT) \qquad (I-36)$$

and that of Frenkel pair

$$n_F/\sqrt{NN_i} = \exp(\Delta S_{th}/2k - \Delta H_F/2kT) \qquad (I-37)$$

where n_S and n_F are the numbers of Schottky and Frenkel pairs respectively, N and N_i are the total number of ions and interstitial sites respectively in the crystal, ΔS_{th} is the change in thermal entropy per vacancy, ΔH_S and ΔH_F are the enthalpi of formation of a Schottky and a Frenkel pair respectively, k is the Boltzman constant and T is absolute temperature. Equations (I-36) and (I-37) represent the temperature dependen of the intrinsic ionic defects in a pure crystal under stoichi metric condition.

According to the mass action law the equilibrium constant of a chemical reaction (K) is expressed in terms of thermodynamic parameters.

$$K = \exp(\Delta S^O/k - \Delta H^O/kT) \qquad (I-38)$$

where ΔS^O and ΔH^O are respectively the entropy and enthalpy change of the reaction under standard state. Assuming these quantities as independent of temperature, equation (I-38) may be modified as

$$K = \text{const.} \exp\left(-\frac{\Delta H^O}{kT}\right) \qquad (I-39)$$

The effect of temperature variation on the individual defect concentration in an oxide having anti-Frenkel disorder can be calculated through Brook's analysis [79] by superimposing this temperature dependence of the equilibrium constant on the types of calculations performed in the earlier section (Sec. I-4.1). The equilibrium constants for the defect reaction presented in equations (I-6) through (I-9) may be expressed as

$$K_1 = K_1^0 \exp\left(-\frac{\Delta H_1^0}{kT}\right) \tag{I-40}$$

$$K_2 = K_2^0 \exp\left(-\frac{\Delta H_2^0}{kT}\right) \tag{I-41}$$

$$K_3 = K_3^0 \exp\left(-\frac{\Delta H_3^0}{kT}\right) \tag{I-42}$$

and

$$K_4 = K_4^0 \exp\left(-\frac{\Delta H_4^0}{kT}\right) \tag{I-43}$$

In the intermediate partial pressure range under a constant P_{O_2} such that $[e'] = [h^\cdot]$, the temperature dependence of $[V_O^{\cdot\cdot}]$ may be found out as follows:

From equation (I-11) and (I-41)

$$[e'] = [h^\cdot] = K_2^{1/2} = K_2^0 \exp\left(-\frac{\Delta H_2^0}{2kT}\right) \tag{I-44}$$

and therefore from equation (I-13) and (I-43)

$$[V_O^{\cdot\cdot}] = \frac{K_4 P_{O_2}^{-1/2}}{[e']^2} = \frac{K_4 P_{O_2}^{-1/2}}{K_2}$$

$$= \frac{K_4^O \exp(-\Delta H_4^O/kT)}{K_2^O \exp(-\Delta H_2^O/kT)} P_{O_2}^{-1/2} \qquad (I-45)$$

$$\therefore \quad \frac{d \ln[V_O^{\cdot\cdot}]}{d(1/T)} = \frac{-\Delta H_4^O + \Delta H_2^O}{k} \qquad (I-46)$$

Equation (I-46) gives the slope of the log concentration vs 1/T curve. Similarly the concentration of other defects may be determined from equations (I-10) through (I-13) and (I-40) through (I-43).

I-5. THERMOELECTRIC POWER

The experimental arrangement for the measurement of thermoelectric power of a crystal MX fitted with electrodes and leads of the same metal M is shown in Fig. 1.4 . The total potential difference $(\emptyset_B - \emptyset_A)$ is made up of three parts.

(i) The homogeneous potential difference $(\emptyset_R - \emptyset_Q)$ which is due to temperature gradient (ΔT) within the crystal.

(ii) The algebraic sum of the contact potential difference $[(\emptyset_S - \emptyset_R) - (\emptyset_P - \emptyset_Q)]$ at the M/MX interfaces, and

(iii) The algebraic sum of the homogeneous potential difference $[(\emptyset_P - \emptyset_A) - (\emptyset_S - \emptyset_B)]$ in the lead wires.
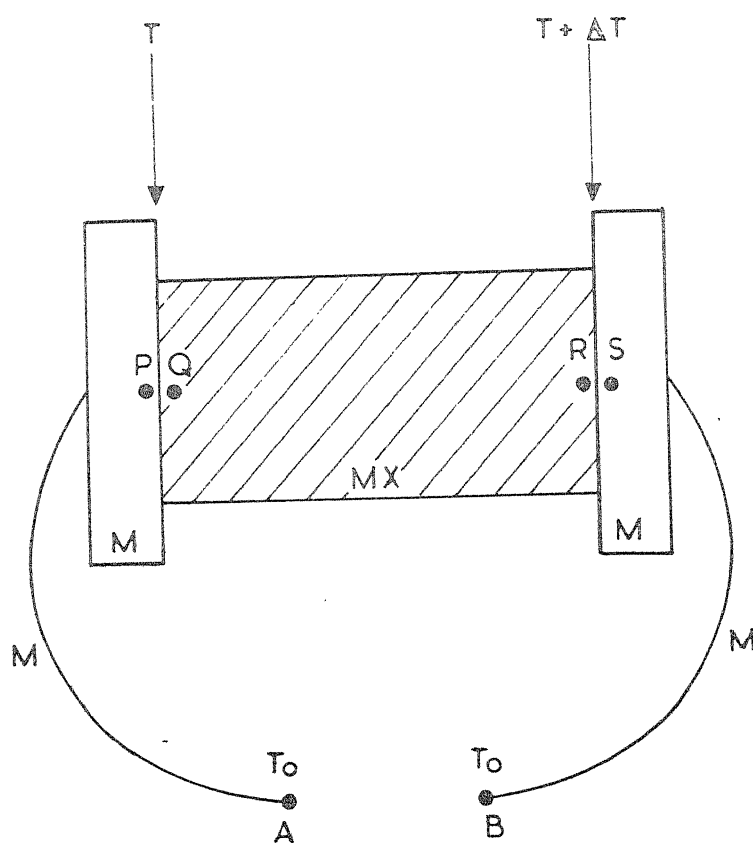
FIG. 1·4 EXPERIMENTAL ARRANGEMENT FOR MEASURE-
MENT OF THERMOELECTRIC POWER IN A CRYS-
TAL MX.

The magnitude of the last term is generally insignificant compared to the other two and may be neglected. Therefore the total thermoelectric power is given by

$$\alpha = \frac{(\phi_R - \phi_Q) + [(\phi_S - \phi_R) - (\phi_P - \phi_Q)]}{dT}$$

$$= \frac{\phi_R - \phi_Q}{dT} + \frac{(\phi_S - \phi_R) - (\phi_P - \phi_Q)}{dT}$$

$$= \frac{d\phi(T)}{dT} + \frac{d\psi(T)}{dT}$$

$$= \alpha_{hom.} + \alpha_{het.} \tag{I-47}$$

$\alpha_{hom.}$ and $\alpha_{het.}$ are the homogeneous and heterogeneous thermo-electric powers respectively and ψ is the M/MX contact potential.

Based on the thermodynamics of irreversible process, the theory of thermoelectric power was developed by de Groet [55] and Holtan et al. [56,57] without considering any particular defect model for the solid and derived an expression for $\alpha_{hom.}$. Later, Howard and Lidiard [80,81] approached the prob by considering Frenkel disorder in the solid and obtained results which are consistent with the thermodynamic analysis. In the kinetic treatment of Howard and Lidiard [80,81], the vacancies were considered as species of effective unit charge moving in a uniform dielectric. Allnatt and Jacobs [82] have reformulated the theory of thermoelectric power with modified

expressions of chemical potentials and considering vacancies as separate thermodynamic species having zero charge and mass. They have derived the expression for Seebeck coefficients for both Schottky and Frenkel type of defects in pure and doped MX crystals. The effects of defect interactions on the thermoelectric power of alkali halide crystals containing Schottky defect has been considered by Shimoji and Hoshino [83]. The problem of thermoelectric power under the situation where the electrode material is different from the metallic constituent of the compound MX has been considered by Allnatt and Jacobs [82] and Shimoji and Hoshino [83]. The theory of thermoelectric power originally developed for MX type of crystals has been successfully extended to oxide electrolytes by several investigators [68-70] and is briefly presented here.

The Seebeck coefficient for a thermocell of the type,

$$(P_{O_2}) \; Pt \Big\| \; Zr_{0.85}Ca_{0.15}O_{1.85} \; \Big\| Pt \; (P_{O_2})$$
$$\hspace{2.5cm} T \hspace{3.5cm} T+\Delta T$$
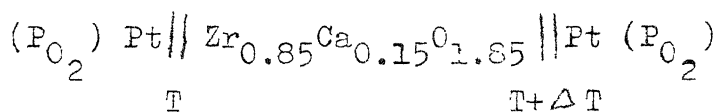
may be expressed as

$$\frac{\Delta \phi}{\Delta T} = \frac{1}{F} [\frac{1}{2} \bar{S}(O^=) - \bar{S}(e^-) - \frac{1}{4} S(O_2)] \hspace{2cm} (I-48)$$

where $\bar{S}(O^=)$ and $\bar{S}(e^-)$ are the entropies of transport of $O^=$ ions in the electrolyte and the electrons in the platinum electrode respectively. $S(O_2)$ is the change in entropy due

to heterogeneous electrode reaction. Tannhauser [84] has pointed out that this quantity has been misleadingly termed as partial molar entropy of O_2 in the gaseous atmosphere at the electrode by Ruka et al. [68] and Tallan and Bransky [70]. The electrode reaction depends on the particular gaseous atmosphere which exists at the electrode. Ruka et al. [68] have assumed that the following reactions take place for the O_2-inert gas and $H_2 - H_2O - N_2$ mixtures respectively.

$$O_2 + 4e^- \rightleftharpoons 2O^= \tag{I-49}$$

$$2H_2O + 4e^- \rightleftharpoons 2H_2 + 2O^= \tag{I-50}$$
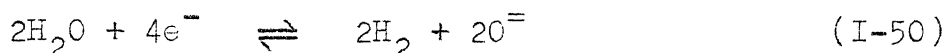
Following the same principle, Tallan and Bransky [70] have derived a general expression for the Seebeck coefficient of a MO_2 type of mixed conductor having a fixed concentration of ionic defect (e.g. nominally pure thoria with a small amount of impurity) and taking into consideration the effect of defect association.

If fully charged oxygen interstitials are present as the compensating defect, the homogeneous Seebeck coefficient can be calculated as

$$\alpha_{hom.} = -\frac{\partial \phi}{\partial T} = \frac{1}{eT}\left[t_h \left\{ \frac{\Delta H_{ox}}{2} + Q(h^\cdot) - \frac{1}{2}\frac{\beta}{1+\beta}\Delta H\beta \right\} \right.$$

$$\left. - t_{ion}\left\{ \frac{1}{2}Q(O_i'') + \frac{1}{2}\frac{\beta}{1+\beta}\Delta H_P \right\} \right] \tag{I-51}$$

where t_h and t_{ion} are the transference numbers for electron hole and oxygen ion respectively. ΔH_{ox} is the enthalpy change for the reaction

$$\tfrac{1}{2} O_2 \rightleftharpoons O_i'' + 2h^\cdot \qquad (I\text{-}52)$$
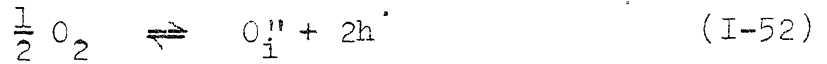
ΔH_p is the enthalpy change of the association reaction

$$F_M^\cdot + O_i'' \rightleftharpoons (F_M O_i)' \qquad (I\text{-}53)$$
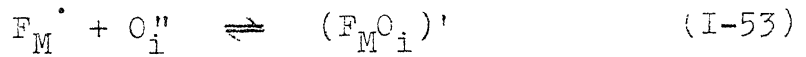
$Q(h^\cdot)$ and $Q(O_i'')$ are the heats of transport of electron hole and oxygen interstitials respectively and β is the degree of association defined by

$$\beta = \frac{[(F_M O_i)']}{[F_M]_T} \qquad (I\text{-}54)$$

$[F_M]_T$ is the total impurity content. Similarly

$$\alpha_{het.} = \tfrac{1}{e} \left[\tfrac{1}{2} S(O_i'')_{MO_2} - \tfrac{1}{4} S(O_2)_g - S(e^-)_{pt} \right] \qquad (I\text{-}55)$$

Combining (I-51) and (I-55) one gets the total Seebeck coefficient. From these general expressions, α_{ion} can be obtained by substituting $t_{ion} = 1$ and $t_h = 0$ and α_h by the substitution of $t_{ion} = 0$ and $t_h = 1$, where α_{ion} and α_h are the ionic and electron hole Seebeck coefficients respectively. The total Seebeck coefficient is given by

$$\alpha_T = t_{ion}\alpha_{ion} + t_h \alpha_h \qquad (I\text{-}56)$$

As yet there is no suitable method to calculate the absolute
Seebeck coefficient. However the Seebeck coefficient
difference for the two gas mixtures. $(\alpha_{ion})_{gas1} - (\alpha_{ion})_{gas2}$
can be calculated for a range of oxygen partial pressures
over which the electrolyte and the electrode material remain
invariant. In that case $\bar{S}(O^=)$ will remain constant and
equation (I-48) can be applied to two different gas mixtures
separately and by substraction one gets

$$\Delta\alpha = (\alpha_{ion})_{gas1} - (\alpha_{ion})_{gas2} = \frac{1}{4F}[S(O_2)_{gas1} - S(O_2)_{gas2}]$$

$$...(I-57)$$

It is generally convenient to choose one reference gas
mixture in the partial pressure range where the electrolyte
is completely ionic. In the case of calcia stabilized
zirconia, pure O_2 can act as the reference gas. Equation (I-57)
shows that the difference in Seebeck coefficient between two
gas mixtures is a linear function of entropy difference
between the two gas phases and not of partial pressure
difference.

This has been verified for $(ZrO_2)_{0.85}(CaO)_{0.15}$
and 'pure' thoria as is evident from Figs. 1.5 and 1.6
respectively. For pure thoria the values of $\Delta\alpha$ in the mixed
conduction region have been plotted with their probable error
limits (the inset of Fig. 1.6). Measurement of Seebeck
coefficient as a function of oxygen partial pressure together
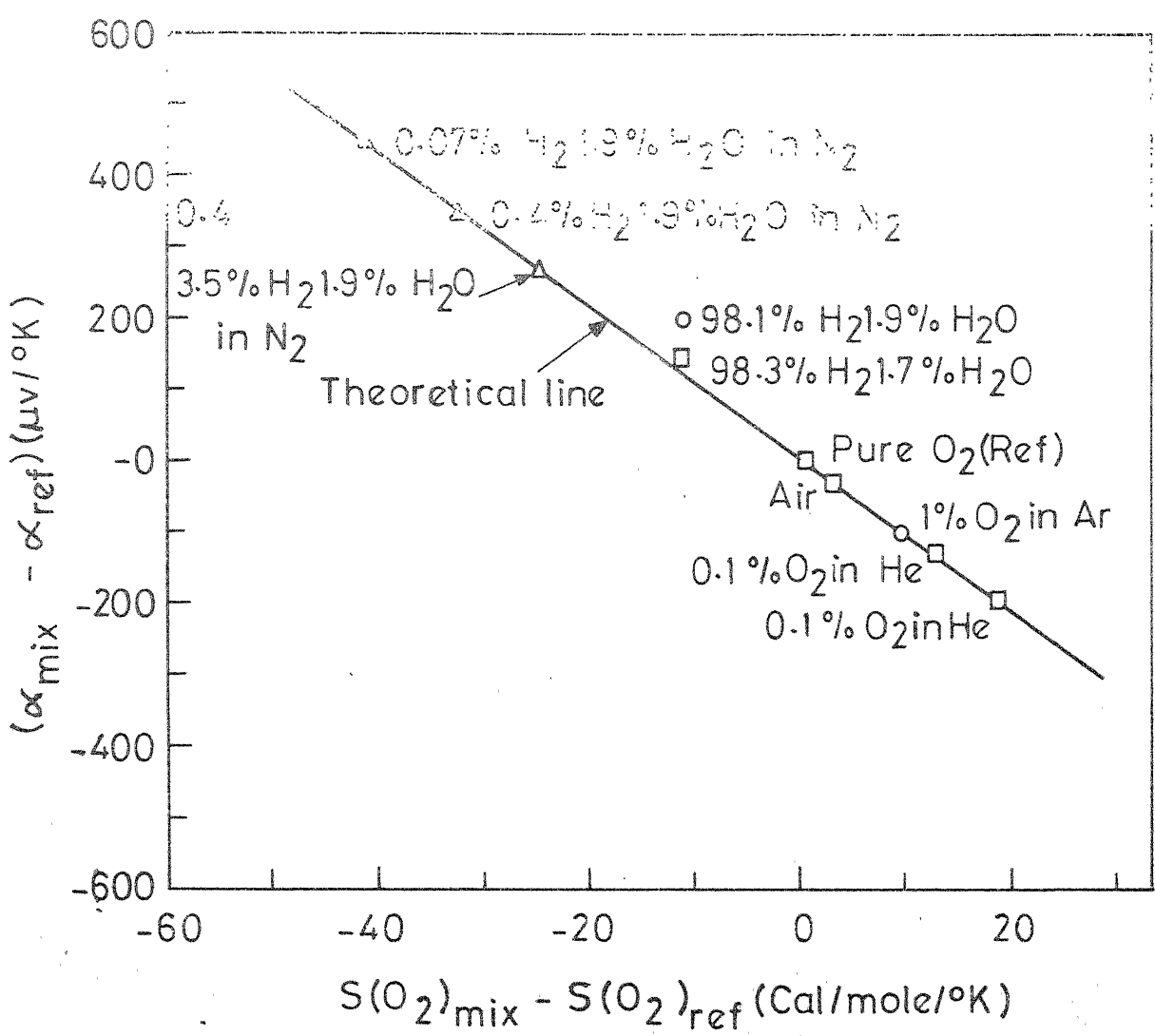
FIG. 1·5 RESULTS ON THERMOELECTRIC POWER OF ZCS OBTAINED 1000°C. [68]
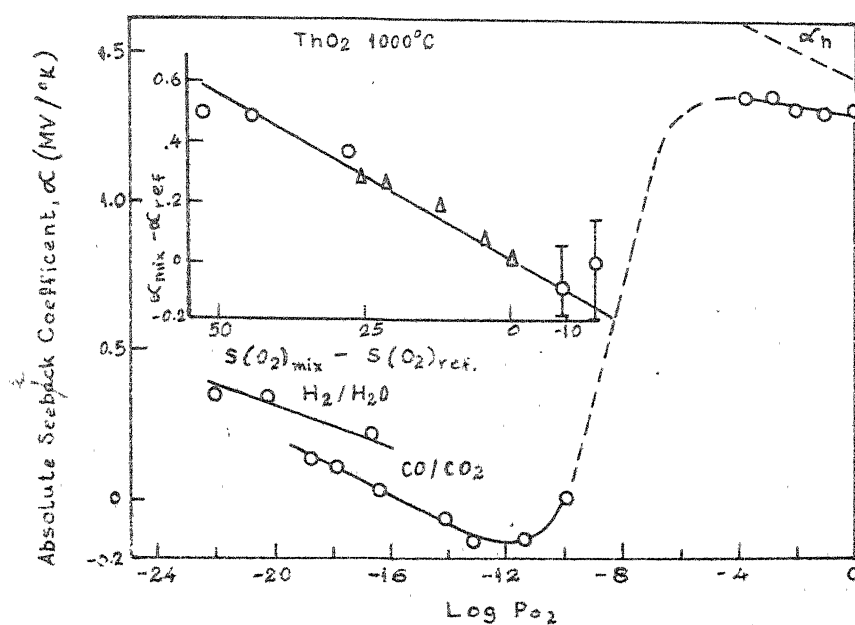
FIG.1·6 ABSOLUTE SEEBECK COEFFICIENT OF PURE ThO_2 AS A FUNCTION OF OXYGEN PARTIAL PRESSURE. [70]

with the reported values of $S(O_2)_{gas}$ and $S(e^-)_{pt}$ gives the enthalpies of transport:

$$\bar{S}(O_i'') = 1.45 \pm 0.5 \text{ eu in ThO}_2 \text{ at } 1000^\circ\text{C over the}$$

P_{O_2} range of 10^{-13} to 10^{-23} atm. and $\bar{S}(V_O^{..}) = 10.3$ to 10.9 eu for $(ZrO_2)_{0.85}(CaO)_{0.15}$ at 1000°C.

I-6. CONDUCTIVITY OF THORIA AND THORIA BASE ELECTROLYTES

I-6.1 Pure ThO_2 and $ThO_2-M_2O_3$ Electrolytes

The experimental results on thoria and thoria base electrolytes have been reviewed by Rapp [26] and later by Etsell and Flengas [27]. The a.c. total conductivity of pure thoria has been measured by several investigators [49,52-54, 85-89] as a function of oxygen partial pressure or temperature. The various oxygen partial pressures were obtained either by different gas mixtures or through various metal-metal oxide equilibria. The results obtained by some of these investigators are compared in Fig. 1.7 in which log has been plotted against log P_{O_2} under different isothermal conditions. Considering the differences in the origin of the specimens, the conductivity values reported by various authors are in good agreement with each other. As predicted by the theory of defect concentration, the P_{O_2} independent plateau in the conductivity plot represents the predominant ionic conduction in 'pure' thoria. Electrical conductivity [52-54,85,87], density [86,90] and thermoelectric power measurements [70]
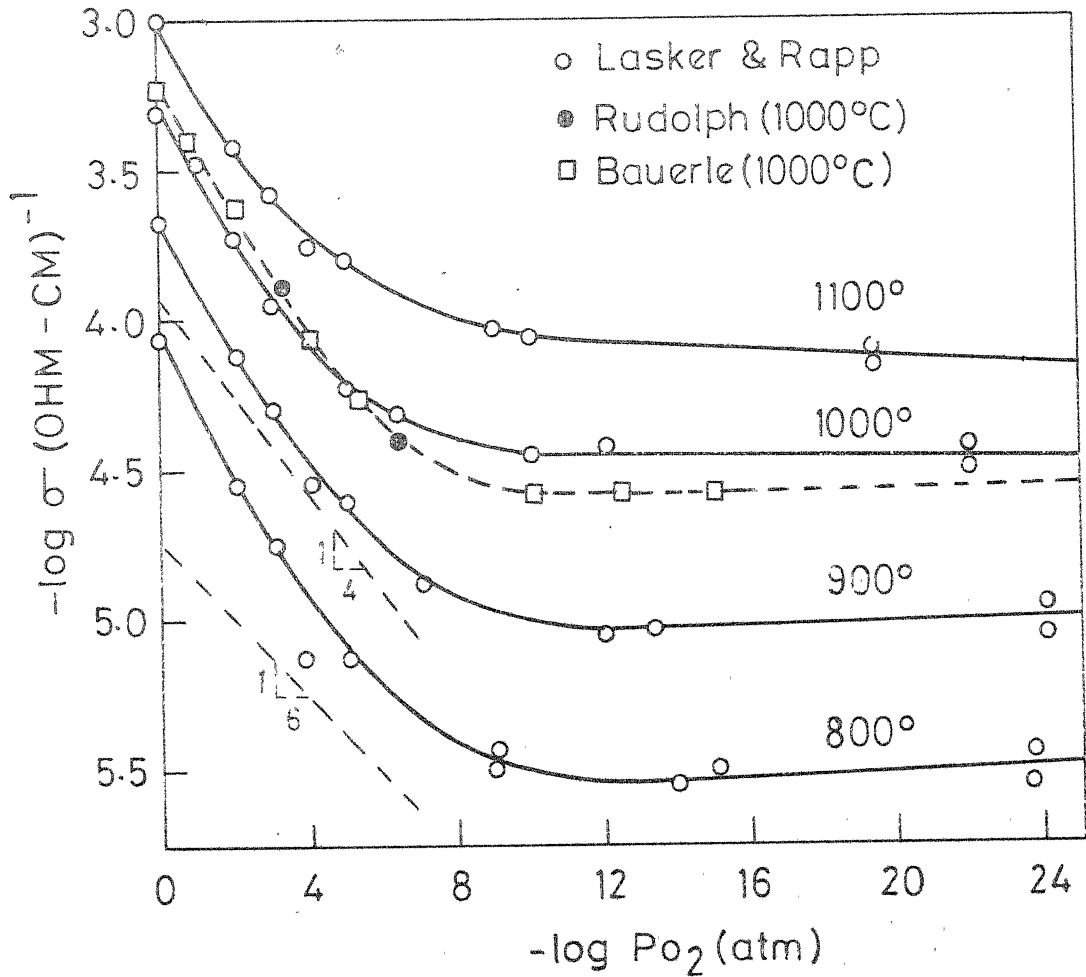
FIG. 1·7   A.C. TOTAL CONDUCTIVITY FOR 'PURE' THORIA AS A FUNCTION OF TEMPERATURE AND OXYGEN PARTIAL PRESSURE. [26]

show that the oxygen vacancies are the predominant ionic defect in 'pure' and doped thoria specimens. It is evident from Fig. 1.7 that the ionic conduction in 'pure' thoria takes place below certain partial pressure range (10^{-6} to 10^{-8} atm.) where it can be used as an electrolyte in galvanic cells. However at higher P_{O_2} the conductivity is proportional to $P_{O_2}^{1/4}$ indicating a p-type semiconduction in this range. According to the predicted variation of defect concentration, the observed pressure dependence of conductivity may be obtained either in a truly pure thoria specimen in which the variation of defect concentration is described by the right hand half of zone II (Mixed conduction region) in Fig. 1.2a or, if the sample contains significant amount of di- or tri-valent impurity ions, so that its conductivity is described by equation of the form (I-33). By plotting the ionic conductivities of thoria samples containing known amount of impurity against the impurity content and extrapolating it to the conductivity value of pure ThO_2, Bauerle [54] has reported the presence of 200-400 ppm of trivalent impurity in his 'pure' thoria sample. Similar observation was also made by Lasker and Rapp [52]. It has been pointed out [87] that the 'pure' ThO_2 samples currently available and earlier used by different investigators contain sufficient amount of the di- or tri-valent impurities and the defect equilibria in such specimens may be better described by that observed in the mixed conduction region of a doped oxide.

However, the observation of the characteristic $P_{O_2}^{1/6}$ dependence of conductivity in the p-type semiconduction region of truly pure ThO_2 as predicted by the postulated defect structure has been claimed by Primas and Rapp [91] only at a very high temperature ($1500^\circ C$) where the concentrations of the extrinsic defects are expected to be negligible compared to that of the native defects. The 1/5 pressure dependence later observed by Bransky and Tallan [87] has been attributed to a transition from P_{O_2} independent ionic conductivity to P_{O_2} dependent hole conductivity. These authors have suggested that the $P_{O_2}^{1/6}$ dependence corresponding to the nonstoichiometric defect equilibrium

$$[h^\cdot] = 2[O_i'']$$

may not be observed until $\sigma_T/\sigma_{ion} \gtrsim 10^3$.

The existence of mixed conduction in 'pure' thoria was earlier demonstrated by Danforth and Bodine [92,93] by a polarization technique, using electrodes blocking to the ions only. The technique has been later used by Vest and Tallan [94] to determine the electronic transference number in calcia stabilized zirconia specimens.

Contrary to the zirconia base electrolytes which are ionic conductors even in a pure oxygen atmosphere, thoria electrolytes are useful below 10^{-6} to 10^{-8} atm. of oxygen partial pressure and remain ionic down to an extremely low P_{O_2}

value. Markin et al. [95] have reported that measurable electronic conduction did not result even by placing thorium pellets on both sides of the electrolyte and flushing with dry hydrogen. The width of the ionic conduction plateau reduces with increasing temperature. Bransky and Tallan [87] have been able to detect n-type semiconduction in 'pure' thoria only at a temperature above $1600^{\circ}C$. Recently Choudhury and Patterson [89] have obtained n-type conductivity at lower temperatures ($800-1100^{\circ}C$) at a partial pressure below the coexistence of $Ti - Ti_xO$ electrode.

The temperature dependence of electrical conductivity in 'pure' thoria under a fixed oxygen partial pressure has been studied by several investigators. The activation energies have been calculated from the Arrhenius-type of plots of $\log\sigma$ vs $1/T$. In the mixed conduction region Bransky and Tallan [87] obtained activation energies of 0.98 ev below $1100^{\circ}C$ and 0.77 ev above this temperature from a plot of log conductance vs $1/T$ while the values obtained by Mehrotra et al. [88] from a plot of $\log\sigma T$ vs $1/T$ are 1.3 ev and 0.95 ev for the corresponding temperature ranges. Similar breaks in the activation energy curve were earlier observed in both 'pure' thoria [53] and pure HfO_2 [96]. In the ionic conduction range, the activation energy for ionic transport as obtained from the conductivity data [87] is 0.89 ev at lower temperatures while the value increases to

1.17 ev at higher temperatures. However the activation energy obtained from Seebeck coefficient measurement is 1.18 ev and remains constant throughout the temperature range. The activation energy for $ThO_2-Y_2O_3$ solid solutions was found to vary between 1.0-1.2 ev [49,52,90].

Among the thoria base electrolytes, Y_2O_3 doped thoria electrolytes have been studied most extensively. The solubility limits for $ThO_2-Y_2O_3$ system have been determined by X-ray diffraction technique [85,86]. On the ThO_2 rich side, the cubic fluorite type phase exists upto 40-50 m/o $YO_{1.5}$ at $2200^{\circ}C$. The limit of solubility decreases to 20-25 m/o $YO_{1.5}$ at $1400^{\circ}C$. The solid solubility limit of various oxides in ThO_2 are presented in Table 1.2. Density measuremen [85,86,90,97] show that the oxygen vacancy is the predominant defect in $ThO_2-YO_{1.5}$ electrolytes.

The conductivities of $ThO_2-YO_{1.5}$ electrolytes containing 0.84 to 25 m/o $YO_{1.5}$ have been measured [52] over a range of P_{O_2} in the temperature range of $(800-1100^{\circ}C)$ and they were found to obey the predicted P_{O_2} and $YO_{1.5}$ content dependencies. However, no detectable electronic conductivity was observed down to an oxygen partial pressure of 10^{-27} atm. at $800^{\circ}C$ or upto 10^{-20} atms. at $1000^{\circ}C$. The effect of $YO_{1.5}$ content on the ionic conductivity observed by different investigators, is shown in Fig. 1.8. The observed dependence is linear only upto a small concentration of $YO_{1.5}$. With

Table 1.2

Solid Solubility of Various Binary Oxides in ThO_2

Oxide	Cation Radius (A°)	Temperature $(^\circ C)$	Solubility m/o MO or M_2O_3	Reference
Se_2O_3	0.91	1750	0.5	98
Y_2O_3	1.07	1200	18	85
		1400	12	86
		1400	14	99
		2000	33	86
La_2O_3	1.21	1200	20	100,101
		1300	35	97
		1400	32	99
		1500	32	102
		1950	39	100
Pr_2O_3	1.16	1400	54	103
Nd_2O_3	1.15	1400	33	99
		1500	33	102
Sm_2O_3	1.13	1400	43	99
Eu_2O_3	1.10	1200	22	104
		1500	36	103,104
		1800	54	103
Gd_2O_3	1.10	800	19	100
		1400	33	99
		1800	45	100
Yb_2O_3	1.04	1000	3	101
		1400	5	103,104
		1800	10	100
CaO	1.10	1700	10	105
		1800	8.	106
		1800	>12	107
SrO	1.24	1800	4.	106
BaO	–	1800	<0.5	106
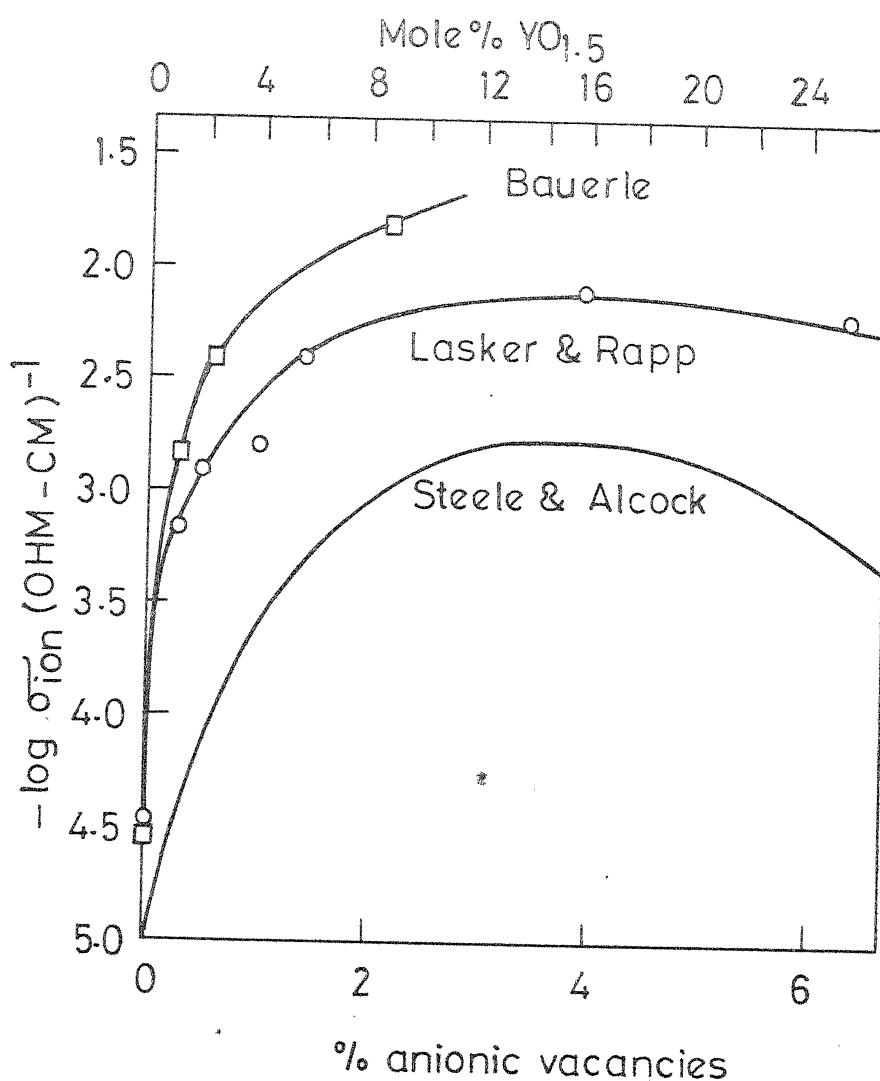
FIG. 1·8 IONIC CONDUCTIVITY AS A FUNCTION OF MOLE % $YO_{1.5}$ OR PERCENTAGE OF ANIONIC VACANCIES AT 1000 °C [26]

increasing impurity content the conductivity goes through a maximum at about 15 m/o $YO_{1.5}$. The deviation from linearity may be ascribed to the decreasing mobility of oxygen vacancies as a result of ordering [108], clustering [109] of the defects or impurity vacancy interactions [73]. The difference in the values of conductivity obtained by various investigators may be attributed to differing conditions employed for sample preparation.

The ionic transference number for $ThO_2-YO_{1.5}$ solid solutions have been calculated from the conductivity data and are shown in Fig. 1.9 as a function of P_{O_2}. As predicted by the dilute solution model, increasing addition of $YO_{1.5}$ (upto 15 m/o $YO_{1.5}$) widens the PO_2 range of exclusive ionic conduction and shifts the limit of predominant ionic conductivity towards higher P_{O_2} side. A knowledge of the variation of t_{ion} as a function of oxygen potential helps the integration of equation (I-3a) to determine the EMF of the galvanic cell formed by the mixed conductors. Subbarao et al. [86] and Lasker and Rapp [52] have measured the EMFs of galvanic cells involving various metal-metal oxide electrodes corresponding to the different oxygen potential and the electrolytes of various $YO_{1.5}$ contents. The measured EMFs, except with 'pure' ThO_2, are in good agreement with those calculated by the graphical integration of equation (I-3a) with the help of Fig. 1.9.
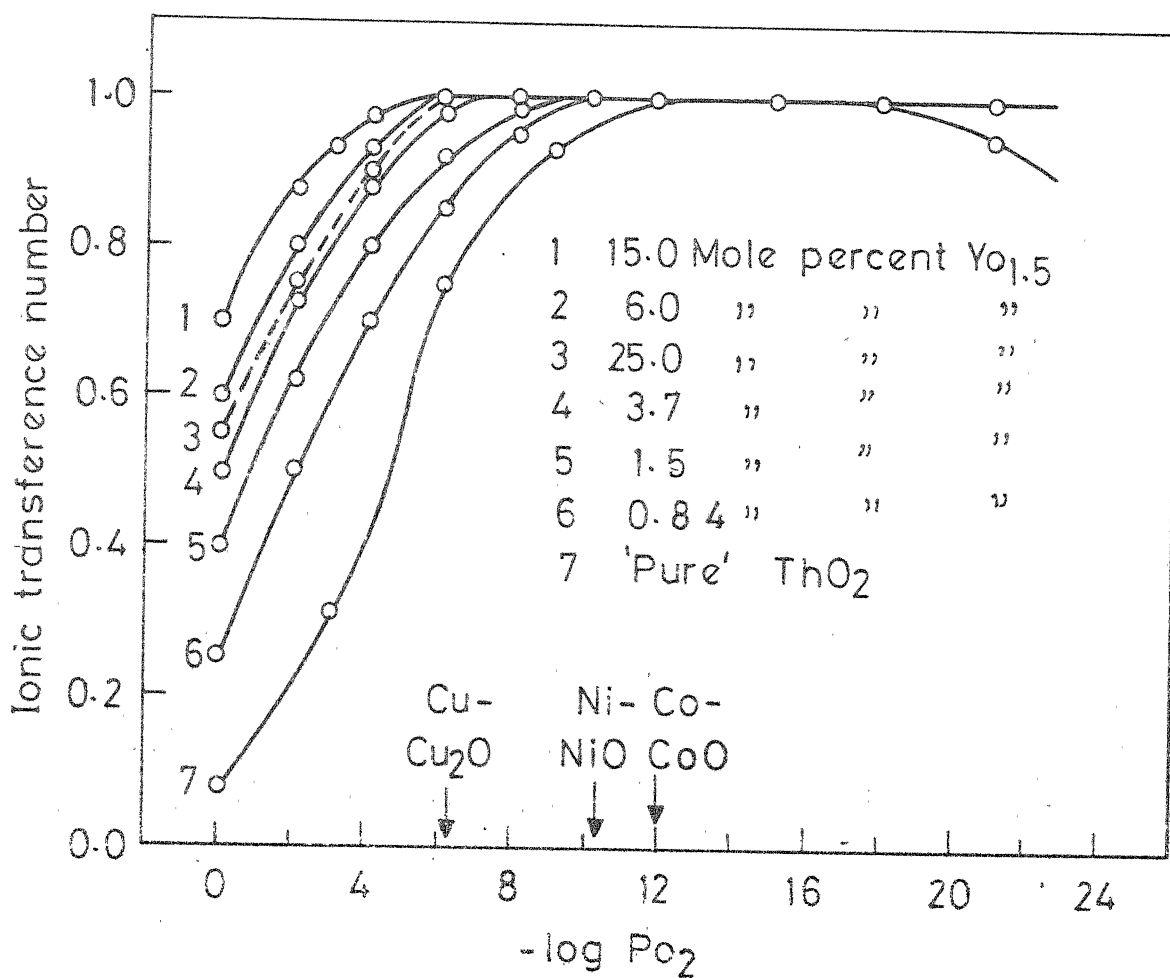
FIG. 1·9   IONIC TRANSFERENCE NUMBER OF ThO_2-$YO_{1.5}$
ELECTROLYTES AS A FUNCTION OF Po_2 AT 1000°C. [52]

It may be pointed out that a significant electronic conduction provides an electrical shunt through the electrolyte and a continuous oxygen transport takes place from the electrode of higher P_{O_2} to that of lower P_{O_2} resulting in a gradual lowering of the cell EMF unless only nonpolarizable electrodes are used. Subbarao et al. [86] calculated the ionic transference number of $ThO_2-YO_{1.5}$ electrolytes as the ratio of measured open circuit EMF to the theoretical EMF corresponding to a fully ionic conductor. These values agree well with those obtained by Lasker and Rapp [52] from the conductivity measurement. Both these investigations provide experimental data for the verification of the dilute solution model developed by Lasker and Rapp [52].

In addition to the conductivity and galvanic cell measurements for the determination of transference numbers, direct measurement of the partial electronic or electron hole contribution in $ThO_{0.85}Y_{0.15}O_{1.925}$ electrolyte has been made by Patterson et al. [51] in the temperature range of $800-1000^{\circ}C$ following Wagner [110] and Hebb's [111] polarization method. The method consists of applying a d.c. EMF across a cell involving a reversible electrode on one side and a nonreversible electrode at the other.

Reversible electrode (Me – MeO)	Electrolyte (oxide)	Non reversible Electrode (Au, Pt)
$X = 0$		$X = L$
+		–

The polarity is chosen such that the conducting ion is attracted towards the reversible electrode which acts as the sink for the ions. Under steady state condition, the ionic current decreases to zero because the nonreversible electrode at $X = L$ is a very poor source of conducting ions. Under this condition, the current (I) consists of only the electronic or electron hole contribution.

$$I_{\infty} = I_h + I_e \qquad (I-58)$$

According to Wagner's [110] theory, local equilibrium exists between the ions, electrons and the neutral species throughout the electrolyte. As has been mentioned earlier, for a doped oxide electrolyte

$$\sigma_h \ \alpha \ P_{O_2}^{1/4} \quad and \quad \sigma_e \ \alpha \ P_{O_2}^{-1/4}$$

and therefore I_{∞} can be calculated by integrating I_h and I_e contributions over the P_{O_2} range of the cell and the resulting expressions

$$I_{\infty} = \frac{RT}{FL} \left\{ \sigma_h^{\ O}[1 - \exp(-u)] + \sigma_e^{\ O}[\exp(u) - 1] \right\} \qquad (I-59)$$

where $\sigma_e^{\ O}$ and $\sigma_h^{\ O}$ are the partial electron and electron hole conductivities at a P_{O_2} of the reversible electrode and $u = |E|F/RT$ where E is the applied EMF.

Patterson et al. [51] have modified Wagner's expression by dividing both sides of equation (I-59) by $[1 - \exp(-u)]$ so that

$$I_\alpha / [1 - \exp(-u)] \;=\; \frac{RT}{FL}[\sigma_h^{\,o} + \sigma_e^{\,o} \exp(u)] \qquad (I-60)$$

A plot of the left hand side of this equation against $\exp(u)$ will yield a slope of $(RT/FL)\,\sigma_e^{\,o}$ and an intercept of $(RT/FL)\,\sigma_h^{\,o}$ and hence the values of $\sigma_h^{\,o}$ and $\sigma_e^{\,o}$ may be derived. The results obtained with $Th_{0.85}Y_{0.15}O_{1.925}$ are shown in Fig. 1.10 along with the total conductivities measured by Lasker and Rapp [52]. The observed P_{O_2} independent σ_e (shunt) was found to be due to some extraneous resistance parallel to the electrode and may be attributed to thermionic emission. Patterson et al. [51] have also estimated the lowest P_{O_2} values for which $t_{ion} > 0.99$ for this electrolyte. The values are $10^{-34.3}$ atm. at $1000^{\circ}C$, $10^{-39.5}$ atm. at $900^{\circ}C$ and $10^{-44.7}$ atm. at $800^{\circ}C$. The complete electrolytic domain of yttria doped thoria electrolytes has been determined [112,113] and the results are shown in Fig. 1.11 along with that of pure thoria and calcia stabilized zirconia.

Aside from the $ThO_2-Y_2O_3$ electrolytes, there are only limited conductivity measurements available on $ThO_2-LaO_{1.5}$ electrolytes. Steele and Alcock [49] reported that the ionic conductivity of $ThO_2-LaO_{1.5}$ electrolytes containing 5-8 m/o La_2O_3 are about 10 percent higher than that of the corresponding $YO_{1.5}$ compositions. Hund [114] has reported a conductivity value of 3.2×10^{-3} σ-cm^{-1} at $1000^{\circ}C$ for ThO_2- 14 m/o La_2O_3. The anion vacancy model has been confirmed
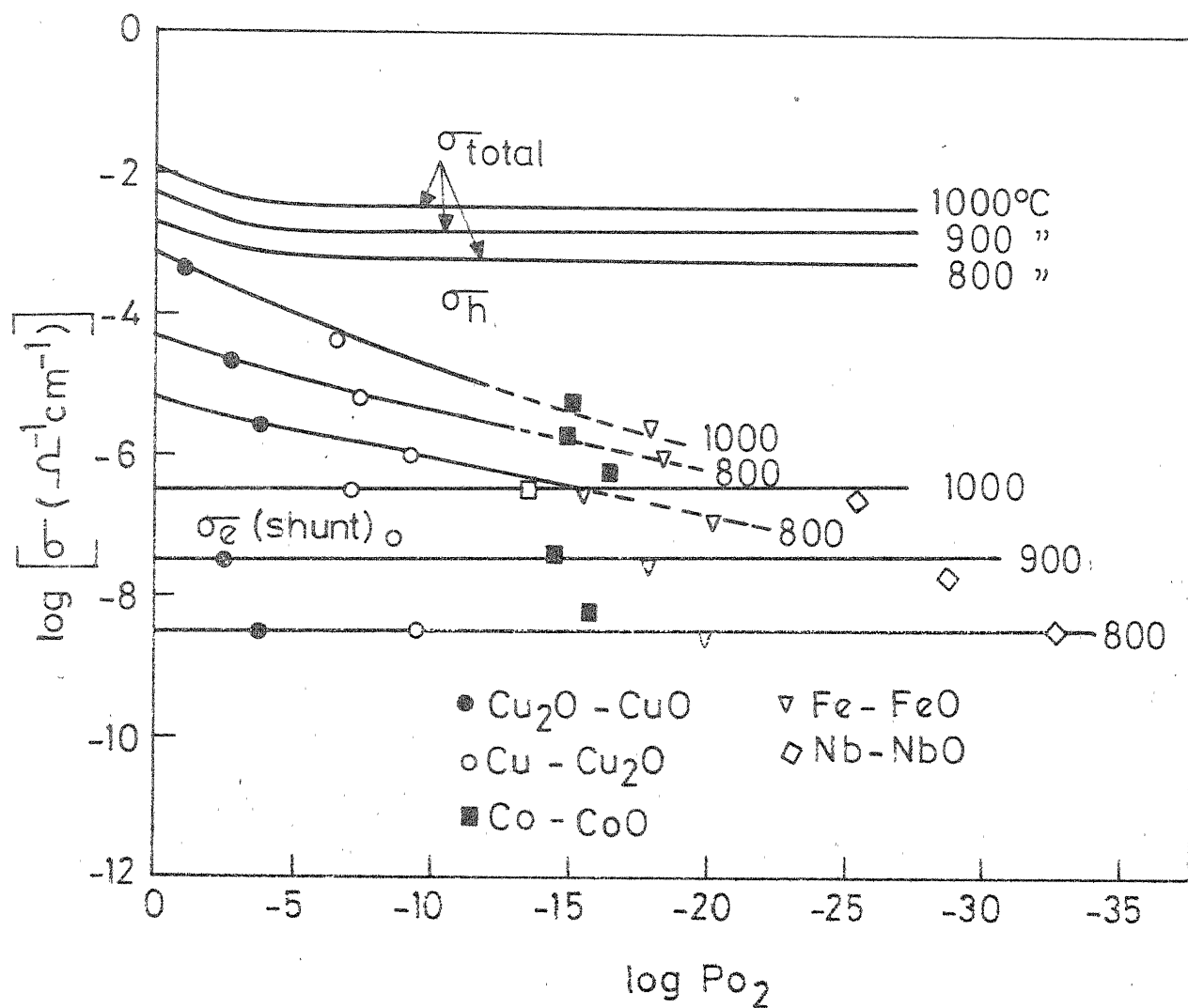
FIG. 1·10   PARTIAL CONDUCTIVITIES IN $Th_{0.85}Y_{0.15}O_{1.925}$ OBTAINED FROM POLARIZATION STUDY [51]

Temerature,°C
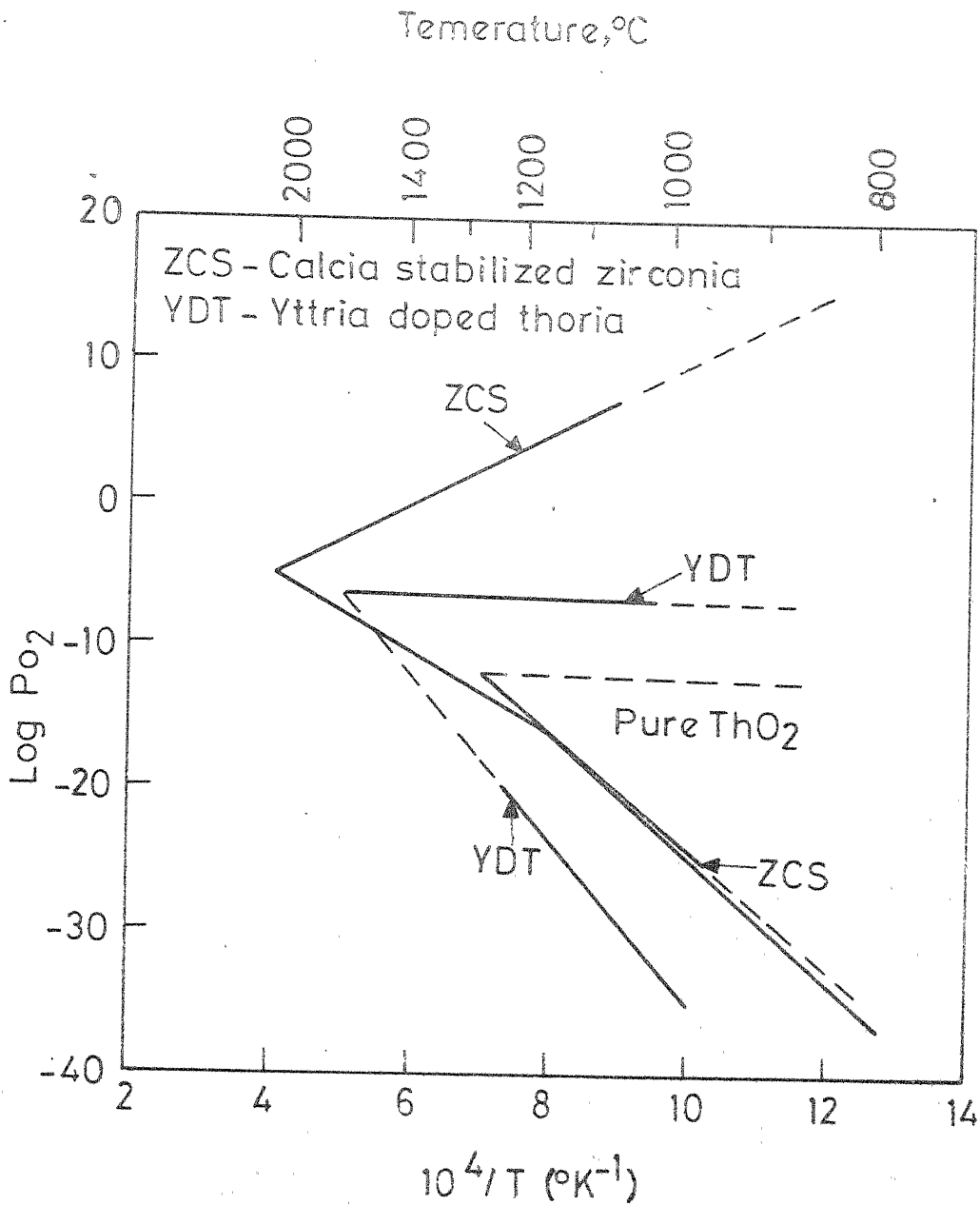
FIG.1·11 ELECTROLYTIC DOMAINS OF VARIOUS ELECTROLYTES
[112]

for $ThO_2-La_2O_3$, $ThO_2-Gd_2O_3$ and $ThO_2-Yb_2O_3$ systems [100].

I-6.2 ThO_2-CaO System

It has been established that calcium oxide which has a NaCl structure, dissolves in ThO_2 to produce a cubic fluorite type solid solution. The ionic sizes for Th^{4+}, Ca^{2+} and O^{2-} in the fluorite lattice are 1.15, 1.10 and 1.27 A^O respectively [72]. Curtis and Johnson [107] have suggested that the maximum solubility of CaO in ThO_2 was at least 12.5 m/o at $1800^O C$ but according to Möbius et al. [72] the solubility is only 8 m/o at $1600^O C$. As has been pointed out earlier, when thoria is doped with CaO, electrical neutrality is maintained by the introduction of O^{2-} vacancies. Wachtman [115] has accounted for the observed internal friction and dielectric loss peak in $ThO_2-1.5$ m/o CaO with a model where by the Ca^{2+} ions are associated with oxygen ion vacancies. The activation energy for the movement of oxygen ions was found to be 0.93 ev. Limited conductivity measurements show that the conductivity values are an order of magnitude lower than the corresponding $ThO_2-Y_2O_3$ compositions and the hole contribution is higher at the same oxygen partial pressure [49] The maximum conductivity seems to occur at 5 m/o CaO and remains constant upto about 15 m/o CaO [49,116]. Ullman [117] has shown that above $1200^O C$ the conductivity was independent

of composition from 0 to 30 m/c CaO and the activation

energy is 2.0 ev compared to that of 0.9 ev below $1200^{o}C$

while Mehrotra et al. [88] have obtained the activation

energies of 1.2 ev below $1100^{o}C$ and 1.0 ev above this

temperature. Such a behaviour was earlier observed in

$ThO_2-Y_2O_3$ solutions.

CHAPTER II

STATEMENT OF THE PROBLEM

As is evident from the discussion presented in the earlier chapter, thoria base materials have been proved to be good solid electrolytes for galvanic cell application in the low oxygen partial pressure range. The defect structure and the electrical properties of pure thoria and yttria doped thoria electrolytes have been extensively studied. Limited experiments carried out with ThO_2-CaO solid solutions indicate their potentialities as good solid electrolytes in the same P_{O_2} range as that of yttria doped thoria electrolytes. However, no detailed and systematic investigation has yet been made on this material and therefore their electrolytic proper-ities are not fully determined.

The present investigation was taken up to make detailed measurements of the electrical properties (electrical conductivity and thermoelectric power) under various experi-mental conditions of temperature, oxygen partial pressure and composition and thereby to ascertain the defect structure as well as to study the electrolytic behaviour of the pure and CaO-doped thoria ceramic electrolytes under these experimental conditions.

Another aim of the study was to determine the characteristics of a solid electrolyte oxygen pump and to test its usefulness in controlling the oxygen activity in a flowing inert gas stream.

CHAPTER III

EXPERIMENTAL PROCEDURE

III-1. SAMPLE PREPARATION

To prepare CaO-doped ThO_2 specimens, reactor grade thorium dioxide (supplied by Indian Rare Earths Ltd., Bombay) and BDH analytical reagent grade calcium carbonate were used as the starting materials. Typical analyses of these materials are given in Table 3.1 and 3.2 respectively. Earlier attempts to coprecipitate oxalates of thorium and calcium from their nitrate solution or to evaporate to dryness the mixture of the same nitrate solution was not successful in this laboratory [118]. Therefore, required quantities of calcined thoria powder and anhydrous calcium carbonate were weighed in a single-pan balance, accurate upto 0.1 mg, and thoroughly mixed under acetone in an agate mortar. The mixing was continued for about an hour. The mixture was dried in an oven at $150^{\circ}C$ and calcined in a platinum crucible at $1100^{\circ}C$ for 3-4 hours. After calcination the powders were pressed into pellets in a 12.5 mm diameter steel die under a pressure of 5 ⊤ bar (~75000 psi) which was applied through a hydraulic press. The pressed pellets were heated at $1400^{\circ}C$ for 2 hours over a platinum foil. To get uniform composition, these pellets were crushed, ground,

Table 3.1

Typical Analysis of Reactor Grade Thorium Dioxide[φ]

Element	Quantity in p.p.m.	Element	Quantity in p.p.m.
Ce	< 0.4	Li	1
Gd	< 0.08	Mn	1
Sm	< 0.2	Ni	4
Er	< 0.2	Mo	< 10
Eu	< 0.08	Pb	< 2
Dy	< 0.2	Sb	< 2
B	0.22	Sn	< 1
Be	< 0.1	V	< 5
Cd	< 0.1	U	1.5
Cu	< 2.0	Sulphate	120
Cr	10	Phosphate	< 25
Fe	90	Ca	< 2000

[φ] Supplied by Indian Rare Earths Ltd., Bombay, India.

Table 3.2

Typical Analysis of Analytical Reagent

Grade Calcium Carbonate[φ]

Impurity	Maximum limits of impurities (percent)
Acid-insoluble matter	0.003
Soluble alkali	0.25 ml N/1
Chloride (Cl)	0.001
Nitrate (NO_3)	0.01
Phosphate (PO_4)	0.001
Silicate (SiO_2)	0.01
Sulphate (SO_4)	0.005
Ba + Sr	0.01
Fe	0.001
Pb	0.001
Mg	0.01
K	0.005
Na	0.02

[φ] Supplied by The British Drug House Ltd., England.

re-mixed and re-pressed either in a 12.5 mm or a 9.5 mm diameter die. The specimens for the conductivity measurement were 2-3 mm thick while those for thermoelectric power measurement were 9.5 mm in diameter and about 1 cm in length. The re-pressed pellets were presintered at $1400^{\circ}C$ for 4 hours and finally fired in a zirconia lined oxy-acetylene gas fired furnace at a temperature of $2000^{\circ}C$ for 4 hours. During firing, the pellets of the same composition were stacked one over the other and placed on a stabilized zirconia setter plate with sufficient amount of powders of the same composition as that of the pellets, in between them to avoid sticking and contamination from the setter plate. After firing, the lower most pellet of each stack was rejected to reduce contamination. The furnace was heated from room temperature to $2000^{\circ}C$ within a time period of 8-10 hours, held there for 4 hours and cooled to $1400^{\circ}C$ within 2 hours after which it was sealed and allowed to cool naturally. The temperature was measured with a Leeds and Northrup optical pyrometer and was controlled within $\pm 10^{\circ}C$ by manual adjustment of the flow rates of the two gases. ThO_2 samples containing 1.0, 2.0, 3.0, 4.0, 5.0, 6.0, 7.0, 10.0 and 15.0 mole percent of CaO were prepared following the above mentioned procedure. Pure ThO_2 samples were also pressed and sintered in the same manner. After firing, the bulk densities of the sintered specimens were measured to calculate the residual porosity.

To measure electrical conductivity as well as thermoelectric power, the flat surfaces of the sintered pellets were ground and polished over different grades of emery paper to remove the surface contaminations as well as to obtain flat and parallel surfaces. The cylindrical surface was ground with a 80 grit diamond file. The flat surfaces of the specimens were finally ground with 120 grit silicon carbide powder so that the platinum electrodes adhere strongly to the pellet. It was earlier observed that the platinum paste did not stick to the smooth and polished surfaces of the specimens. Thin coatings of unfluxed black platinum paste (Engelhard No. 6926) were applied to the ground surfaces of the specimens and they were heated to about $900^{\circ}C$. The process of painting and heating was repeated until electrodes of surface resistance of less than 0.5 ohms were obtained. Normally three coatings were needed to obtain a proper electrode.

III-2. X-RAY STUDIES

X-ray diffraction patterns of the sintered and powdered (-325 mesh) samples were taken on a General Electric XRD-6 diffractometer using the instrument parameters given in Table 3.3.

Table 3.3

Instrument Parameters for X-ray
Diffraction Studies

Radiation	CuK_α
Excitation Voltage	30 KV
X-ray Current	15 mA
Beam Slit	3°
Soller Slit for Incident Beam	Medium Resolution
Soller Slit for Diffracted Beam	Medium and High Resolution
Detector Slit	0.1° and 0.02°
Scanning Speed	2°/min
Chart Speed	1"/min
Time Constant	1 sec. to 2 sec.

Fig. 3.1:   Alumina Tube Specimen Holder.

Brass rod
'O' Ring seals

Gas outlet ◄

Brass fork to
hold the alumina tube.

Gas inlet

Brass tube

Stainless steel rod

Stabilized zirconia tube

Alumina sheath
for gas outlet

Alumina pressing rod

Alumina tube

Sample

Platinum electrode
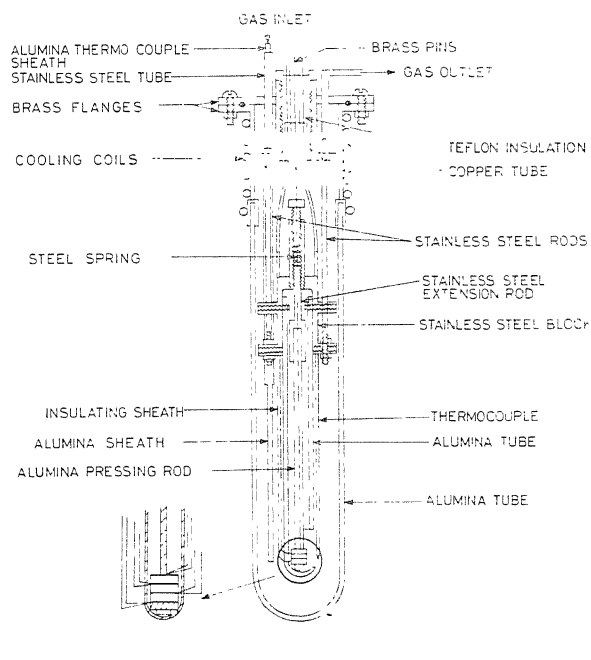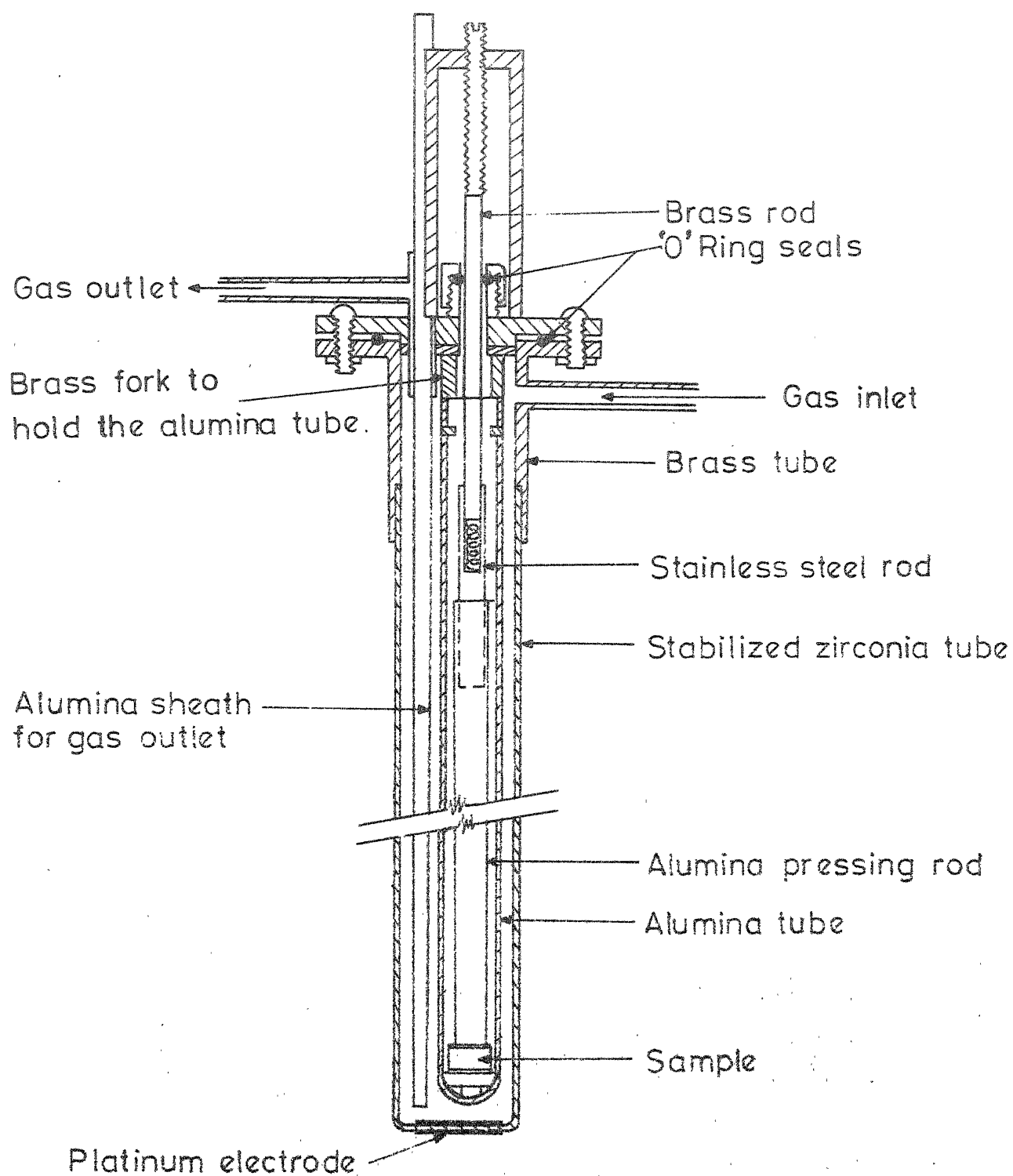
FIG. 3.2 ZIRCONIA TUBE SPECIMEN HOLDER.

and through teflon insulation in the cold area. Two platinum
leads were attached to each surface of the specimen so that
two probe as well as four probe measurements could be done
with the same set up. For attaching the leads to the
platinum electrodes on the specimen surface, the ends of the
two lead wires were welded in a flame and flattened in the
form of a foil which was pressed against the specimen
surfaces. In both the specimen holders 'O' ring seals were
used between the two parts of the brass flanges and the gas
inlet was through an alumina thermocouple sheath.

The zirconia tube specimen holder had the
advantage that a part of the tube could be used in forming
an electrochemical cell to measure the oxygen partial pressure
prevailing inside the holder. For that, the inside and the
outside surfaces of the flat bottom of the zirconia tube were
painted with platinum paste and the EMF developed across the
oxygen concentration cell, utilizing air as the reference,
was measured with a high impedance electrometer. However,
as will be discussed later (Chapter IV) the leak rate of
oxygen through the zirconia tube increases very fast with
increasing temperature and hence this holder could not be
used above $900^{\circ}C$ except for the measurements in air atmosphere.
The alumina tube sample holder has been used for constant
partial pressure measurements over the temperature range of
$600-1400^{\circ}C$ as well as for high temperature isothermal

measurements with varying oxygen partial pressure. For that
purpose, the oxygen partial pressure of the incoming gas was
measured before it entered the specimen holder, by passing
the gas through a hot zirconia tube fitted with two platinum
electrodes and measuring the EMF of the cell thus formed.

The a.c. conductance of the specimens was
measured with a General Radio 1608-A type impedance bridge
with an internal frequency of 1 KHz. It was found that at
low temperatures where the sample resistances were quite high,
the platinum lead resistances could be neglected and the two
probe bridge method which has been used frequently in earlier
investigations, gave quite accurate results. However, at
higher temperatures, the sample resistances became very low
and were comparable to the increased value of the lead
resistances. Therefore it was necessary to eliminate the
lead resistances for accurate measurement of the sample
conductance and a technique similar to that of four probe
measurement was used. For that purpose two of the four
leads attached to the two surfaces of the specimen were used
to apply an a.c. voltage of a frequency 1 KHz. The remaining
leads were utilized for the measurement of potential drop
across the specimen with an a.c. V.T.V.M. (internal impedance
1 MΩ). The current through the specimen was determined by
measuring the potential drop across a standard resistance
placed in series with the specimen. In Fig. 3.3 a comparison
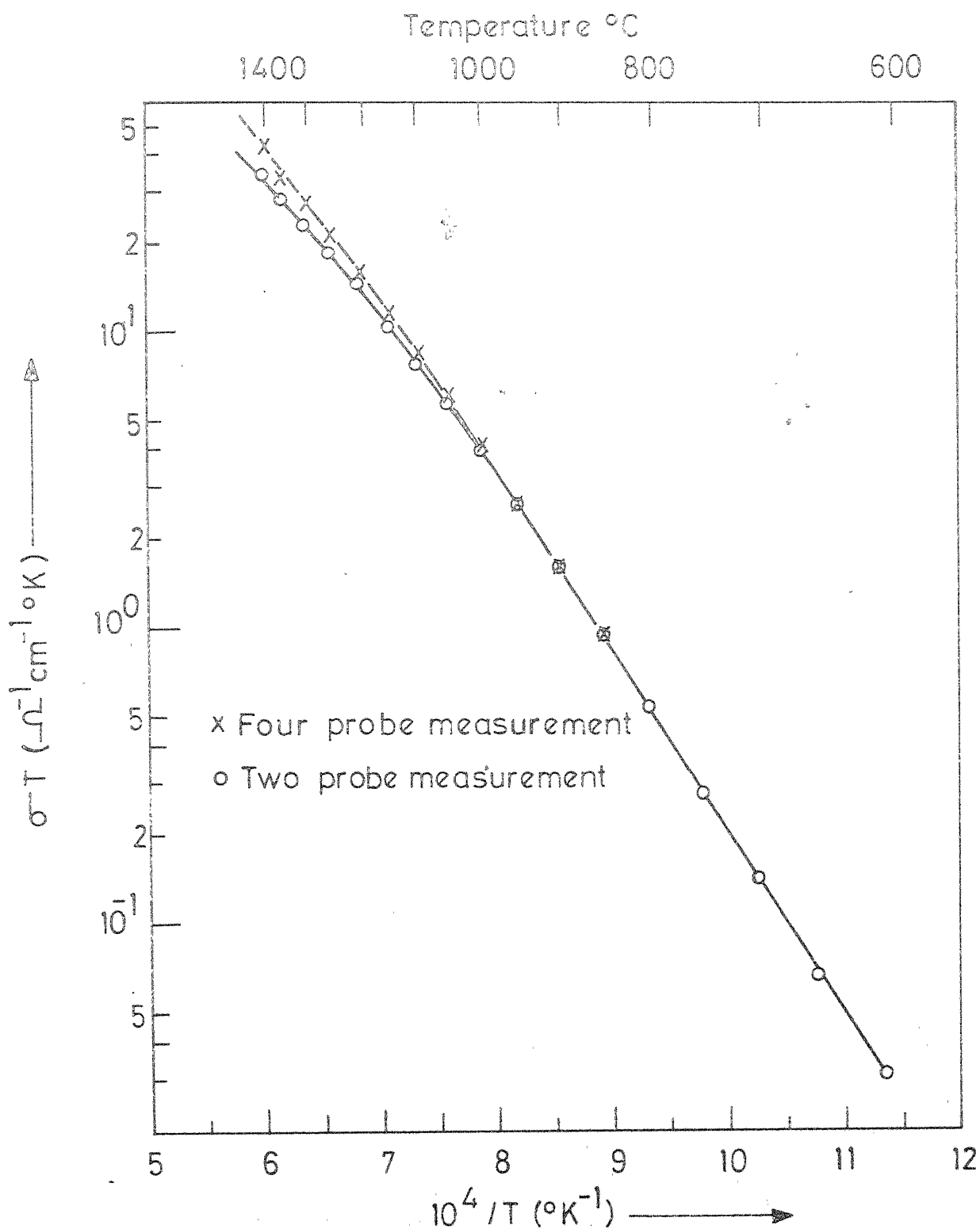
FIG. 3·3   Log σT VS. 1/T PLOT FOR 3 MOLE % CaO DOPED ThO$_2$ SAMPLE MEASURED IN AIR BY TWO DIFFERENT TECHNIQUES.

of the results by these two techniques has been made. It may be noted that above 1000°C the measurement by the two probe technique resulted in an increasingly lower conductivity than that by the four probe method. Therefore in the present investigation the two probe method was used only in the low temperature range while the four probe method was adopted at higher temperatures. In practice, the conductance of the specimens at each temperature above 900°C was measured by both the techniques but the values obtained by the two probe method were not considered if they were lower than those obtained by four probe method.

The specimen holders were heated inside a resistance heating furnace and the temperature was controlled within ± 0.5°C by a Leeds and Northrup Electromax type temperature controller. The exact temperature of the specimen was measured by a Pt/Pt-10% Rh thermocouple kept very close to the specimen and the EMF was measured by a Leeds and Northrup K-3 potentiometer. The technique used for the control of oxygen partial pressure within the specimen holder is discussed in the next chapter.

To obtain better electrical contacts between the platinum electrodes and the lead wires, freshly loaded samples were first heated directly to 1400°C so that the lead wires became welded to the electrodes. At each temperature and partial pressure sufficient time was allowed for equilibration.

When the conductivity values for two consecutive readings
at an interval of one hour remained unchanged, equilibrium
was assumed to have been attained.

III-4.   MEASUREMENT OF THERMOELECTRIC POWER

Thermoelectric power measurements were carried
out in the alumina tube specimen holder under various oxygen
partial pressures and temperatures. Sintered specimens of
9 mm diameter and about 1 cm in length were used for the
purpose. Electroded specimens were kept pressed against
the bottom of the inner alumina tube by means of the spring
loaded alumina rod. To maintain the necessary temperature
gradient, a small platinum resistance heater was wound over
the alumina pressing rod just above the specimen surface.
A d.c. voltage was applied to the heater from a constant
current d.c. power supply (Harrison 6201B). The temperature
gradient was varied by changing the current through the
heater. The temperature of the specimen surfaces were
measured by two Pt/Pt-10% Rh thermocouples, the tips of
which were kept pressed against the surfaces of the specimen.
A Leeds and Northrup K-3 potentiometer was used to measure
the thermocouple EMFs. The EMF developed across the
specimen was measured by using the platinum leads of the
thermocouples and a Phillips d.c. micro voltmeter having an
interval impedance of 100 MΩ. The furnace temperature and

the oxygen partial pressure within the specimen holder were
controlled in the same manner as that used during the
conductivity measurement. At a fixed P_{O_2} and furnace
temperature, the thermal EMFs were measured corresponding to
different temperature gradients of upto $15^{\circ}C$ and the Seebeck
coefficient was calculated as the slope of the straight line
obtained by plotting the EMF against temperature gradient.
The sign of the Seebeck coefficient was determined from the
polarity of the cold end of the specimen. Using this
convention the sign of the coefficient was the same as that
of the charge carrier.

III-5. SPECIMEN PREPARATION FOR METALLOGRAPHIC OBSERVATION

Sintered specimens were first ground over v
belt grinders of 1/0, 2/0 and 4/0 grades followed by emery
papers of 3/0 and 4/0 grades. The ground specimens were
polished over polishing wheels initially with 15 μ and 5 μ
alumina powders and finally with 1 μ diamond paste. The
specimens were etched with boiling orthophosphoric acid for
20-30 seconds.

CHAPTER IV

CONTROL AND MEASUREMENT OF OXYGEN ACTIVITY BY
ELECTROCHEMICAL OXYGEN PUMP AND PROBE

It is customary to maintain oxygen partial pressure of a gaseous system at a desired level either with an inert gas-oxygen mixture or through thermodynamic equilibrium in reactive gas mixtures like H_2-H_2O or CO-CO_2. These processes become cumbersome especially as they require accurate control of gas flow rates. In the present investigation an attempt has been made to control the oxygen activity inside the specimen holder by an electrochemical method using an oxygen ion conducting solid electrolyte (calcia stabilized zirconia).

Stabilized zirconia has been used as a solid electrolyte to form the galvanic cells of the following type with porous platinum electrodes.

$$P'_{O_2}, \; Pt/\underset{zirconia}{Stabilized}/Pt, \; P''_{O_2}$$
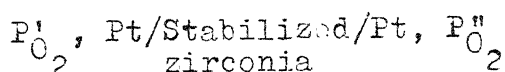
where $P'_{O_2} < P''_{O_2}$

On maintaining two different oxygen partial pressures which are within the range of predominant ionic conduction ($t_{ion} = 1$), on the two sides of the electrolyte, an open circuit EMF (E_{open}) is developed which is given by

$$E_{open} = \frac{RT}{4F} \ln \frac{P_{O_2}''}{P_{O_2}'} \tag{IV-1}$$

Such cells can be used as fuel cells as well as to measure the oxygen partial pressure in an unknown system with reference to a known P_{O_2} (e.g. air with $P_{O_2} = 0.21$ atm.). On the other hand if an external voltage (V) is applied to the cell, essentially all of the current flowing through the electrolyte is carried by the oxygen ions from the cathode to the anode while in the external circuit the current corresponds to the transport of electron again from the cathode to the anode. The electrode reaction at the cathode may be represented as

$$\tfrac{1}{2} O_2(g) + 2e' + V_O^{\cdot\cdot} \rightarrow O_o \tag{IV-2}$$

The reaction proceeds in the reverse direction at the anode.

In cases where the electrolyte shows a small amount of electronic conduction, the EMF arises as a consequence of the simultaneous migration of ionic and electronic defects. Under the open circuit condition, the total current carried by the defects is zero and therefore

$$J = J_e + J_i = 0$$

or

$$J_e = - J_i \neq 0 \quad at \quad V = E_{open}$$

where J is the current density. E_{open} under this condition
is given by

$$E_{open} = \frac{RT}{4F} t_{ion} \ln \frac{P_{O_2}''}{P_{O_2}'} \qquad (IV-3)$$

The ionic or the electronic current may be stopped by the
application of an external voltage given by

$$E_{stop} = \frac{RT}{4F} \ln \frac{P_{O_2}''}{P_{O_2}'} \qquad (IV-4)$$

Since, $t_{ion} \leqslant 1$, comparing equations (IV-3) and (IV-4) one gets

$$E_{stop} \geqslant E_{open}$$

Application of a voltage higher than E_{open} (for $t_{ion} \leqslant 1$)
causes transport of oxygen from one electrode to the other
depending upon the sign and magnitude of the net voltage
across the electrolyte and the phenomenon has been termed as
'Oxygen pumping'. The rate of oxygen transport is determined
by the ionic conductance of the electrolyte, area of the
electrodes and the magnitude of voltage loss (E_p) due to
polarization at the electrodes. The pumping rate is directly
proportional to the ionic current passing through the electroly
and is given by

$$I_{pump} = \frac{V - E_{stop} - E_p}{R_{pump}}$$

where R_{pump} is the net resistance of the pumping cell.

Earlier, Kröger and his co-workers [41,119,120] have pointed out the use of calcia stabilized zirconia as an oxygen pump. Yuan and Kröger [41] have used a stabilized zirconia tube to pump residual oxygen from a streaming mixture of nitrogen and oxygen and also measured the oxygen content of the purified gas after pumping. Recently Agrawal et al. [44] have used a modified electrode arrangement along with an electronic feedback control system to keep the oxygen content in a flowing Argon gas to a desired level.

A schematic diagram of the oxygen pump used in the present investigation is shown in Fig. 4.1. The stabilized zirconia tube (obtained from Zirconium Corporation of America) used for the purpose, was of 22 mm I.D., 27 mm O.D., 45.7 mm in length and was closed at one end. Platinum paint electrodes were applied to the tube surfaces following the procedure described previously (Section III-1). In the present investigation, four different electrodes, two for the pumping cell and two for the measuring cell, were used for the experiment. The flat bottom of the electrolyte tube was used to form the measuring cell while the side wall was used for the oxygen pump. The pumping electrodes were 18 cm long and were at a distance of 5 cm from the bottom of the tube. Argon gas direct from the cylinder, was introduced at the top of the electrolyte tube with a flow rate of 0.5 to 1.0 c.c./sec.
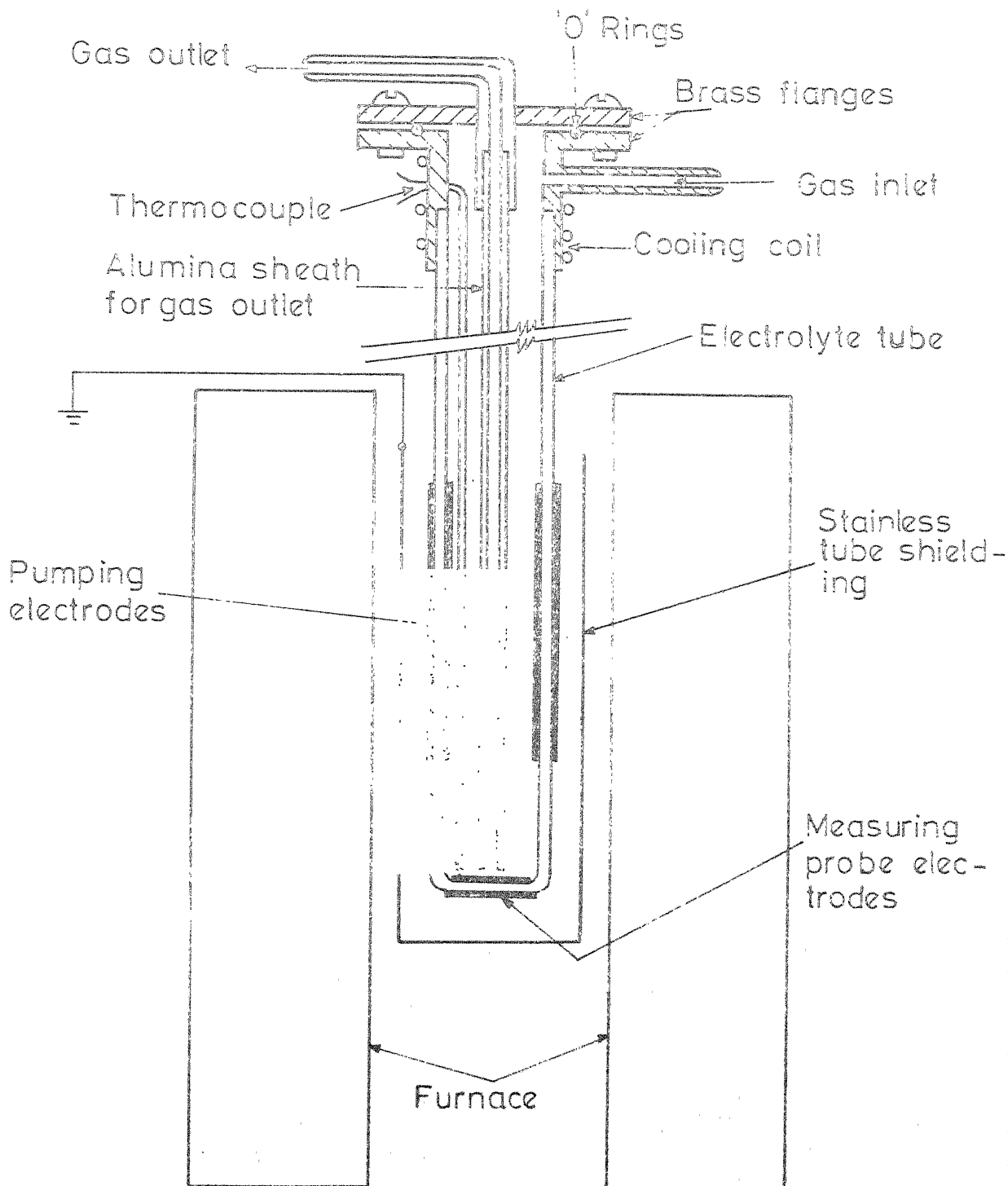
FIG. 4·1   STABILIZED ZIRCONIA OXYGEN PUMP

The oxygen content of the gas was controlled by the application of a suitable d.c. voltage from a constant voltage power supply unit (Harrison 6201B). The final oxygen content of the gas was measured by the measuring cell electrodes using air (out side the tube) as the reference. The gas was taken out through a recrystallized alumina thermocouple sheath the receiving end of which was kept at a distance of 5 mm from the measuring electrode. The oxygen content of Argon gas is reduced when the inner pumping electrode is used as the cathode and the phenomenon may be termed as 'pumping out'. On the other hand by reversing the polarities of the applied voltage the oxygen content of the gas is increased and it may be termed as 'pumping in'. To measure the exact temperature of the oxygen probe, a Pt/Pt-10% Rh thermocouple tip was welded to the inner electrode and the EMF was measured with a Leeds and Northrup K-3 potentiometer. The platinum lead of the thermocouple was used to measure the EMF across the measuring probe with the help of a Phillips d.c. microvolt meter, having an internal impedance of 100 MΩ. The electrolyte tube was heated inside a kanthal wire wound resistance furnace. The temperature at the centre of the pumping electrode was about 100°C higher than that of the probe. Temperature of the furnace was controlled within $\pm$ 1°C by a Leeds and Northrup Electromax type temperature controller.

Yuan and Kröger [41] earlier used a three electrode system in which the inside electrode was made common to both the pump and the probe and two separate electrodes were made on the outside of the tube. It may be pointed out that such an arrangement gives rise to an erroneous probe EMF.

In the present investigation a four electrode system was used in which both the pump and the probe electrodes were electrically separated by bare areas of the electrolyte tube. Such an arrangement has been recently used by Agrawal et al. [44]. To see the effect of a common cathode during the 'pumping out' operation, the lead wires from the pump and the probe cathodes were shorted externally and it was observed that there was an immediate increase in the probe EMF followed by a slow rise to a steady state value which was slightly lower than the applied pump voltage. On the other hand, no change in the probe EMF was observed when the anode of the pump and the probe were shorted. It may be mentioned that on shorting the inner electrodes, the cathodes of the pump and the probe were at the same potential with respect to the pump anode. Thus the probe cathode also started functioning as an extension of the pump cathode and inspite of the complicated cell configuration (Fig. 4.2) small amount of oxygen transport took place from the probe cathode to the pump anode giving rise to polarization effect and
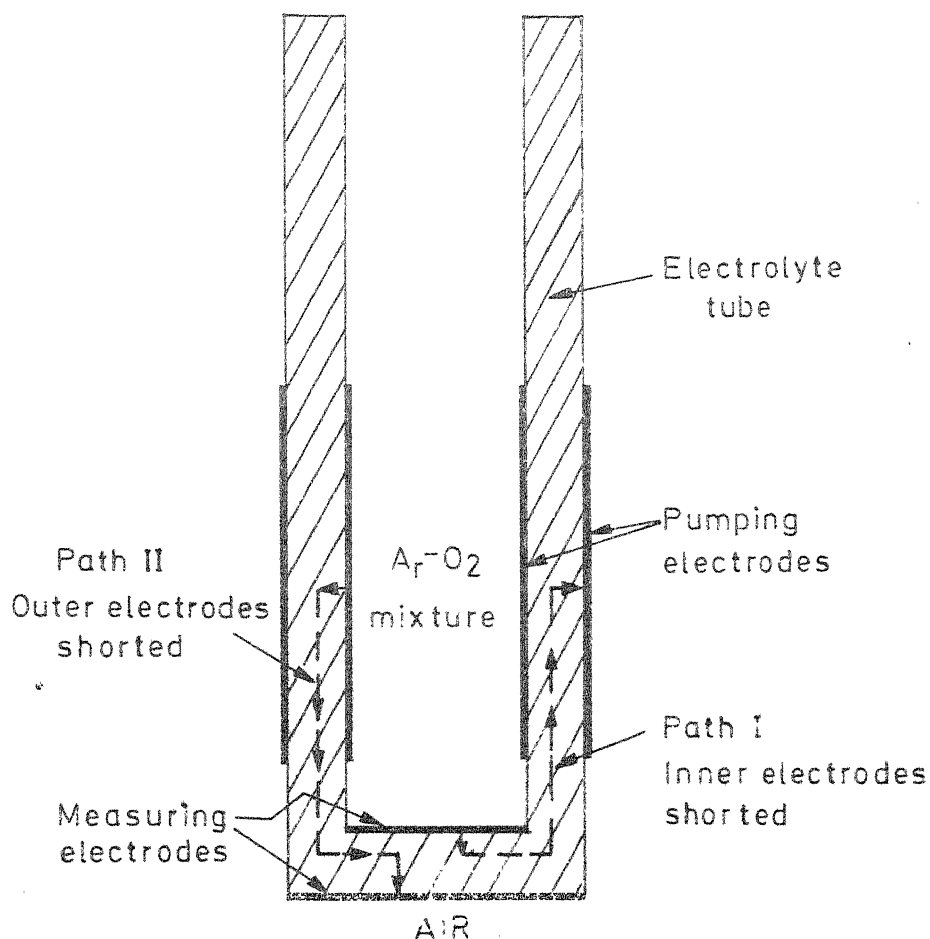
Fig. 4.2   Flow of oxygen when the pumping
and measuring electrodes are shorted

resulting in a lower partial pressure at the electrolyte-electrode interface of the probe cathode. The indicating equipment of the probe under this condition, measured a quantity equal to the sum of the correct probe EMF and the cathodic over potential at the probe cathode. With shorted outer electrodes, the probe anode acted as the extension of the pump anode (Fig. 4.2). Since the probe anode was in contact with the reversible air electrode which did not lead to any polarization effect, eventhough there was a small amount of current flow from the probe anode to the pump cathode, the probe EMF remained unchanged under this condition.

To investigate the possibility of controlling the oxygen partial pressure to a desired level in a flowing Argon-oxygen mixture with the help of this electrochemical pump, its characteristics were studied under different experimental conditions. The EMF, which is a measure of the oxygen content of the flowing gas, was measured as a function of applied voltage under a constant gas flow rate at different pump and probe temperatures. The current flowing through the pumping cell was also determined and the pumping cell resistance was calculated. The results are shown in Figs. 4.3 and 4.4 corresponding to probe temperatures of 700°C and 800°C respectively. It may be observed that the pump characteristics are identical for both these
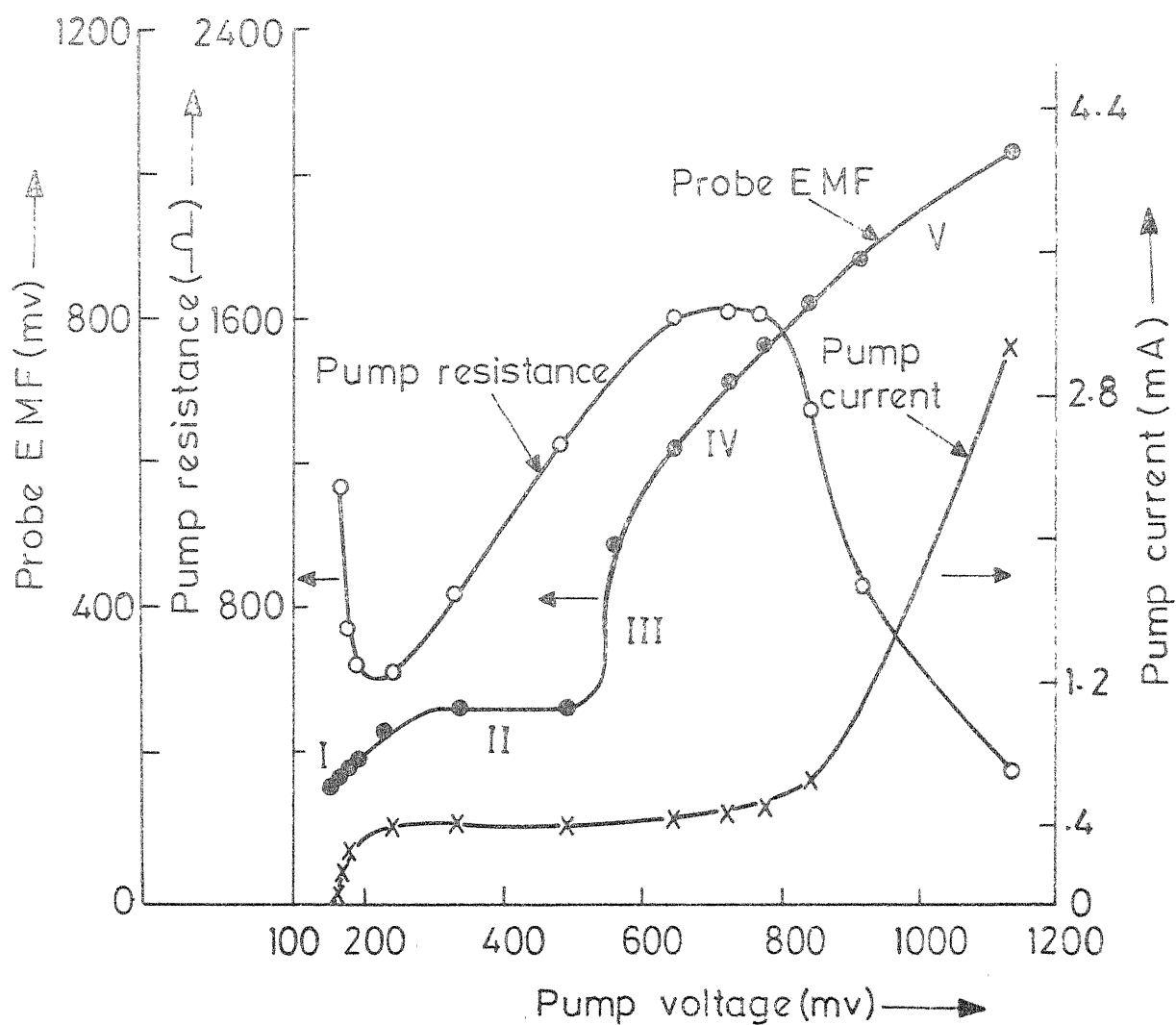
FIG. 4·3   PUMP AND PROBE CHARACTERISTICS AT A PROBE
TEMPERATURE OF 700 °C
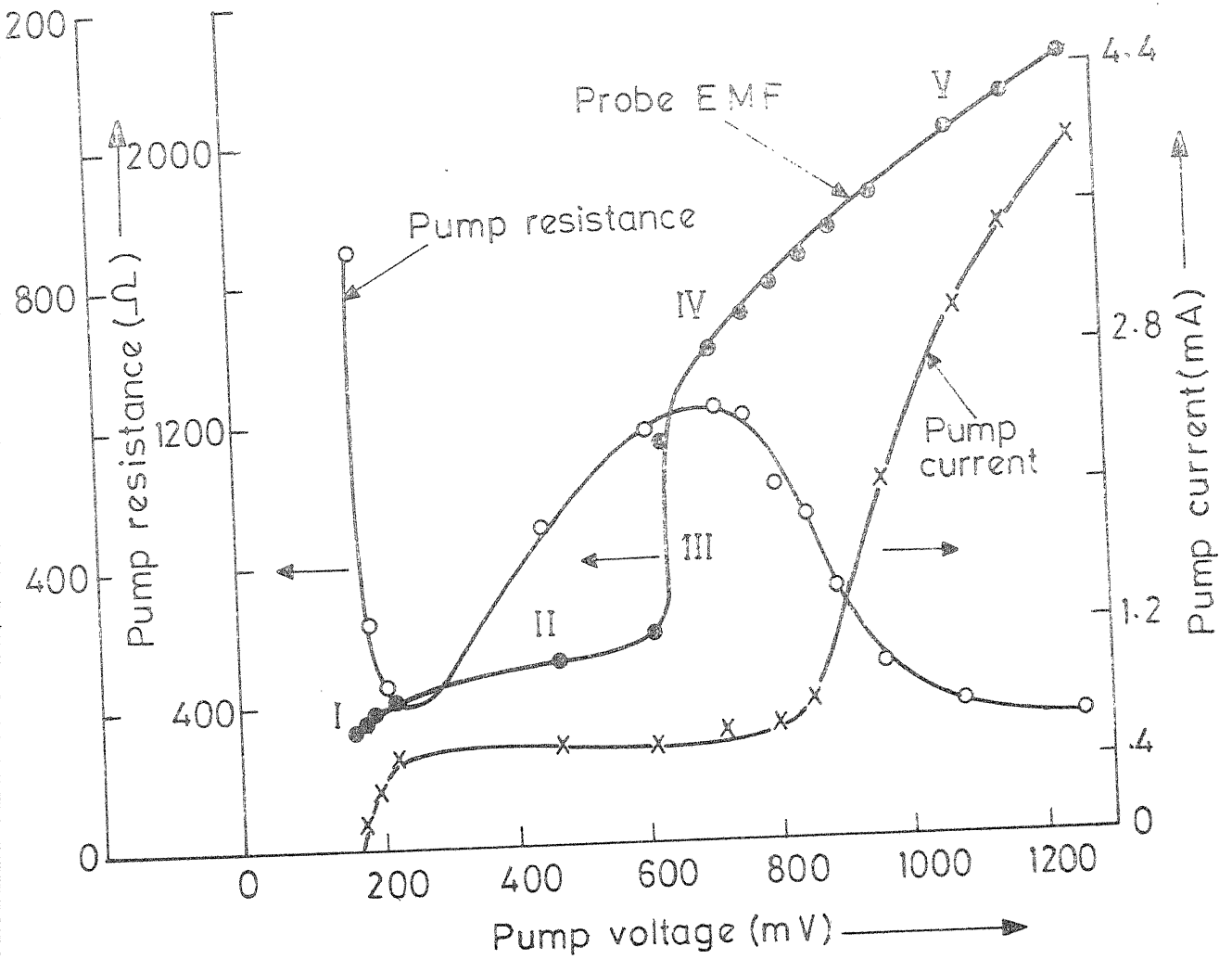
FIG. 4.4   PUMP AND PROBE CHARACTERISTICS AT A PROBE TEMPERATURE OF 800°C

temperatures. At a very low applied voltage (region I)
there is an increase in the probe EMF value with increasing
voltage, indicating a gradual removal of oxygen from the
gas phase. In region II, the resistance of the cell
increases while the pumping current as well as the probe
EMF remain almost unchanged. This is followed by a sudden
rise in the EMF value (region III) within an extremely
narrow range of applied voltage. Beyond this voltage range,
the current continues to remain constant but the probe EMF
increases in a gradual manner and the resistance goes through
a peak (region IV). When the probe EMF becomes quite high
indicating a very low oxygen content in the flowing gas.,
the resistance of the cell starts decreasing (region V) and
as a result the pumping current increases rapidly while the
probe EMF continues to increase at almost the same rate as
in region IV. Similar characteristics of an oxygen pump have
also been observed by Agrawal et al. [44]. The oxygen
partial pressure of the gas inside the pumping tube, fed
directly from the cylinder was measured with the measuring
probe and was found to be 1.0×10^{-4} atm. and 2.0×10^{-4} atm.
at the probe temperatures of $700^{\circ}C$ and $800^{\circ}C$ respectively.
With 3.0 mA of pumping current, the partial pressure went
down to 6×10^{-23} atm. at a probe temperature of $700^{\circ}C$ and
3×10^{-20} atm. at $800^{\circ}C$. The results suggest that the
extent of purification that could be achieved by this technique

was dependent upon the temperature of the pump and the probe. To verify the effect of temperature, the cylinder gas was passed through the zirconia tube kept at different temperatures and the oxygen content inside the tube was measured by the measuring probe under a constant gas flow rate. The results are shown in Fig. 4.5 in which the probe EMF is plotted against temperature. At lower temperatures, the EMF value, as expected from equation (IV-1), increased with temperature. However, with further increase of temperature the curve goes through a peak at about $850^{o}C$ followed by a sharp fall at higher temperature. The lowering of the probe EMF should be interpreted as an increase in the oxygen content of the gaseous atmosphere prevailing inside the tube and may be due to an increased rate of oxygen leakage through the electrolyte tube at these temperatures. In this respect it may be pointed out that the gas flow rate has also an important role in maintaining the oxygen content of the incoming gas. The effect of gas flow rate on the probe EMF is shown in Fig. 4.6. With reduced gas flow rates the probe EMF is decreased due to an increase of oxygen partial pressure of the inside gas. Etsell and Flengas [121] earlier observed that at a fixed temperature the probe EMF increased with increasing gas flow rate and reached an asymptotic value which corresponded to the initial oxygen content of the Argon gas. The effect of
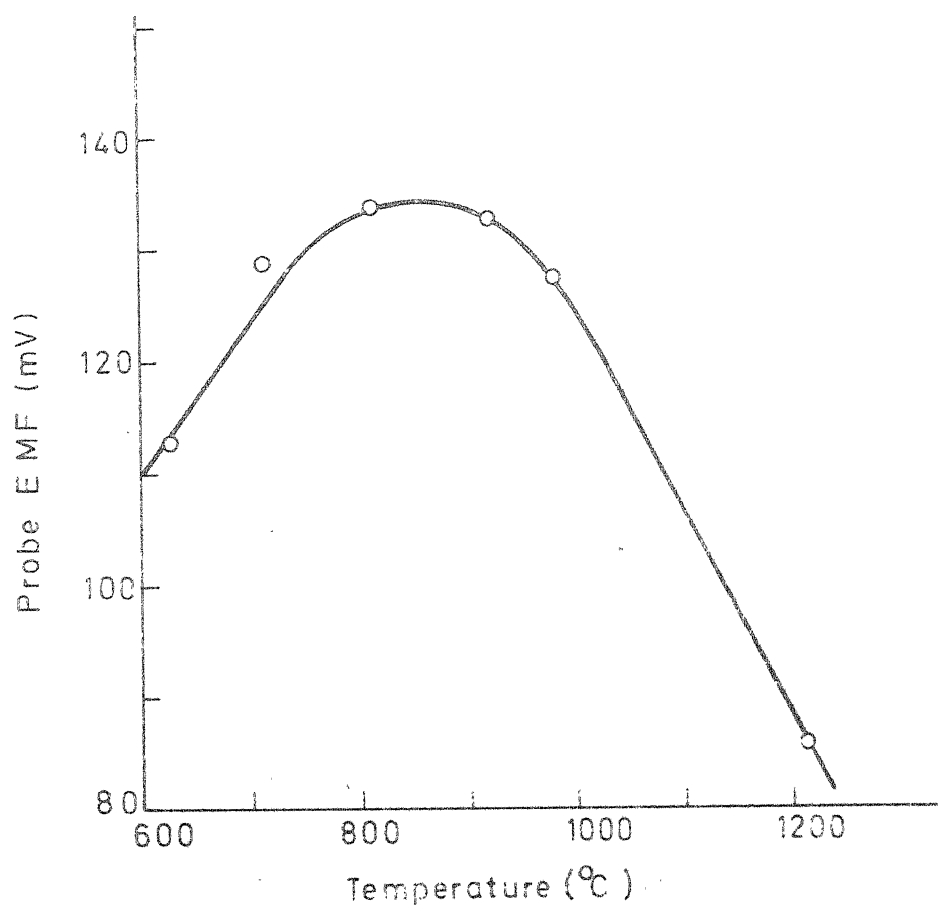
Fig. 4.5 Effect of temperature on the probe
E.M.F at a constant gas flow rate
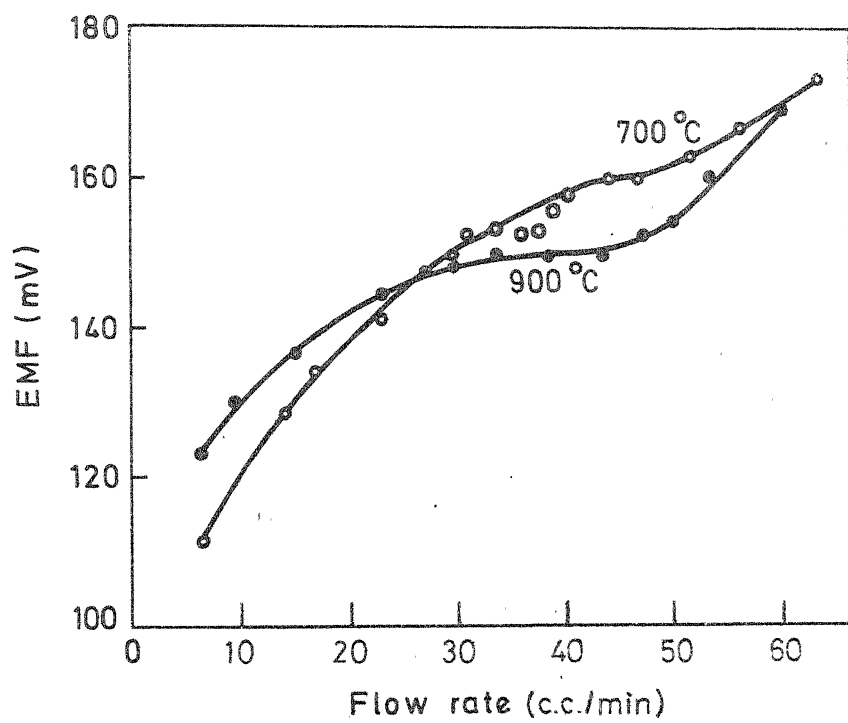
FIG. 4.6 Effect of gas flow rate on the
Probe. EMF.

gas flow rate was more prominent for gases with very low initial oxygen content. It has been mentioned [121,122] that the change in the probe EMF was due to the polarization effect at the electrode electrolyte interface resulting from a small amount of electronic current through the electrolyte and therefore the question may be raised whether at a lower flow rate the measured probe EMF corresponds to the average oxygen content inside the tube. However, in the present investigation an indirect evidence of the change in average oxygen content of the inside atmosphere with the gas flow rate, has been obtained by measuring the conductivity of some ThO_2-CaO specimens as a function of gas flow rate within the zirconia tube specimen holder. The results are shown in Table 4.1. At higher flow rates the conductivity of the sample was decreased indicating lower oxygen partial pressures inside the tube.

The leakage of oxygen may be either due to a small electronic conductivity in the solid electrolyte or due to molecular diffusion through the fine pores in the ceramic tube. However recent experiments [42,43] performed under ultra high vacuum and the gas analysis by mass spectrometer showed that the oxygen content inside a hot zirconia tube was increased due to the oxygen leak through the tube, but there was no change of the nitrogen concentration. This may be an indication that the leakage is mainly due to the

Table 4.1

Effect of Flow Rate on the Conductivity Measured in the Zirconia Tube Specimen Holder

Flow rate c.c./min	P_{O_2} measured by probe at $800^{\circ}C$ (Atm.)	Conductivity of 99% ThO_2 - 1% CaO specimen ($\mu\,\text{v}$)
80	$10^{-4.39}$	31.28
50	$10^{-4.22}$	32.56
15	$10^{-3.74}$	39.08
5	$10^{-3.23}$	46.42

electronic conductivity. Mogab [43] has calculated the effect of oxygen leak due to the electronic conductivity on the probe EMF and found that it becomes important below 10^{-7} torr of oxygen partial pressure.

The shape of the curve of pumping current vs pumping voltage shown in Fig. 4.3 and 4.4 qualitatively represents the polarization behaviour observed by earlier investigators [119,120]. However, any quantitative explanation becomes difficult at this stage because the oxygen partial pressure and the temperature are not uniform throughout the length of the pumping electrodes. From the probe EMF vs voltage plot, it may be suggested that in region III where the oxygen content of the gas mixture changes drastically with an insignificant change in the pumping voltage, the control of oxygen partial pressure of the flowing gas at a desired level becomes impossible. The extent of P_{O_2} jump in this region is from 5×10^{-7} atm. to 1×10^{-12} atm. and therefore the conductivity of the ThO_2-CaO specimens could not be measured with certainty within this P_{O_2} range. To obtain oxygen partial pressure higher than that of cylinder Argon, oxygen was pumped in to the tube by reversing the polarity of the applied voltage. The highest value of oxygen partial pressure obtained was of the order of 10^{-3} atm.

Experiments were carried out to test the efficiency of transferring the purified Argon gas from the

oxygen pump to the specimen holders and also to find out the oxygen leak rate through the alumina or the zirconia tube of the specimen holders. For this, Argon gas, from cylinder, was passed through the zirconia tube specimen holder kept at $700^{\circ}C$, at a constant flow rate of 40 c.c./min. and the oxygen content inside the tube was measured by the measuring probe. In a separate experiment, the gas was passed through the alumina tube specimen holder before introducing into the zirconia tube, keeping the temperature and the gas flow rate at the same level as that of the earlier experiment. The temperature of the alumina tube was slowly raised from room temperature to $1400^{\circ}C$ and the oxygen content inside the zirconia tube was measured with a constant measuring probe temperature. The results are shown in Table 4.2. At lower temperatures, the EMFs measured during both the experiments are equal but at higher temperatures, there is a gradual lowering of the EMF value indicating slow oxygen diffusion through the alumina tube. However the change in the oxygen partial pressure is not significant and may be neglected for most purposes. From this experiment it may be concluded that the leakage through the alumina tube or in the gas transfer line is not significant in this partial pressure range.

To test the behaviour of the zirconia tube specimen holder, the oxygen pump was connected in series

Table 4.2

Experiments to Test the Leak Rate in the Alumina Tube

(1)   Argon from cylinder ⟶ Zirconia tube specimen holder at 700°C

Probe temperature   –   700°C

Gas flow rate   –   40 c.c./min

Probe EMF   –   150 mV.

(2)   Argon from cylinder ⟶ Alumina tube specimen holder ⟶ Zirconia tube specimen holder at 700°C

Alumina tube temperature (°C)	Probe EMF at 700°C (mV)	$-\log P_{O_2}$ (atm.)
R.T.	150	3.78
300	150	3.78
600	150	3.78
800	150	3.78
1000	148	3.74
1100	148	3.74
1200	148	3.74
1300	144	3.66
1400	140	3.58

with the holder and purified Argon gas from the pump was passed through it. The probe temperature in both the tubes were kept at $700^{\circ}C$ and the EMFs across both the probes were measured as a function of pumping voltage. The results are shown in Fig. 4.7 in which the EMF values corresponding to the two probes are plotted against the pumping voltage. It may be observed that at low voltages when the oxygen partial pressure inside both the tubes is high, the differences between the two values are small. However, the difference becomes quite large in the range where there is a sudden rise in the EMF value with an insignificant change in pumping voltage. The probe EMFs become closer again at very low oxygen partial pressures corresponding to regions IV and V of Figs. 4.3 and 4.4. The oxygen partial pressure inside specimen holder is always more than that at the pumping tube. However, the difference is comparatively smaller except in the range corresponding to the region III in Figs. 4.3 and 4.4. The difference between the two readings is attributed mainly to the oxygen leakage through the specimen holder tube. Since the transition from the high P_{O_2} to low P_{O_2} does not take place at the same pumping voltage it may be concluded that the effect corresponds to a particular oxygen partial pressure rather than a pumping voltage. However no satisfactory explanation of this effect is available at present.
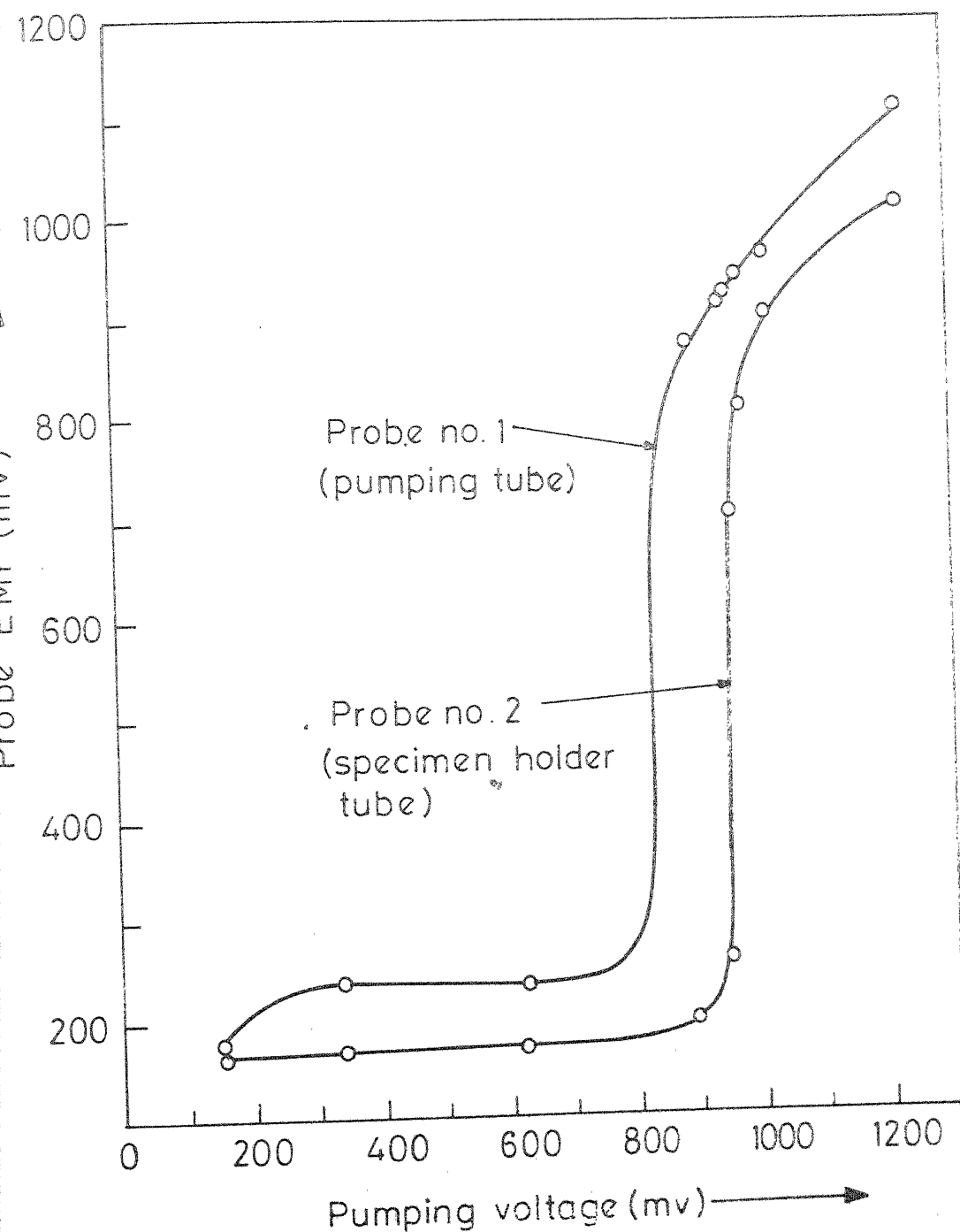
FIG. 4·7 CHANGE OF OXYGEN PARTIAL PRESSURE
INSIDE THE ZIRCONIA TUBE SPECIMEN HOLDER
AS A RESULT OF OXYGEN PUMPING.

As has been mentioned earlier the zirconia tube specimen holder could not be used at higher temperatures due to its extremely high oxygen leak rate. Above $900^C C$, the leak rate was such that the P_{C_2} inside the holder could not be lowered below about 10^{-6} atm. even with the maximum amount of purification achieved in the pumping tube. Measurements at higher temperatures were made in the alumina tube sample holder and the P_{O_2} inside the tube was measured before the gas entered the tube. Therefore it was necessary to test the accuracy of such measurements. It has been already mentioned that in the high P_{O_2} range ($\sim 10^{-5}$ atm.) the oxygen leakage through the alumina tube even at higher temperatures is negligible. To test the behaviour of the alumina tube at very low P_{O_2} range, two oxygen probes, one in the up stream and the other in the down stream side, were used in series with the alumina tube. Both the probes were kept at $700^C C$. Initially Argon gas, directly from cylinder was passed through the system at a constant flow rate and the two probe EMFs were measured by varying the temperature of the alumina tube. The experiment was repeated with highly pure Argon ($P_{O_2} \simeq 10^{-21}$ atm.) purified by the oxygen pump. The results obtained from both the experiments are presented in Table 4.3. It may be observed that in both the cases the EMF in the probe No. 2 does not change significantly with increasing temperature

Table 4.3

Results on the Leak Test of Alumina Tube

EMF at Probe No. 1 at 700°C	Alumina tube temperature (°C)	EMF at Probe No. 2 at 700°C	$-\log P_{O_2}$ (atm.)
170 mV $(P_{O_2} = 10^{-4.2})$	600	158 mV	3.95
	800	157 mV	3.93
	1000	160 mV	3.99
	1200	157 mV	3.93
	1350	154 mV	3.86
990 mV $(P_{O_2} = 10^{-21.19})$	800	930 mV	19.95
	1000	930 mV	19.95
	1200	920 mV	19.74
	1300	910 mV	19.53

of the alumina tube. This may be taken as an indication
of the insignificant leak rate in the alumina tube even
at very low P_{O_2} values and the observed differences between
the two probe readings may be assumed to be mainly due to
the leakage through the second zirconia tube which increases
with decreasing oxygen partial pressure.

CHAPTER V

EXPERIMENTAL RESULTS

V-1.   DENSITY, X-RAY AND METALLOGRAPHIC OBSERVATION

The bulk densities of the sintered specimens
containing varying quantities of Ca have been measured and
the approximate residual porosity, based on the theoretical
densities of doped thoria, has been calculated. The results
are presented in Table 5.1. The porosity of the samples was
found to vary between 1 and 5 percent except that of pure
thoria which was comparatively less dense. X-ray diffraction
patterns of the powdered specimens were taken to find out
the presence of any second phase in the specimens. However,
no such phase could be detected in the specimens containing
upto 10 m/o Ca. It may be pointed out that the ionic sizes
of Th^{4+} (1.15 A°) and Ca^{2+} (1.10 A°) ions in the CaF_2 lattice
are almost equal and therefore the changes in the lattice
parameter could not be detected in the X-ray analysis. The
X-ray pattern of pure thoria, taken on the diffractometer, is
given in Table 5.2.

Some of the typical microstructures of the
sintered specimens are shown in Fig. 5.1 corresponding to
(a) 1 m/o, (b) 3 m/o, and (c) 7 m/o Ca specimens. It may be
observed that there is a marked difference between the grain

Table 5.1

Density and Porosity of Sintered Specimens

Specimen	Theoretical density (gm/c.c.)	Measured bulk density (gm/c.c.)	Approx. Porosity (Percent)
'Pure' ThO_2	10.04	8.94	11.1
1 m/o CaO	9.96	9.57	3.92
2 m/o CaO	9.88	9.60	2.84
3 m/o CaO	9.80	9.29	5.21
4 m/o CaO	9.73	9.52	2.16
5 m/o CaO	9.65	9.49	1.66
6 m/o CaO	9.57	9.44	1.36
7 m/o CaO	9.49	9.40	1.00

Table 5.2

X-ray Pattern of Pure ThO$_2$

Radiation: CuK$_\alpha$

2θ	d(A^o)	hkl	Relative intensity
27.60^o	3.229	111	100
32.05^o	2.790	200	40
45.80	1.979	220	75
54.35	1.715	311	75
56.80	1.619	222	20
66.70	1.402	400	10
73.80	1.283	331	40
76.15	1.249	420	25
84.80	1.142	422	30
102.35	0.988	440	10
109.00	0.946	531	3
111.50	0.932	600	15

96
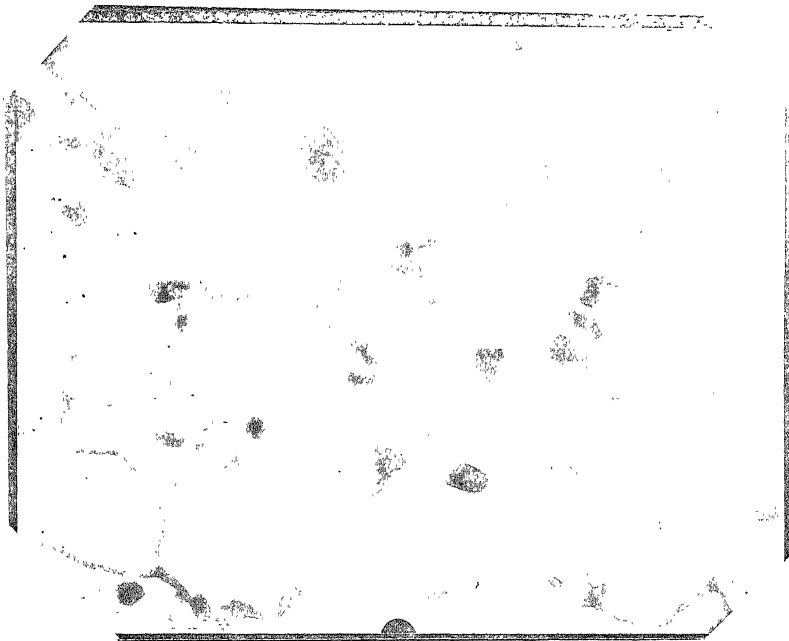
(a) 1 m/o Calcium Oxide

(b) 3 m/o Calcium Oxide

Fig. 5.1: Photomicrographs of ThO_2-CaO Specimens.
(X300)
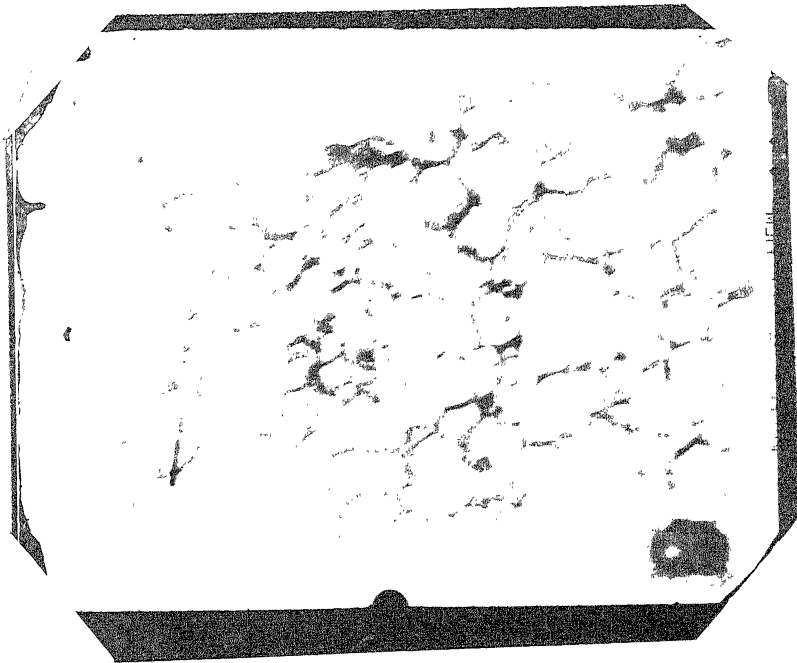
(c)   7 m/o Calcium Oxide

Fig. 5.1:   Photomicrograph of ThO_2-CaO Specimen.
(X300)

sizes of the various specimens. With increasing CaO content
the grain size of the specimen reduces drastically. The grain
size changes from 180 μ in 1 m/o CaO to 30 μ in 7 m/o CaO
specimen. However, none of these microstructures show any
evidence of a second phase in these specimens.

V-2 ELECTRICAL CONDUCTIVITY

The a.c. total conductivity of pure ThO_2 and
ThO_2-CaO solid solutions with CaO contents ranging from 1 to
15 m/o was initially measured in air within the temperature
range of 600-1400°C. The values obtained at various temper-
atures have been plotted as a function of m/o CaO (Fig. 5.2).
The relevant experimental data are presented in the Appendix
(Tables Al.1 series). It is observed that at each temperature,
small additions of CaO sharply increases the conductivity.
However, the effect becomes less prominent beyond about 2 m/o
CaO. The conductivity at each temperature goes through a flat
maximum at about 10 m/o CaO. The variation of the conductivity
values between 7 and 10 m/o CaO is not very significant and
therefore the specimens containing a maximum of 7 m/o CaO were
used for the rest of the experiments. The conductivity of
'pure' and CaO doped thoria specimens were measured in the
P_{O_2} range of 1 to 10^{-25} atm. at temperatures between 600 and
1200°C. In Fig. 5.3, the conductivity of 'pure' ThO_2 has
been plotted as a function of oxygen partial pressure at
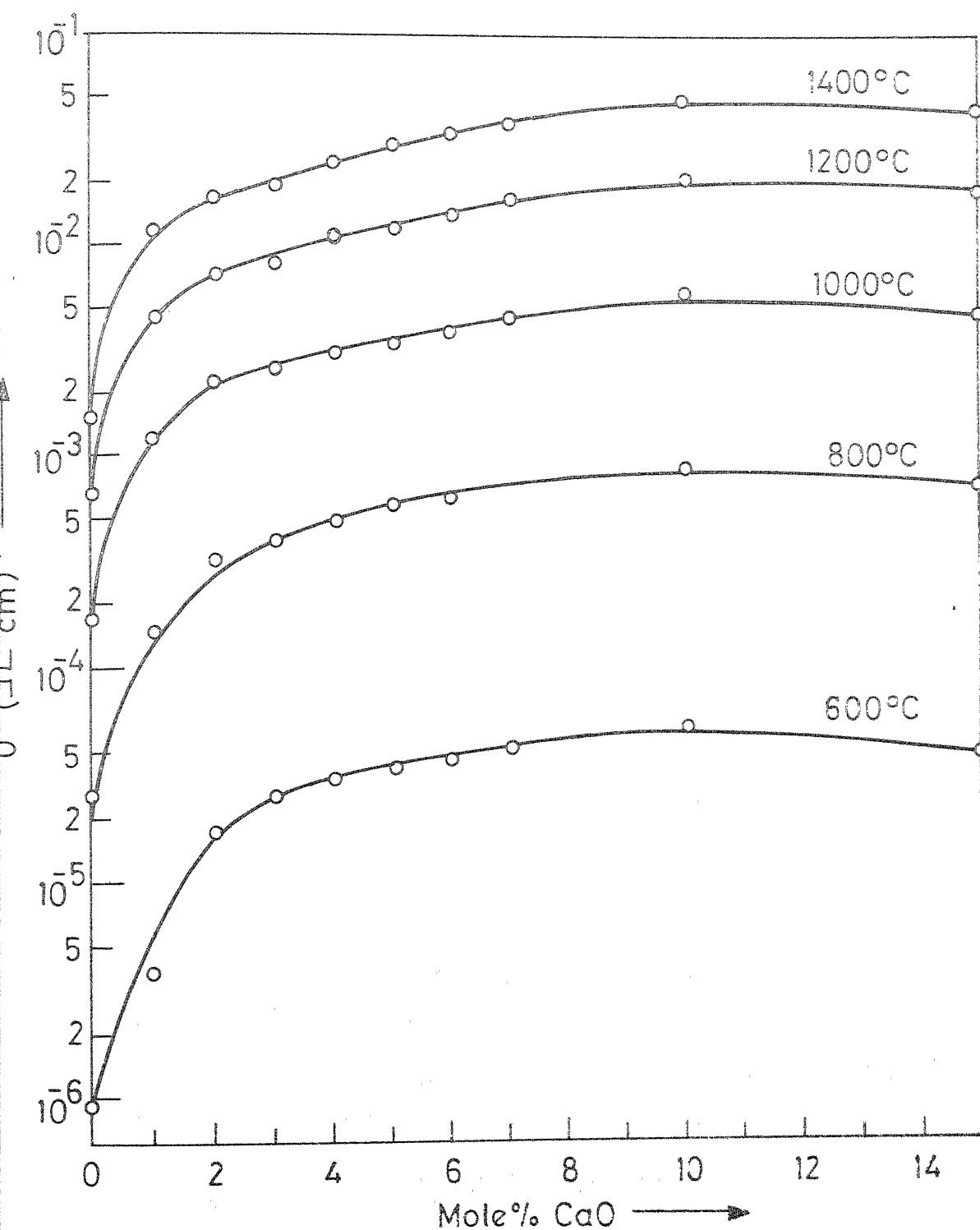
FIG. 5.2 CONDUCTIVITY ISOTHERMS FOR ThO$_2$-CaO ELECTRO-
LYTES MEASURED IN AIR.
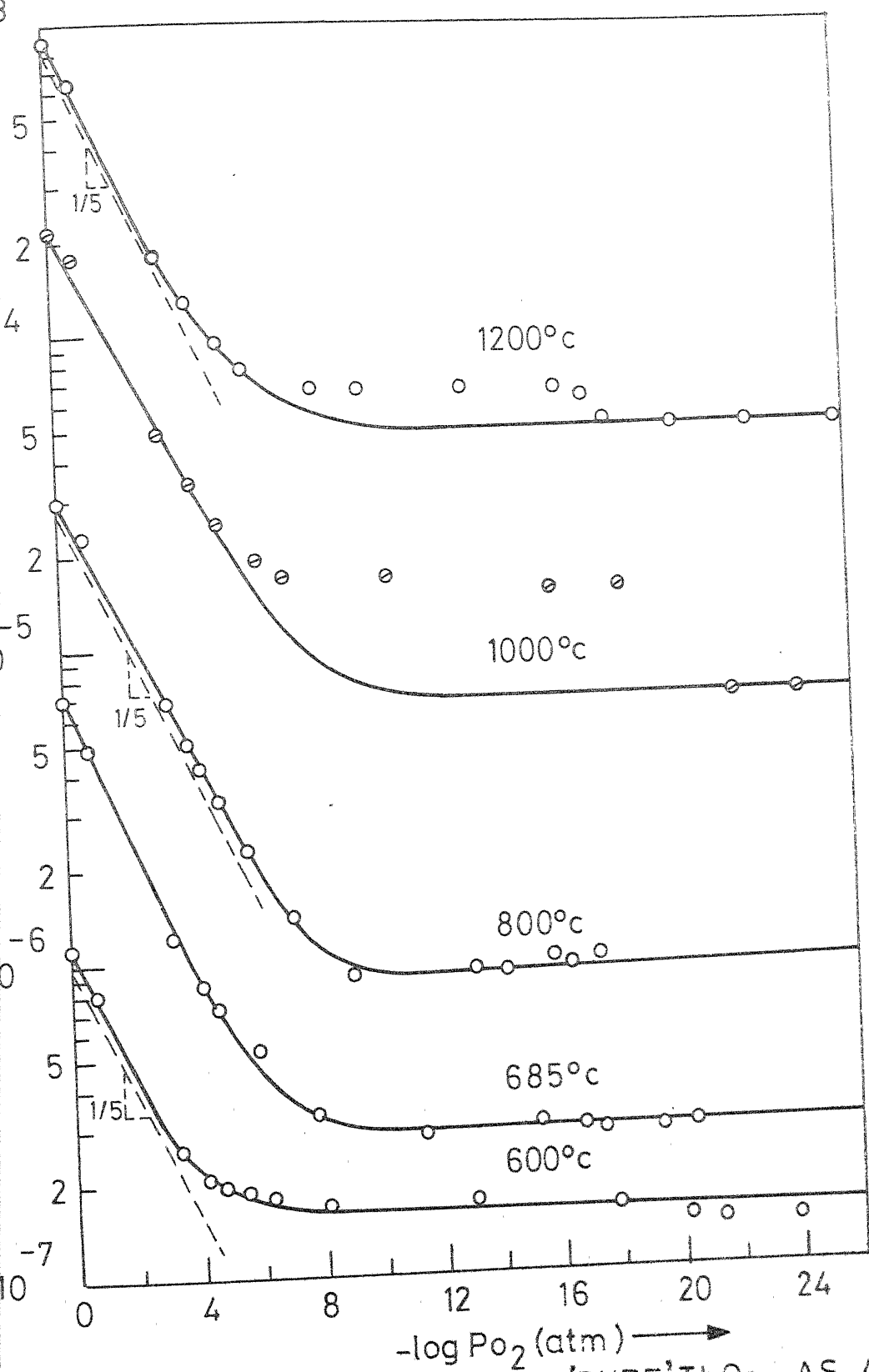
FIG 3 ELECTRICAL CONDUCTIVITY OF 'PURE' ThO_2 AS A FUNCTION OF OXYGEN PARTIAL PRESSURE AT DIFFERENT TEMPERATURES

The figure shows conductivity curves plotted against $-\log P_{O_2}$ (atm) for different temperatures: 1200°C, 1000°C, 800°C, 685°C, and 600°C. Dashed lines with slope 1/5 are indicated.

different temperatures. At higher partial pressures, the conductivity at each temperature decreases with decreasing P_{O_2}. The conductivity in this partial pressure range is found to be proportional to $P_{O_2}^{1/5}$. Below a certain value of oxygen partial pressure, the conductivity becomes independent of pressure and the transition from the pressure dependent to a pressure independent region occurs at lower oxygen partial pressure as the temperature is increased. The conductivity curve reaches its plateau at a partial pressure of 10^{-8} atm. at 600°C and the value decreases to 10^{-10} atms. at 1200°C.

Similar plots of the logarithm of conductivity vs. logarithm of oxygen partial pressure at different temperatures have been made for ThO_2-CaO solid solutions containing 1, 2, 3, 4 and 7 m/o CaO and are shown in Figs. 5.4, 5.5, 5.6, 5.7 and 5.8 respectively. The corresponding basic experimental data are given in Appendix (Tables A2 series). The behaviour in each case is very similar to that of 'pure' ThO_2. The conductivity value at any fixed oxygen partial pressure increases steadily with temperature as well as with the impurity content. The slopes of the curves in the pressure dependent region are different at different temperatures. In most cases the slope of the line decreases with increasing temperature for a given composition as also with increasing CaO content at any temperature. The horizontal portion of the conductivity plot extends upto a higher oxygen pressure as
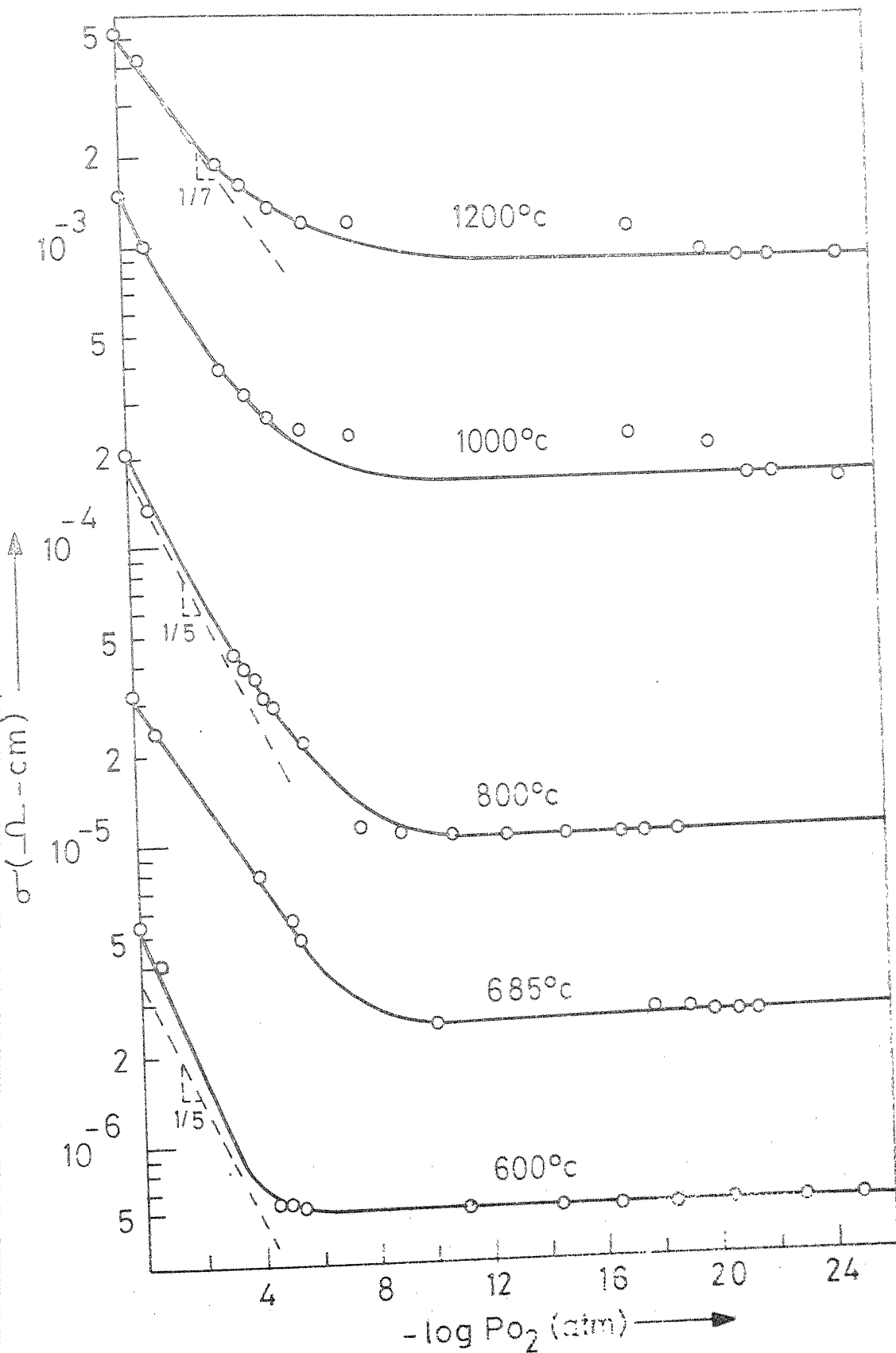
FIG. 5.4 ELECTRICAL CONDUCTIVITY OF $ThO_2 - 1\%$ CaO SAMPLE AS A FUNCTION OF OXYGEN PARTIAL PRESSURE AT DIFFERENT TEMPERATURES.
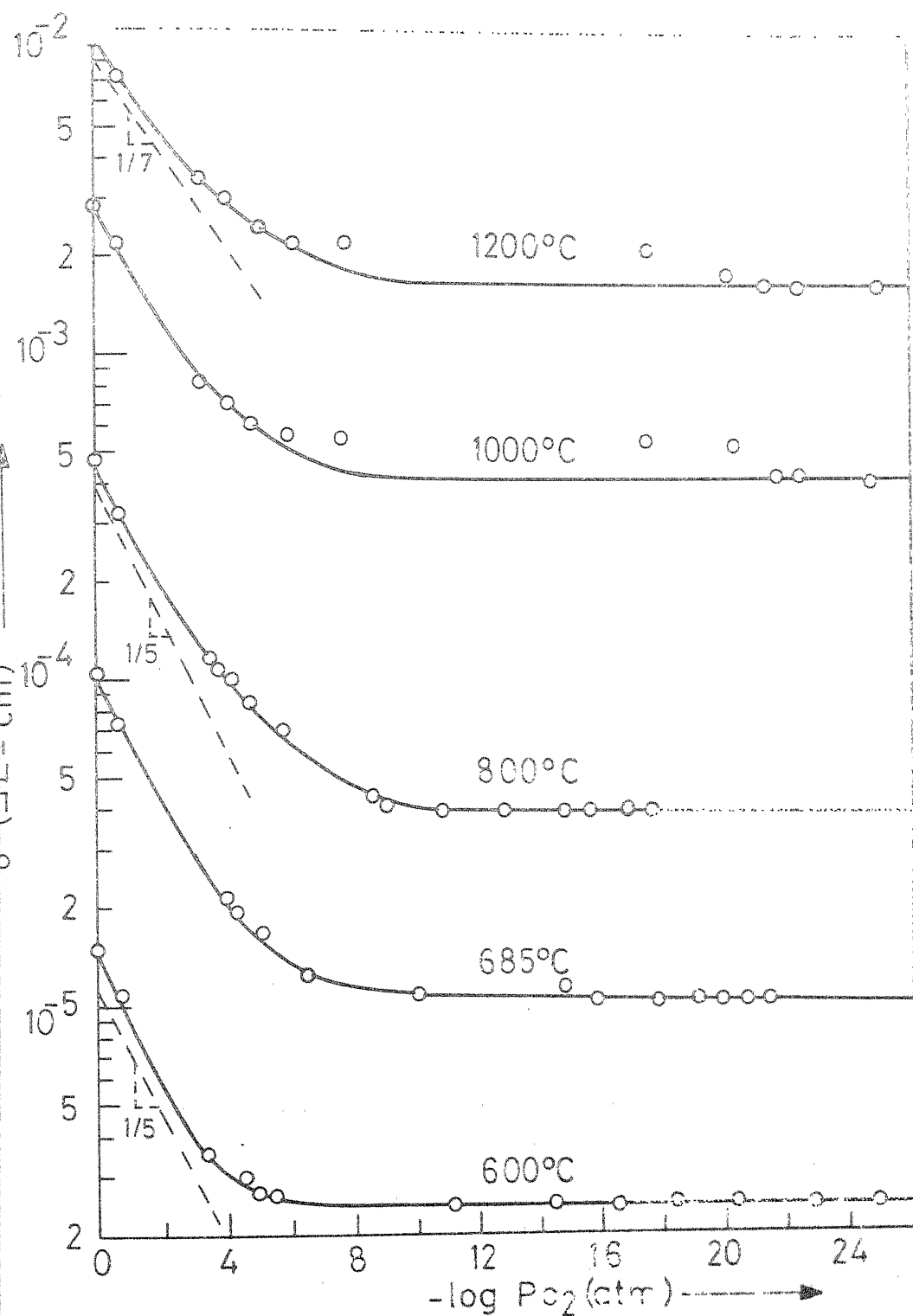
FIG 5·5 ELECTRICAL CONDUCTIVITY OF ThO₂ -2% CaO
SAMPLE AS A FUNCTION OF OXYGEN PARTIAL
PRESSURE AND TEMPERATURE
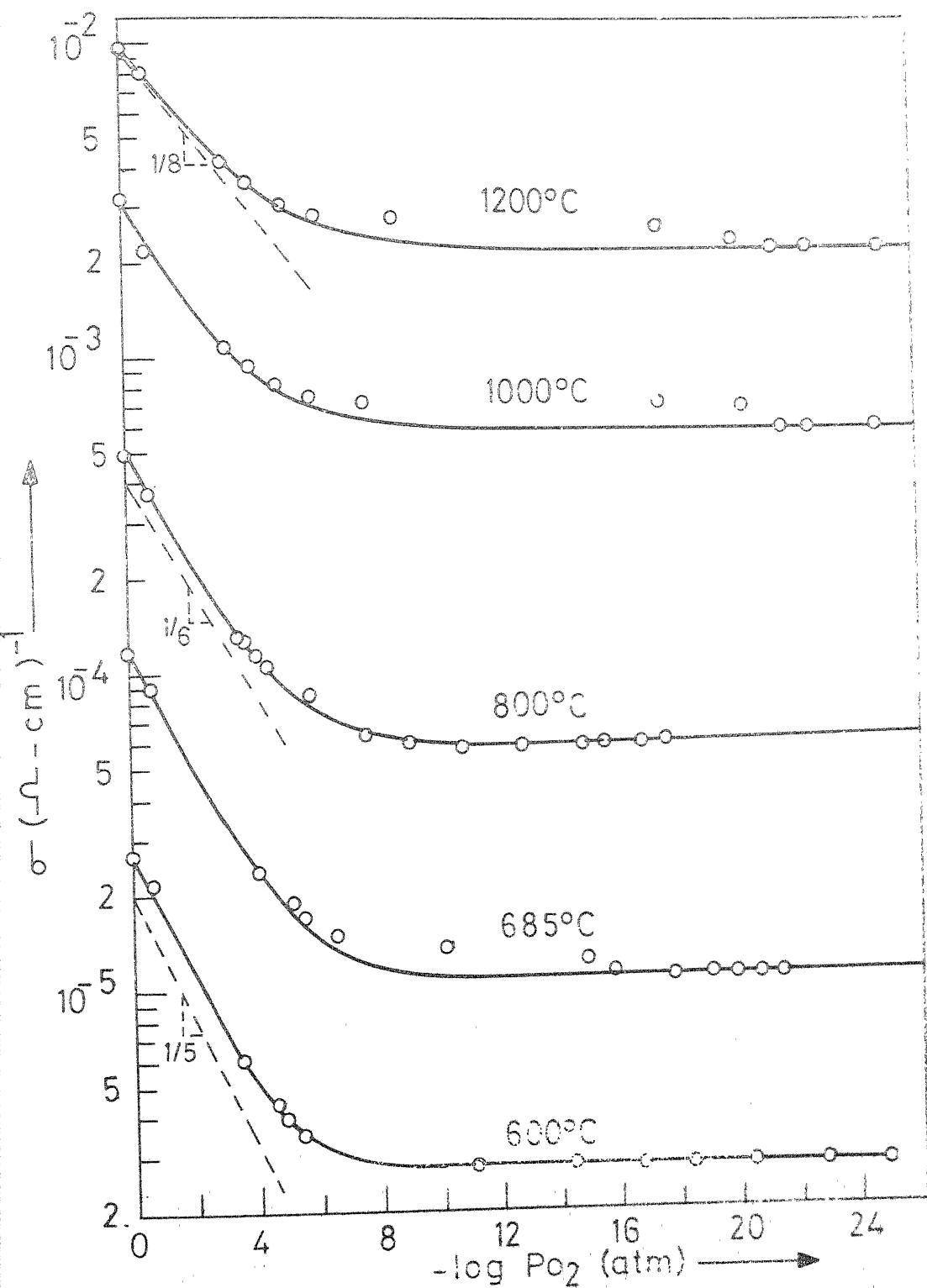
FIG. 5·6 ELECTRICAL CONDUCTIVITY OF $ThO_2 - 3\%CaO$ SAMPLE AS A FUNCTION OF OXYGEN PARTIAL PRESSURE AT DIFFERENT TEMPERATURES.
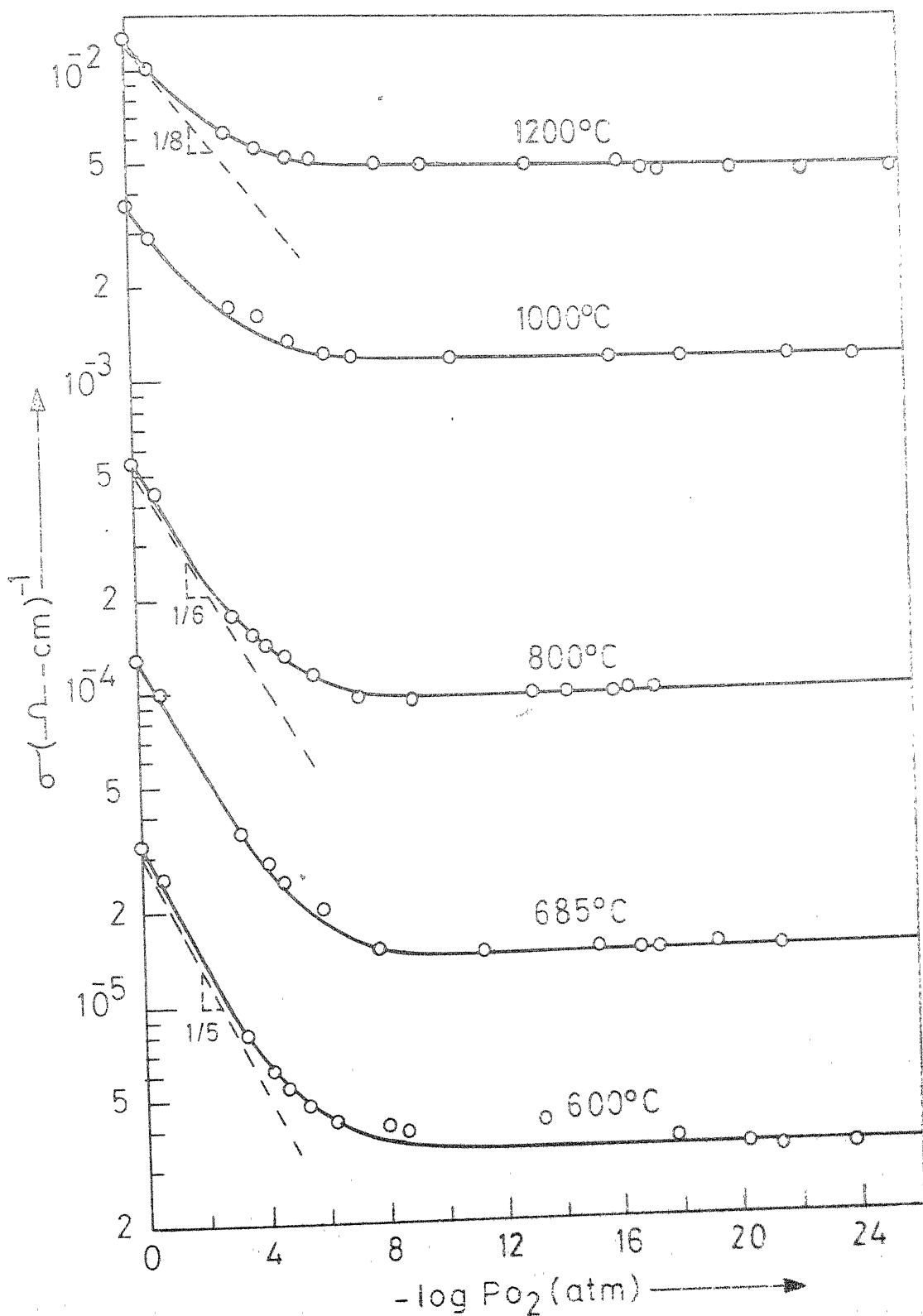
FIG. 5.7 ELECTRICAL CONDUCTIVITY OF $ThO_2-4\% \, CaO$
SAMPLE AS A FUNCTION OF OXYGEN PARTIAL
PRESSURE AND TEMPERATURE.
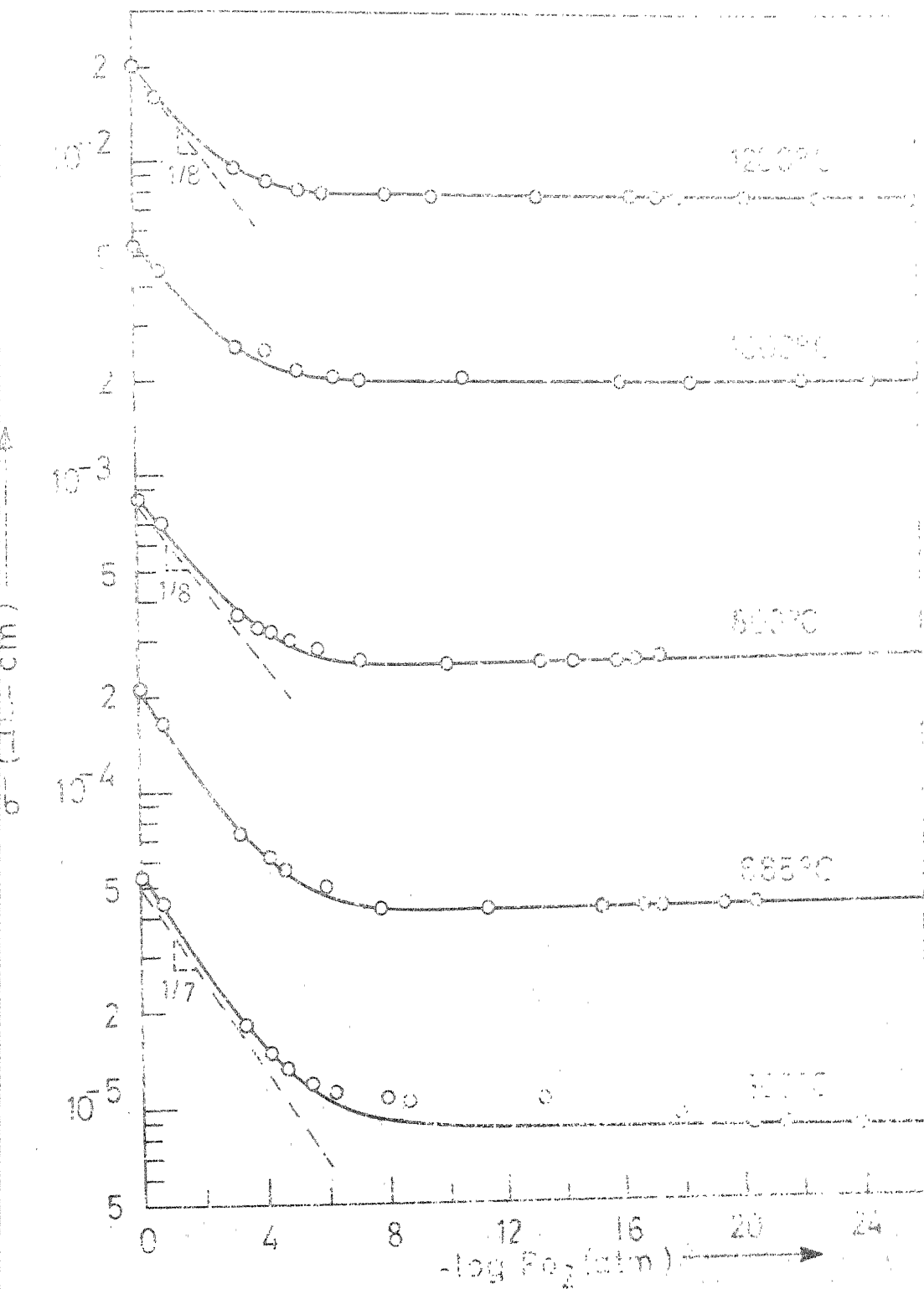
FIG.5.8 ELECTRICAL CONDUCTIVITY OF ThO₂ + 1% CaO SAMPLE
AS A FUNCTION OF OXYGEN PARTIAL PRESSURE AT
DIFFERENT TEMPERATURES.

the CaO content of the sample is increased. In a 7 m/o CaO sample which shows the highest conductivity throughout the partial pressure range, the transition from a pressure dependent to a pressure independent conductivity takes place in the range of 10^{-4} - 10^{-8} atm. at almost all the temperatures studied (Fig. 5.8). At 1000 and $1200^{\circ}C$, except for 4 and 7 m/o CaO solid solutions in which the transition takes place above 10^{-6} atm. (Figs. 5.7 and 5.8), the figures include some experimental points between 10^{-6} to 10^{-16} atm. of oxygen partial pressure which lie above the pressure independent portion of the conductivity curves. This is due to an experimental difficulty in controlling the oxygen partial pressure in this range.

It has been mentioned earlier that the high temperature conductivity measurements were carried out in the alumina tube specimen holder in which case the oxygen content of the flowing gas was measured before it entered the specimen holder. It was observed that the oxygen content inside the tube could not be measured accurately in the partial pressure range corresponding to the region III of Figs. 4.3 and 4.4. Similar to the behaviour of zirconia tube specimen holder (Fig. 4.7) the oxygen content inside the alumina tube remained constant at around 10^{-6} atm. even when the oxygen content inside the pumping tube as shown by the measuring probe was reduced to a very low value. However,

a sudden lowering of P_{O_2} inside the alumina tube was observed when the oxygen content in the pumping tube reached a certain critical value (around 10^{-18} atm.). As a result, the oxygen content inside the alumina tube did not correspond to the measured probe EMF between 10^{-6} to 10^{-18} atm. of oxygen partial pressure. However, beyond these limits the P_{O_2} inside the alumina tube was very close to that measured by the measuring probe. This was verified by measuring the conductivity of a particular ThO_2-CaO specimen at $800^\circ C$ as a function of P_{O_2} inside both the alumina and the zirconia tube specimen holders. The conductivity of the specimen inside the alumina tube was found to remain fixed at a value corresponding to $P_{O_2} = 10^{-6}$ atm. when the P_{O_2} in the pumping tube was changed from 10^{-6} to 10^{-18} atm. But it suddenly changed to a lower value corresponding to the conductivity of the specimen at $800^\circ C$ as measured by the zirconia tube specimen holder, when the P_{O_2} in the pumping tube was lowered beyond this limit. Similar effect was observed in the plots of log σT vs $-log P_{O_2}$ at $1000^\circ C$ and $1200^\circ C$. However, it was not detected in the samples (4 and 7 m/o CaO) for which P_{O_2} independent plateau was reached above 10^{-6} atm.

To see the effect of composition on the conductivity values, the data presented in Figs. 5.3 to 5.8 have been replotted in Figs. 5.9, 5.10, 5.11, 5.12 and 5.13 in which the log σ vs $-log P_{O_2}$ curves corresponding to various compositions
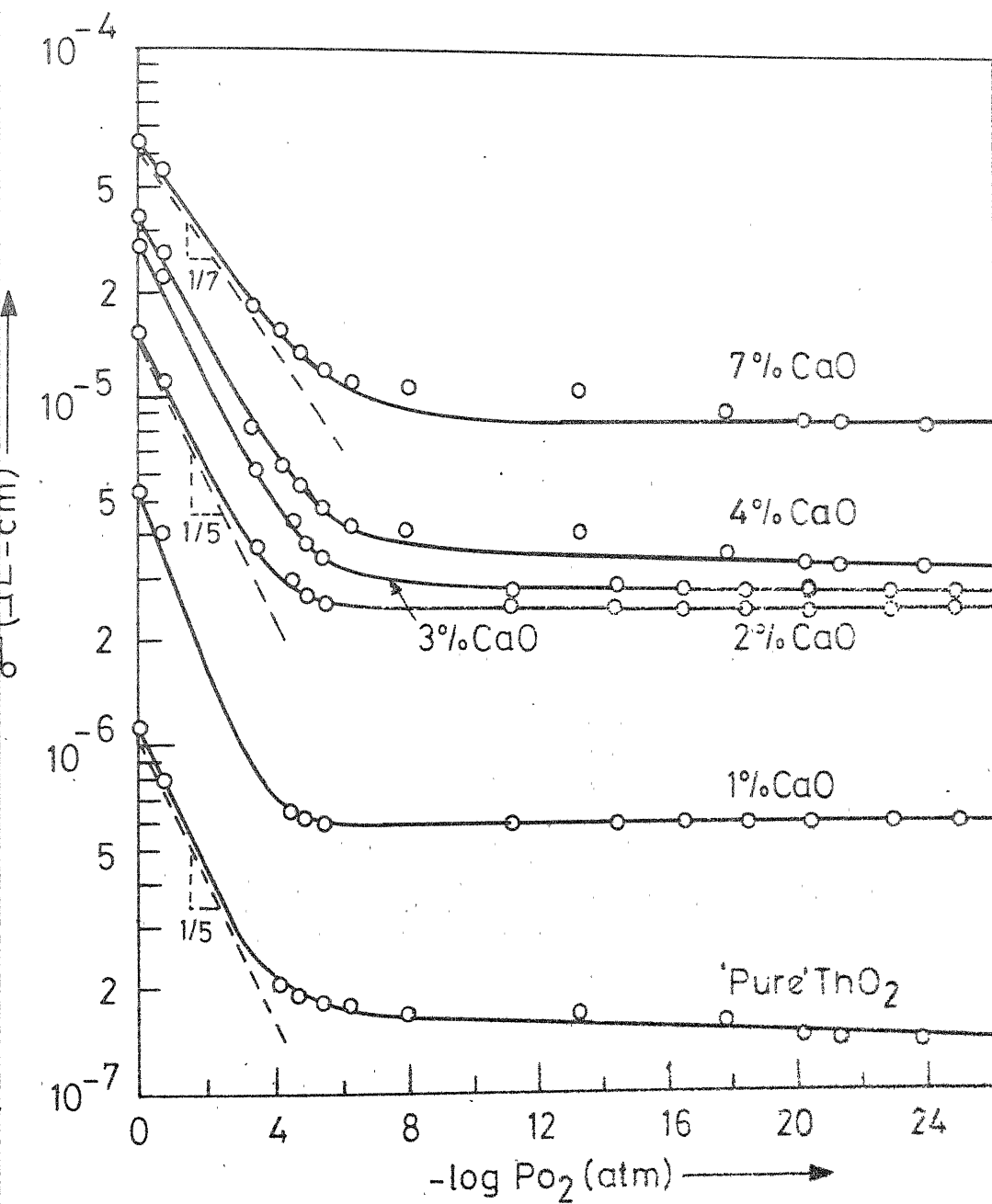
G.5.9 ELECTRICAL CONDUCTIVITY OF ThO$_2$-CaO SOLID
SOLUTIONS AS A FUNCTION OF OXYGEN PARTIAL
PRESSURE AT 600°C.
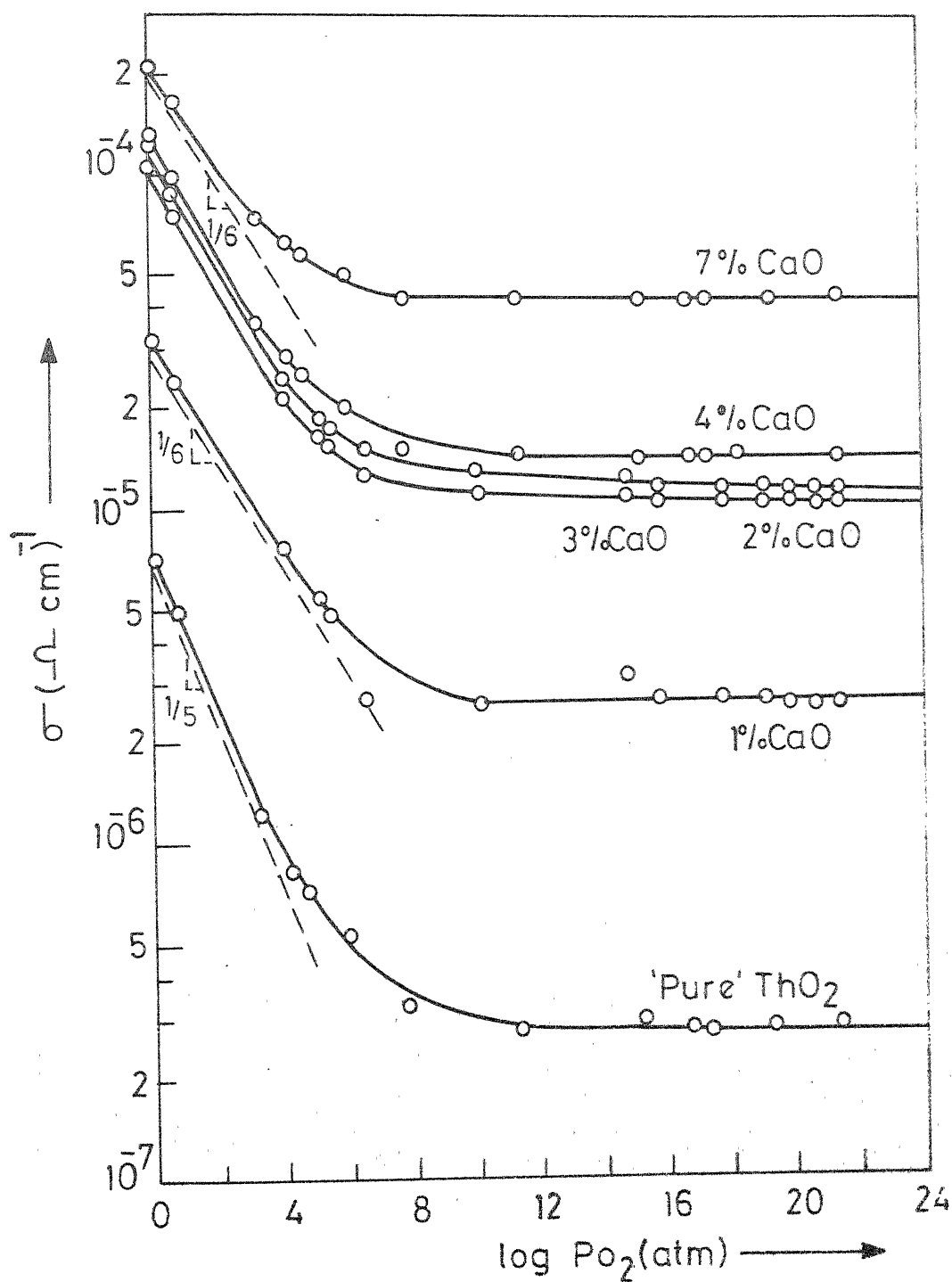
FIG.5.10 ELECTRICAL CONDUCTIVITY OF ThO₂⁻CaO SOLID
SOLUTIONS AS A FUNCTION OF OXYGEN PARTIAL
PRESSURE AT 685°C.
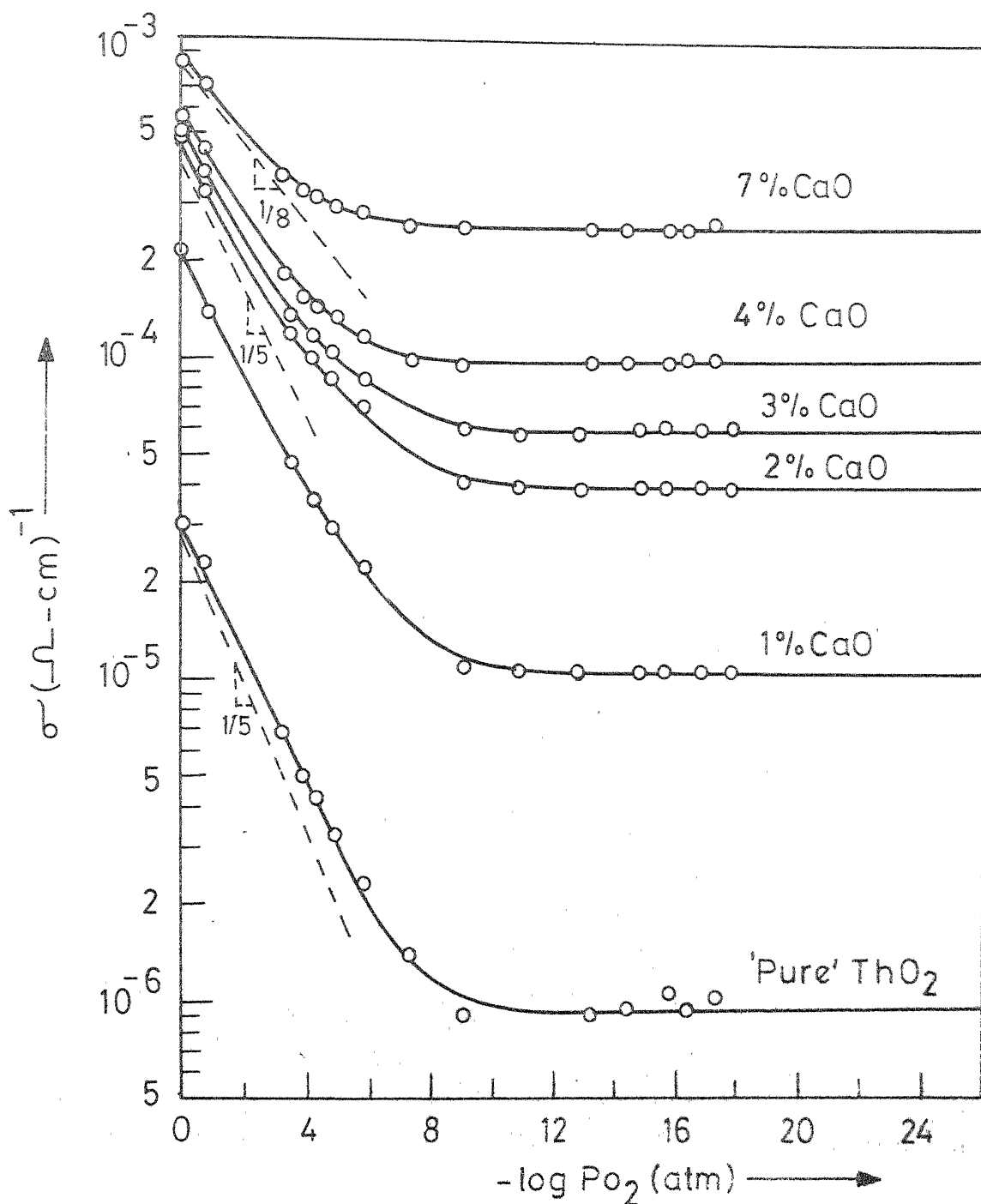
FIG.5·11 ELECTRICAL CONDUCTIVITY OF ThO$_2$–CaO SOLID
SOLUTIONS AS A FUNCTION OF OXYGEN PARTIAL
PRESSURE AT 800°C.

10^{-2}

5

2

10^{-3}

5

2

10^{-4}

5

2

10^{-5}

5

$\sigma - (\Omega - cm)^{-1}$

1/8

1/5

1/5

7% CaO

4% CaO

3% CaO

2% CaO

1% CaO

'Pure' ThO$_2$

0   4   8   12   16   20   24

$-\log P_{O_2}$ (atm)
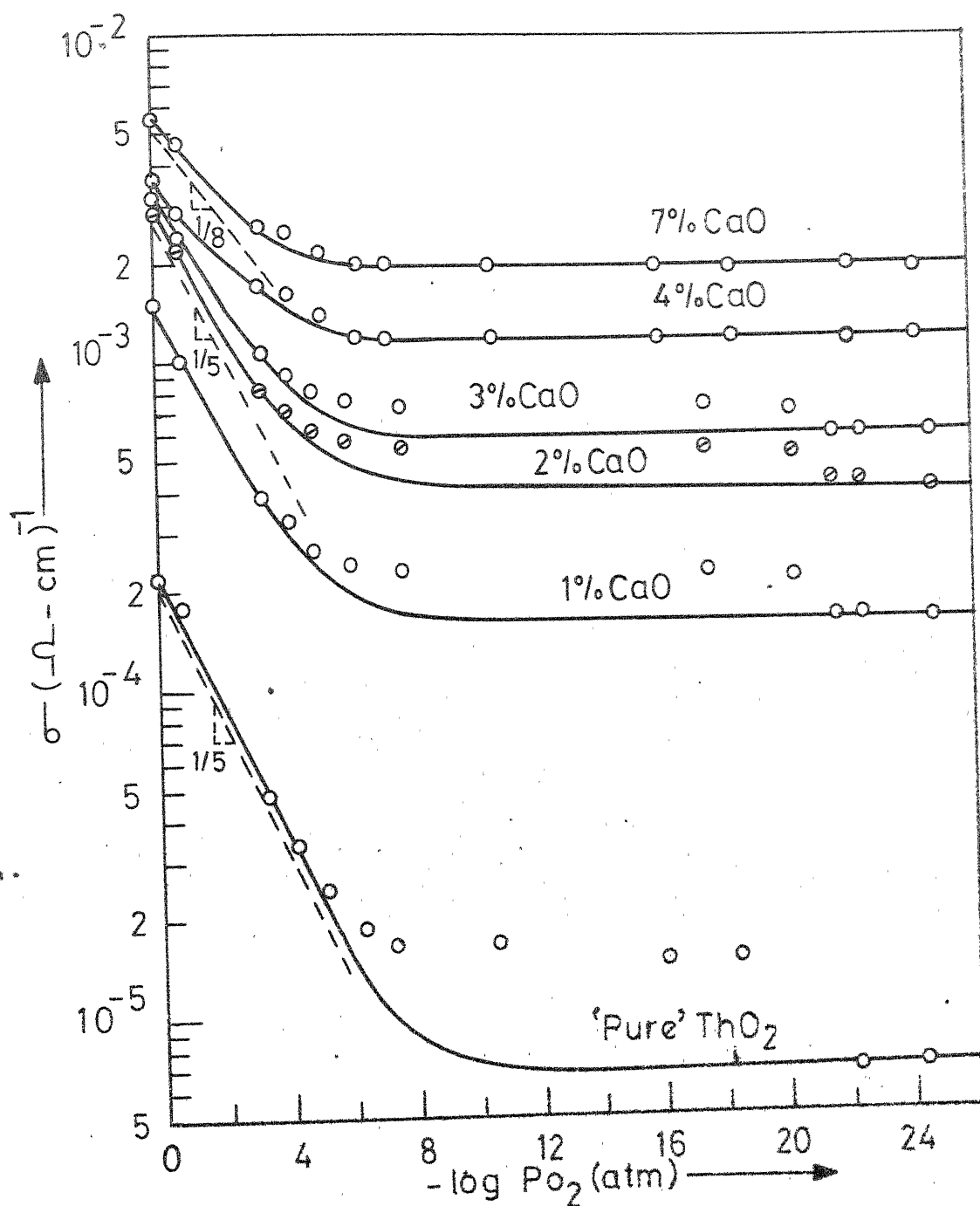
FIG. 5·12 ELECTRICAL CONDUCTIVITY OF ThO$_2$–CaO SOLID SOLUTIONS AS A FUNCTION OF OXYGEN PARTIAL PRESSURE AT 1000°C.
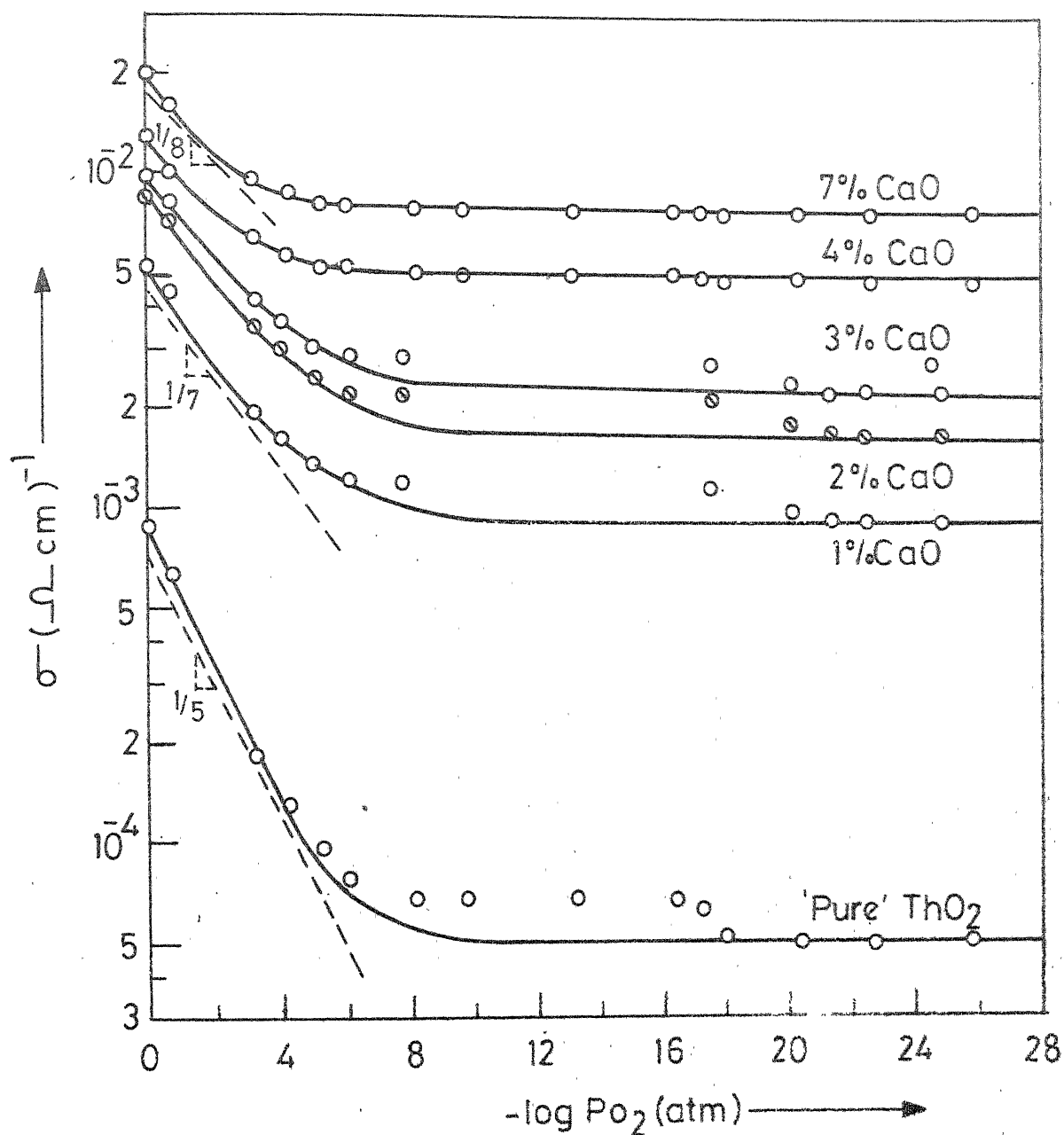
FIG. 5.13 ELECTRICAL CONDUCTIVITY OF ThO$_2$-CaO SOLID SOLUTIONS AS A FUNCTION OF OXYGEN PARTIAL PRESSURE AT 1200°C.

have been reproduced for fixed temperatures of 600, 685, 800, 1000 and 1200°C respectively. The variation of the slope of the curves in the pressure dependent region, as a function of CaO content, is evident from these figures. The slope decreases from 1/5 to either 1/7 or 1/8 (depending upon temperature) as the CaO content is increased, along with a shift of the transition region towards the higher partial pressure side.

Ionic transference numbers (t_{ion}) for 'pure' and doped samples have been calculated at different oxygen partial pressures and temperatures following the procedure adopted by Lasker and Rapp [52]. These results have been plotted as a function of oxygen partial pressure in Figs. 5.14 and 5.15 corresponding to various temperatures. Under a fixed partial pressure and temperature the value increases with increasing CaO content. The transference number becomes unity when the conductivity becomes independent of partial pressure. At 1000°C 'pure' ThO_2 becomes fully ionic below 10^{-12} atm. while by addition of 7 m/o CaO the value goes up to 10^{-8} atm. At 800°C the corresponding values are 10^{-10} and 10^{-6} atm. respectively.

To determine the activation energy of the conduction process, the conductivity of 'pure' thoria and ThO_2-CaO solid solutions has been measured as a function of temperature between 600-1400°C under fixed oxygen partial
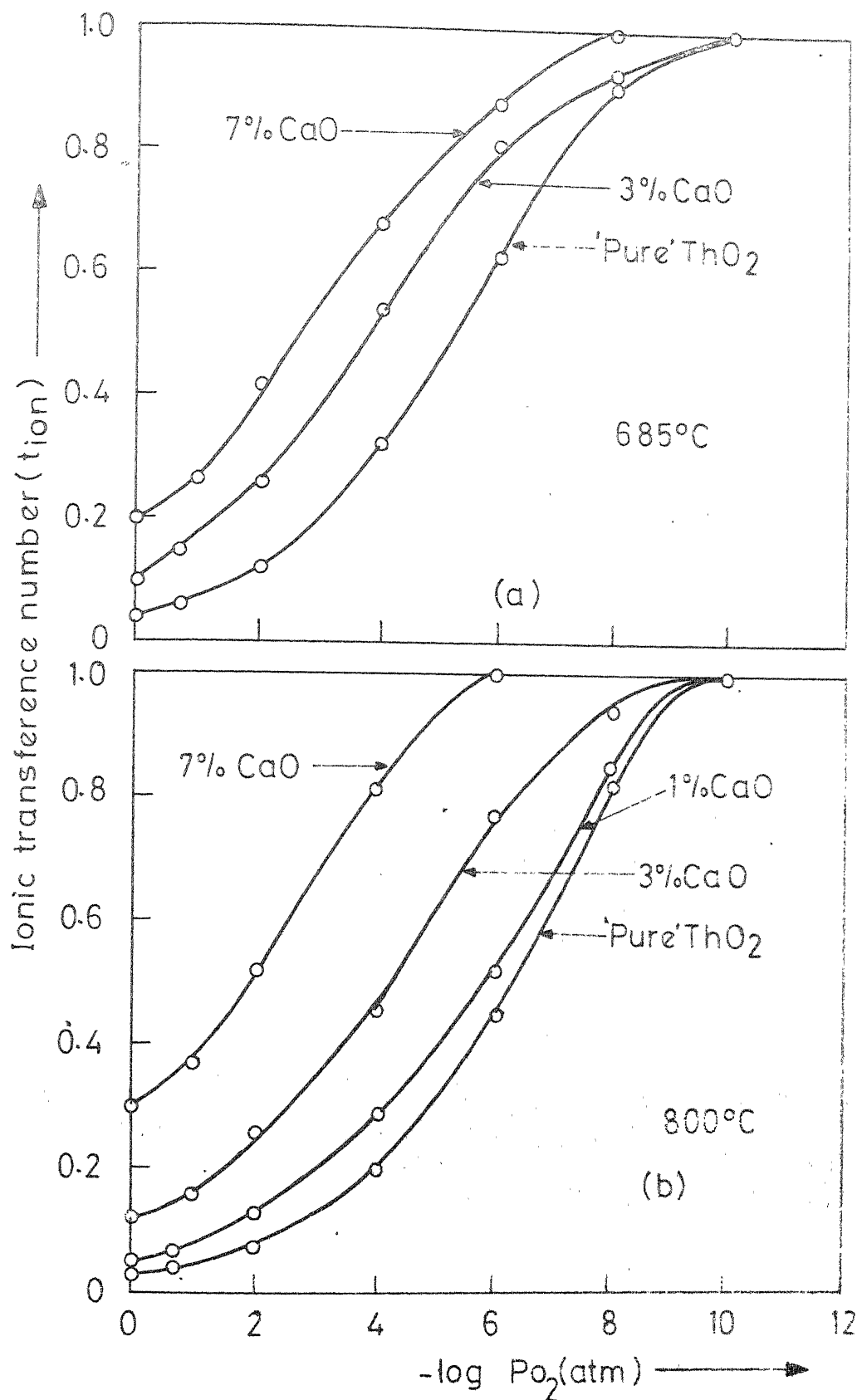
FIG. 5.14 IONIC TRANSFERENCE NUMBERS OF ThO₂ -CaO SOLID
SOLUTIONS AS A FUNCTION OF OXYGEN PARTIAL PRESS-
URE AT 685°C(a) & 800°C(b).
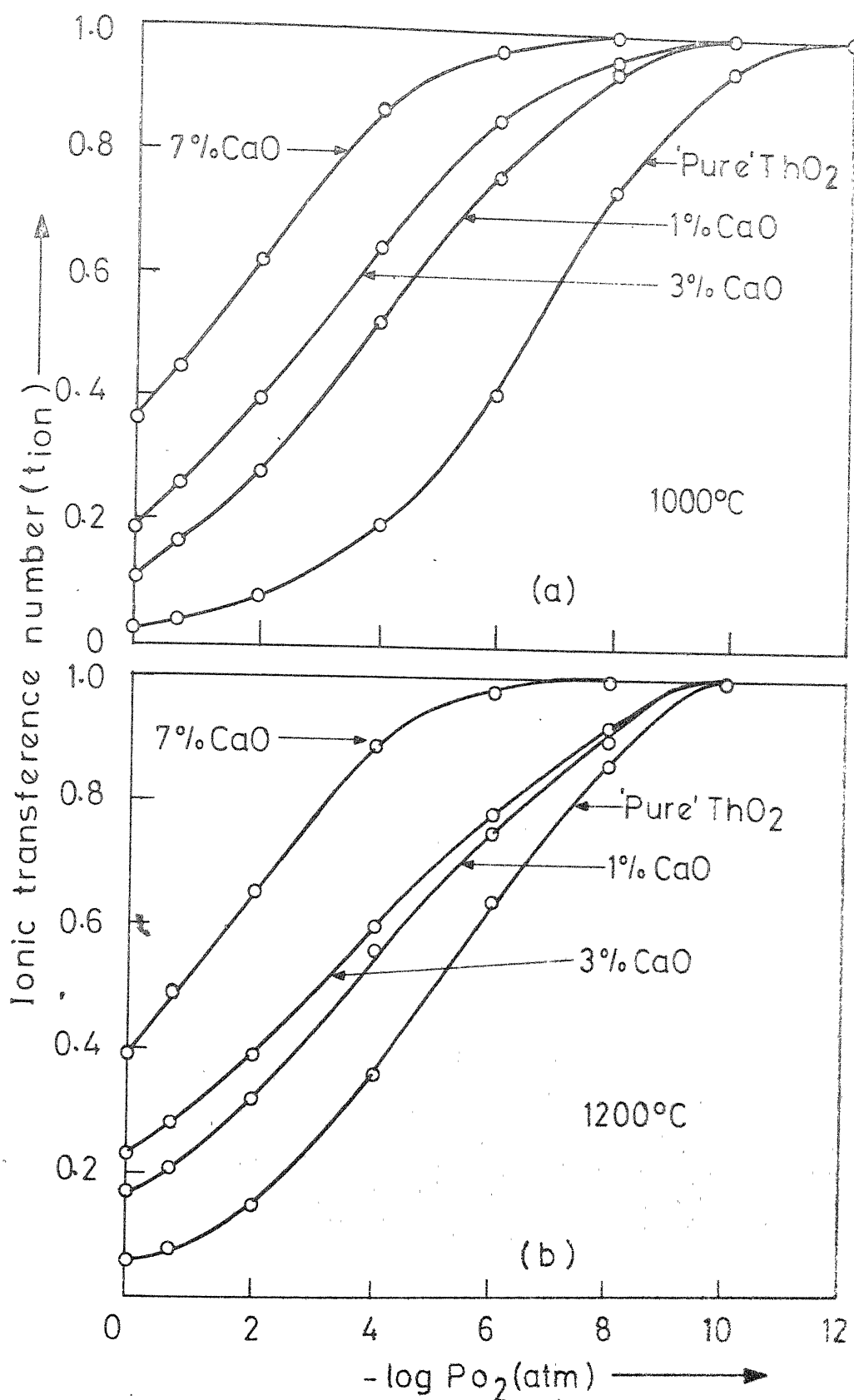
FIG. 5.15 IONIC TRANSFERENCE NUMBERS OF ThO₂-CaO SOLID
SOLUTIONS AS A FUNCTION OF OXYGEN PARTIAL
PRESSURE AT 1000°C (a) & 1200°C (b).

pressures of 10^C (oxygen), $10^{-0.7}$ (air), 10^{-5} and 10^{-23} atm.
and the results are presented in Figs. 5.16 to 5.19 in which
Arrhenius-type plots of log σT vs $1/T$ have been made as a
function of CaO content. The basic experimental data are
given in the Appendix (Tables A1 series). It may be observed
that the straight lines having different slopes are obtained
in different temperature regions. In each region, the
activation energy was calculated from the slope of the
straight line which was fitted to the experimental points
by a least square method. Table 5.3 gives a complete list of
observed activation energies under different experimental
conditions. The error limits of the calculated activation
energies were found to be $\pm$ 0.05 ev. At a very low oxygen
partial pressure (10^{-23} atm.) where all the specimens may be
considered as exclusive ionic conductors, three distinctly
different temperature ranges having different activation
energies are evident (Fig. 5.19). The activation energy is
the highest in the intermediate temperature range while it is
lower both in the low and high temperature regions. The
activation energy in the low temperature region does not
change significantly with the CaO content of the specimens.
It varies between 0.96 ev to 1.06 ev in this temperature range.
However in the intermediate temperature range, the activation
energies for the highly doped specimens (containing 3-7 m/o
CaO) are lower compared to that of 'pure' thoria as well as
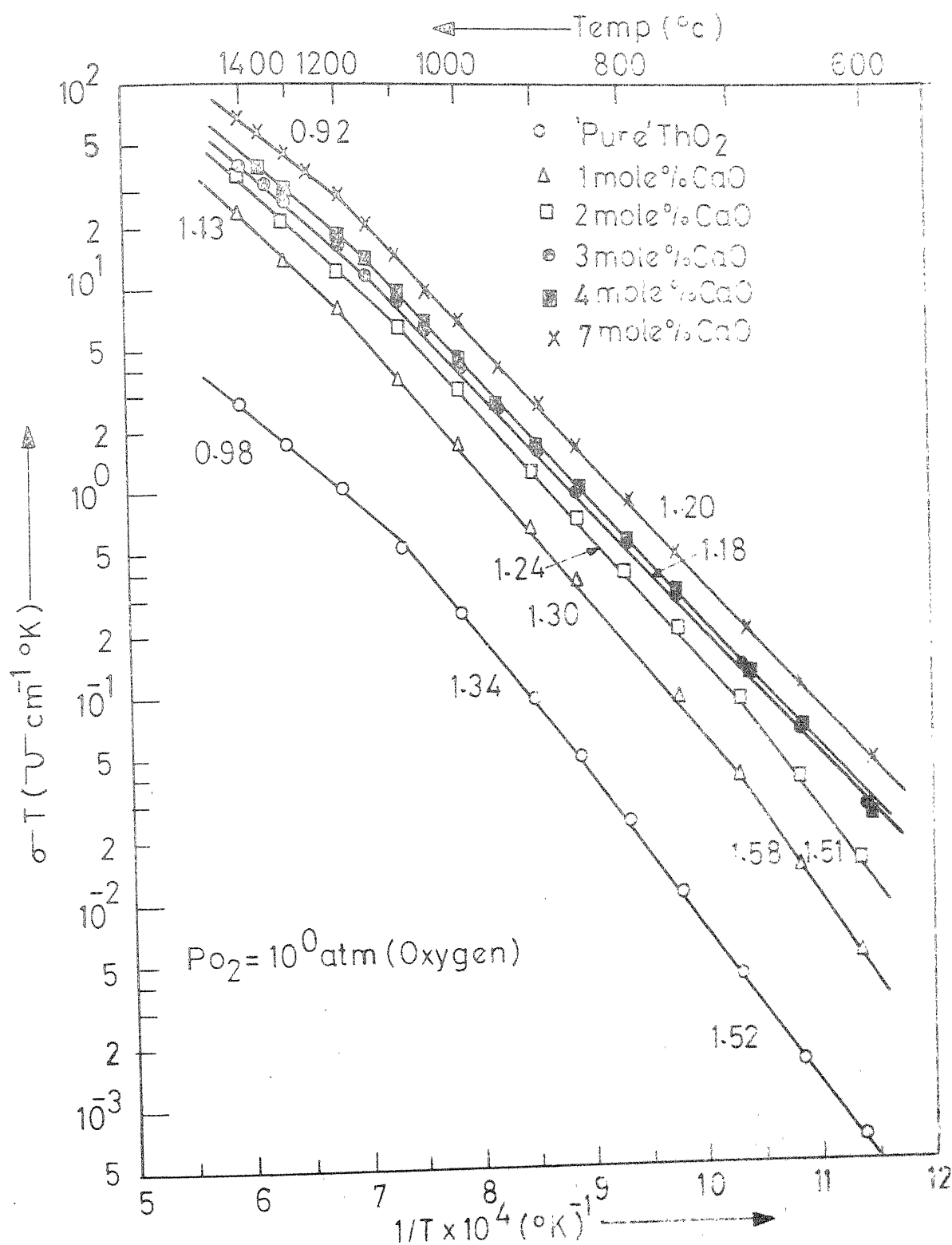
FIG. 5.16 ELECTRICAL CONDUCTIVITY OF ThO_2 – CaO SOLID SOLUTION AS A FUNCTION OF TEMPERATURE IN OXYGEN ATMOSPHERE
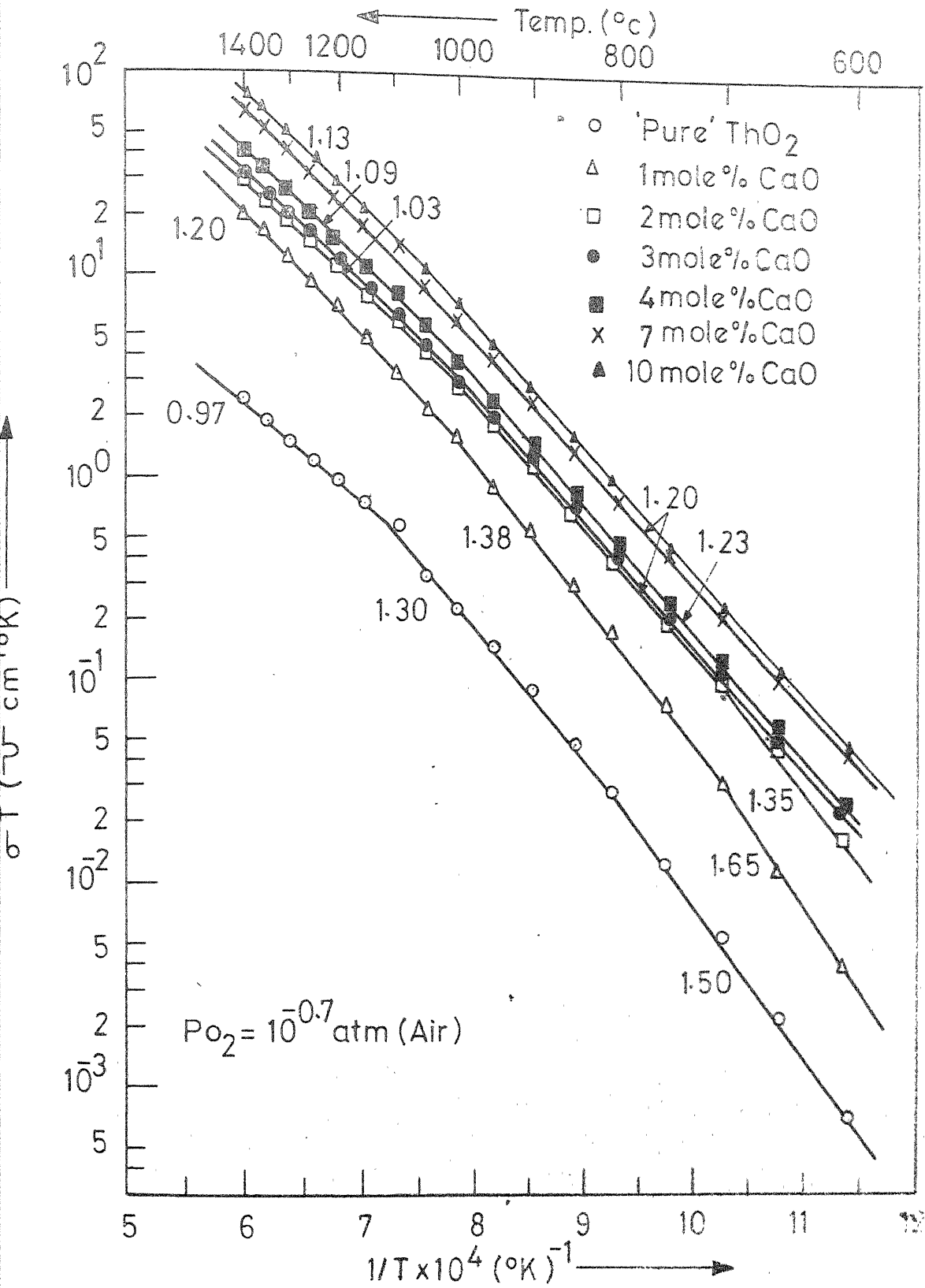
FIG. 5·17   ELECTRICAL CONDUCTIVITY OF ThO$_2$ - CaO SOLID SOLUTION
AS A FUNCTION OF TEMPERATURE IN AIR - ATMOSPHERE.
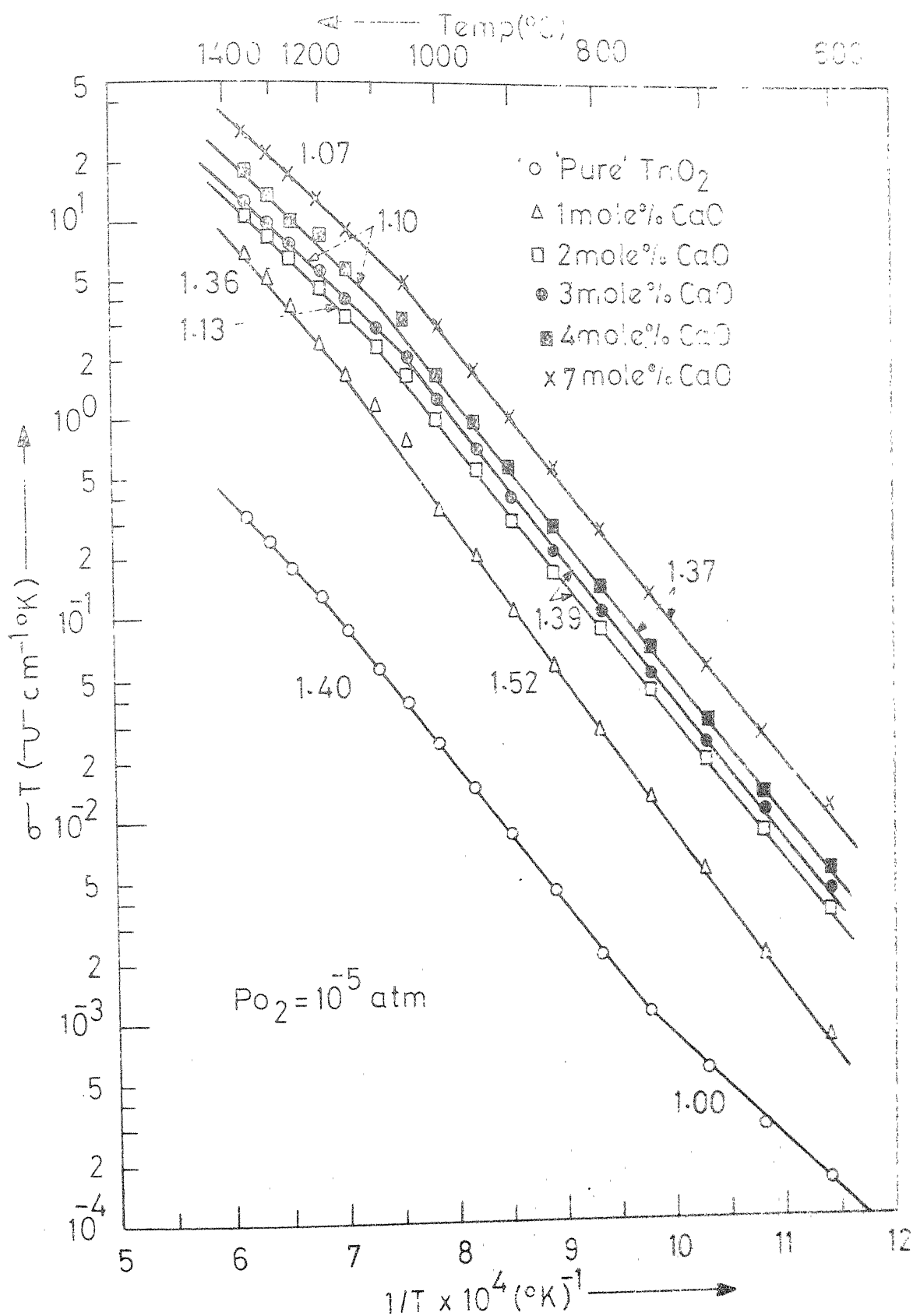
FIG.5.18 ELECTRICAL CONDUCTIVITY OF ThO_2-CaO SOLID SOLUTI-
ONS AS A FUNCTION OF TEMPERATURE AT AN OXYGEN
PARTIAL PRESSURE AT 10^{-5} Atm
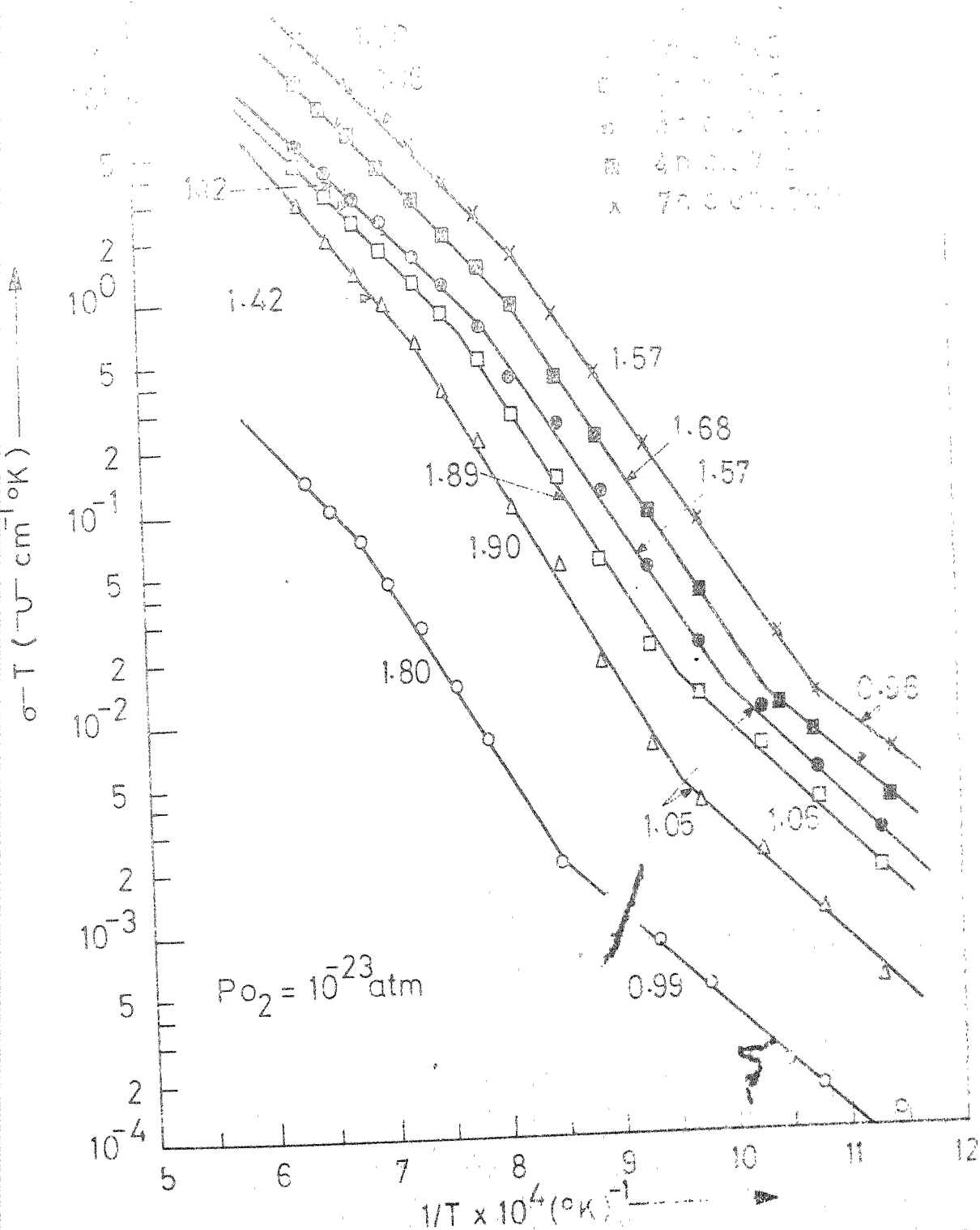
FIG. 5.19 ELECTRICAL CONDUCTIVITY OF THO₂·CeO₂ SOLID SOLUTIONS AS A FUNCTION OF TEMPERATURE AT AN OXYGEN PARTIAL PRESSURE OF 10⁻²³ Atm.

Table 5.3

Activation Energy of Conduction Under Various Experimental Conditions

Composition	Low temperature region				Intermediate temperature region				High temperature region			
	10^0	$10^{-0.7}$	10^{-5}	10^{-23}	10^0	$10^{-0.7}$	10^{-5}	10^{-23}	10^0	$10^{-0.7}$	10^{-5}	10^{-23}
'Pure' ThO$_2$	1.52	1.50	1.00	0.99	1.34	1.30	1.40	1.80	0.98	0.97	—	1.28
1 m/o CaO	1.58	1.65	—	1.05	1.30	1.38	1.52	1.90	1.13	1.20	1.36	1.42
2 m/o CaO	1.51	1.35	—	1.06	1.24	1.20	1.39	1.89	1.13	1.03	1.13	1.20
3 m/o CaO	—	—	—	1.06	1.18	1.20	1.39	1.57	1.13	1.03	1.10	1.12
4 m/o CaO	—	—	—	0.96	1.18	1.23	1.37	1.68	1.10	1.09	1.10	1.20
7 m/o CaO	—	—	—	0.96	1.20	1.20	1.37	1.57	0.92	1.13	1.07	1.16

those with lower dopant concentration (1-2 m/o CaO). The
activation energy of 'pure' thoria in this range, is 1.80 ev
and a value as high as 1.90 ev is obtained in 1 and 2 m/o CaO
specimens. However with increasing CaO content the value
decreases to around 1.6 ev. The activation energy in the high
temperature region varies between 1.12 ev to 1.42 ev but
does not follow any definite trend with the variation of CaO.

The temperature corresponding to the change over
from the intermediate temperature range to either low or high
temperature region changes with CaO content. In both these
cases the transition temperature decreases with increasing
CaO content. Table 5.4 gives a list of such transition
temperatures in samples containing varying quantities of CaO.
In 'pure' ThO_2, the low temperature break occurs at $900^{\circ}C$
but in a specimen containing 7 m/o the corresponding temperature
is $650^{\circ}C$. Similarly, the high temperature break occurs at
$1200^{\circ}C$ in 'pure' thoria and at $950^{\circ}C$ in 7 m/o CaO specimen.

It may be noted that the activation energy of
conduction in the different temperature ranges varies in
different ways with oxygen partial pressure and therefore the
shape of the log σT vs $1/T$ plots also changes accordingly.
The effect of P_{O_2} on the activation energy of specimens of
different compositions may be observed in Figs. 5.20 to 5.25 in
which the data for a particular composition obtained from
Figs. 5.16 to 5.19 have been reproduced with various oxygen

Table 5.4

Transition Temperatures at 10^{-23} atms.

Composition	High-Intermediate temperature region ($^{\circ}C$)	Intermediate-Low temperature region ($^{\circ}C$)
'Pure' ThO_2	1200	900
1 m/o CaO	1100	770
2 m/o CaO	1030	770
3 m/o CaO	1000	720
4 m/o CaO	950	700
7 m/o CaO	950	650
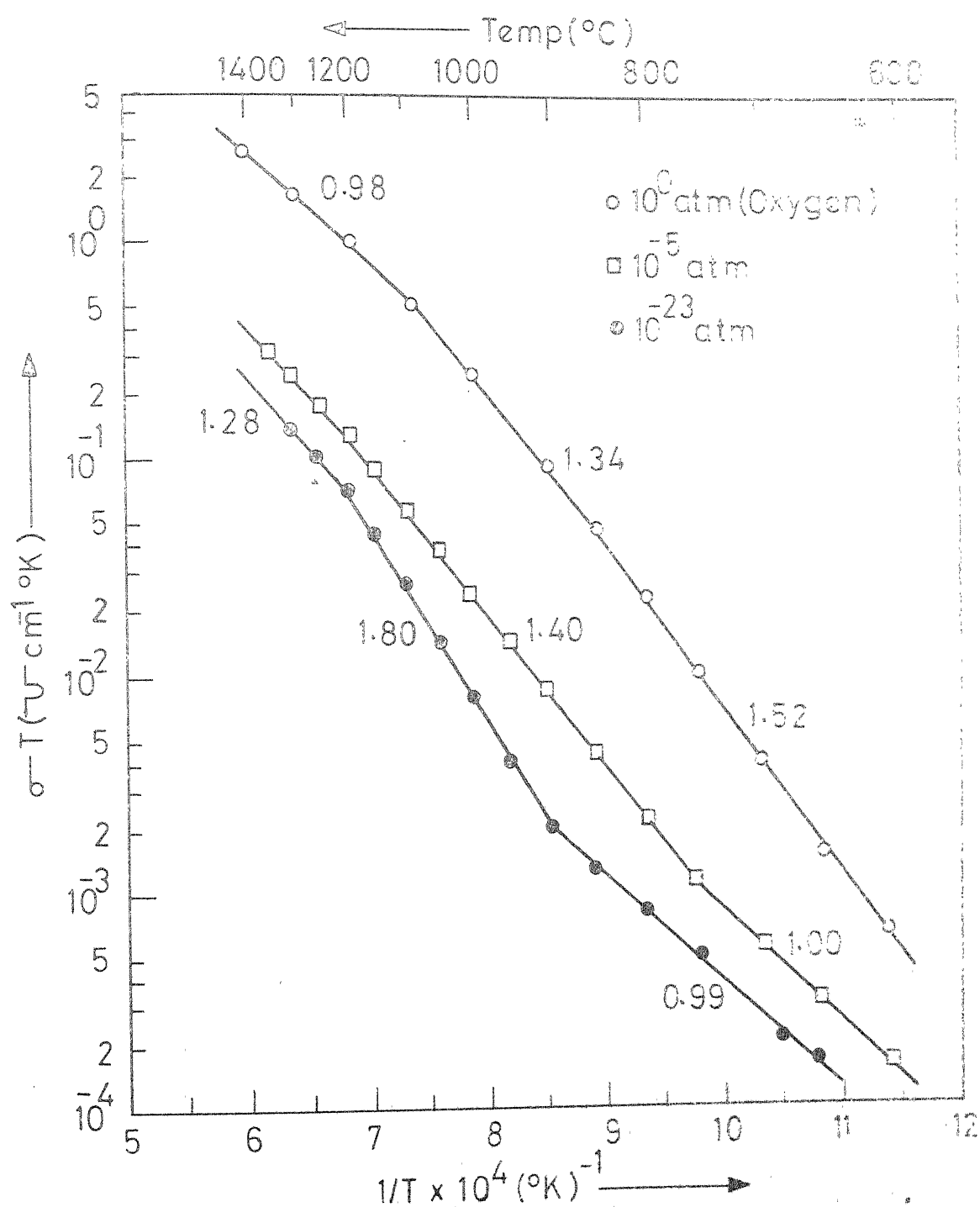
FIG. 5·20 ELECTRICAL CONDUCTIVITY OF PURE TnO₂ AS A
FUNCTION OF TEMPERATURE AT DIFFERENT OXYGEN
PARTIAL PRESSURES.
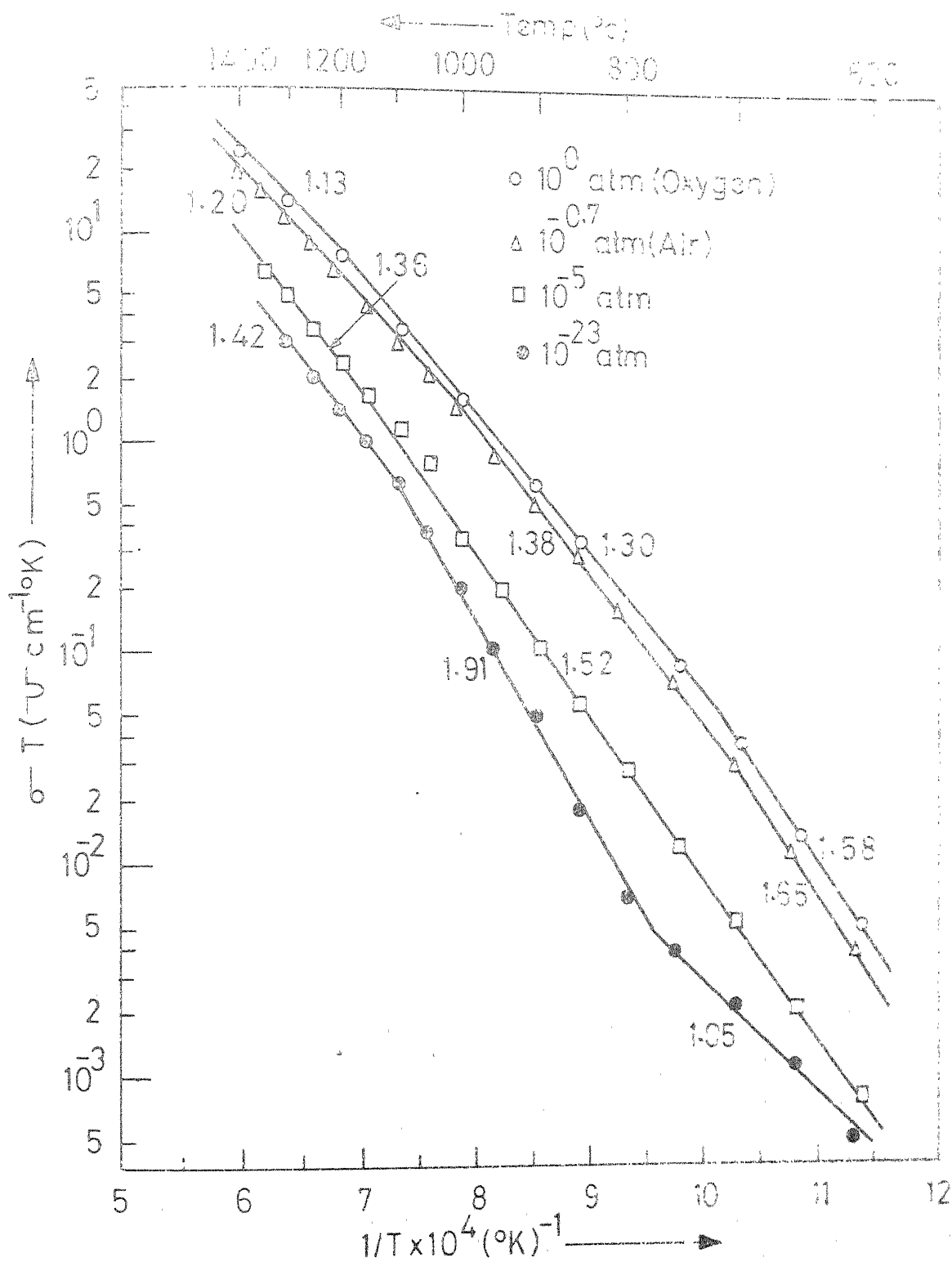
FIG.5.21 ELECTRICAL CONDUCTIVITY OF ThO₂-1mole% CaO
SAMPLE AS A FUNCTION OF TEMPERATURE AT
DIFFERENT OXYGEN PARTIAL PRESSURES
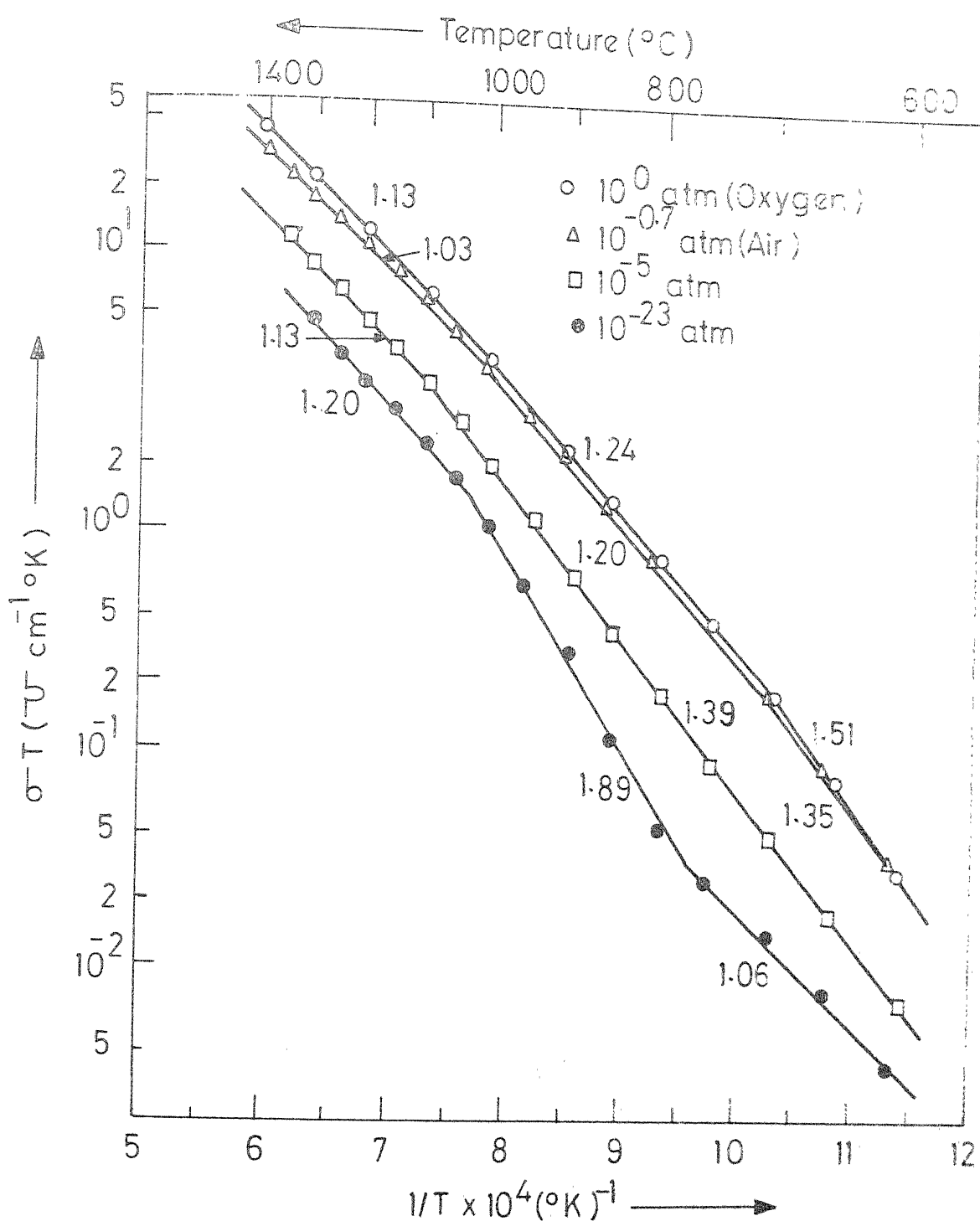
FIG. 5.22 CONDUCTIVITY OF ThO$_2$ - 2% CaO SPECIMEN AS A FUNCTION OF TEMPERATURE AT A DIFFERENT OXYGEN PARTIAL PRESSURES.
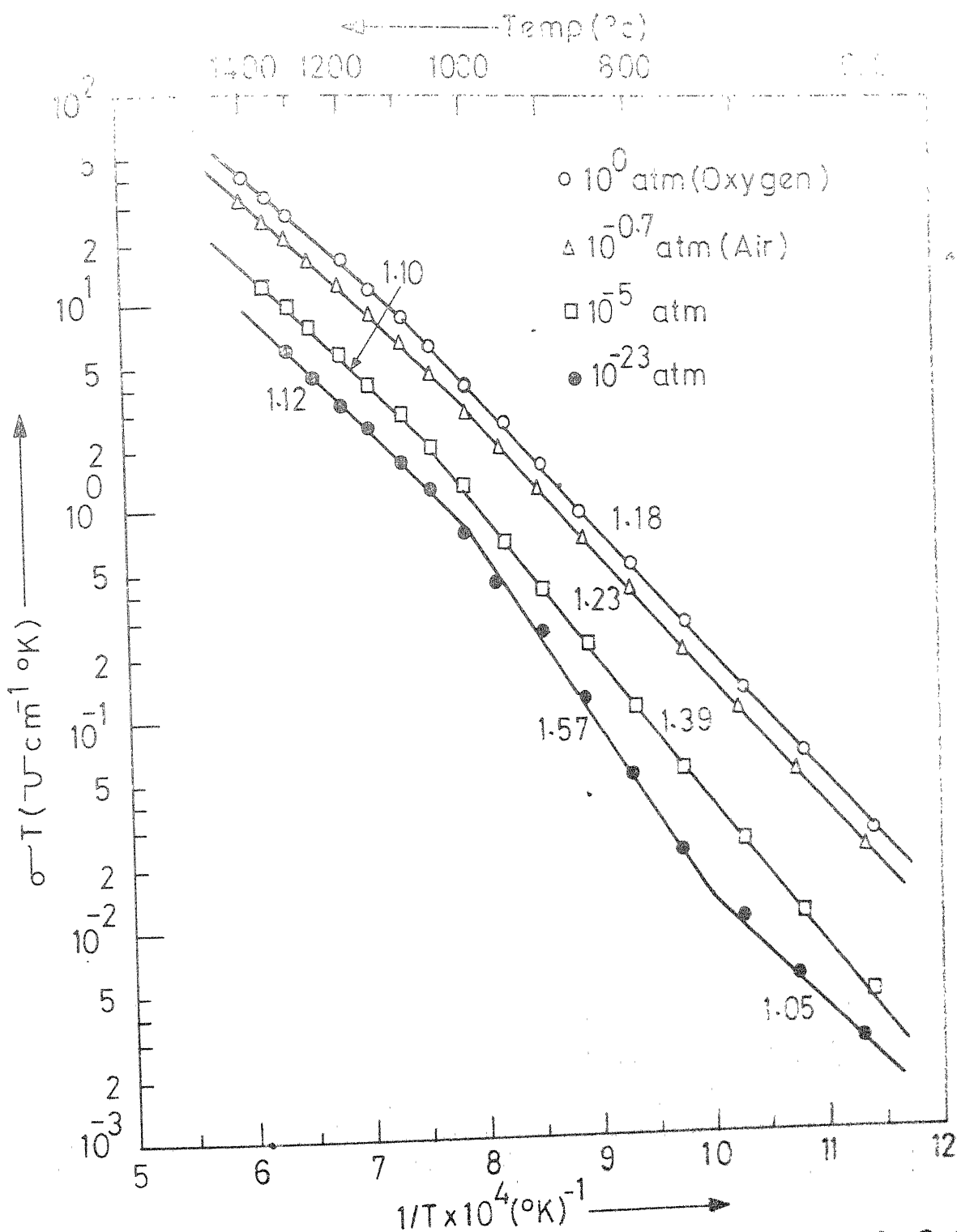
FIG.5.23 ELECTRICAL CONDUCTIVITY OF ThO$_2$-3 mole% CaO
SAMPLE AS A FUNCTION OF TEMPERATURE AT
DIFFERENT OXYGEN PARTIAL PRESSURES.
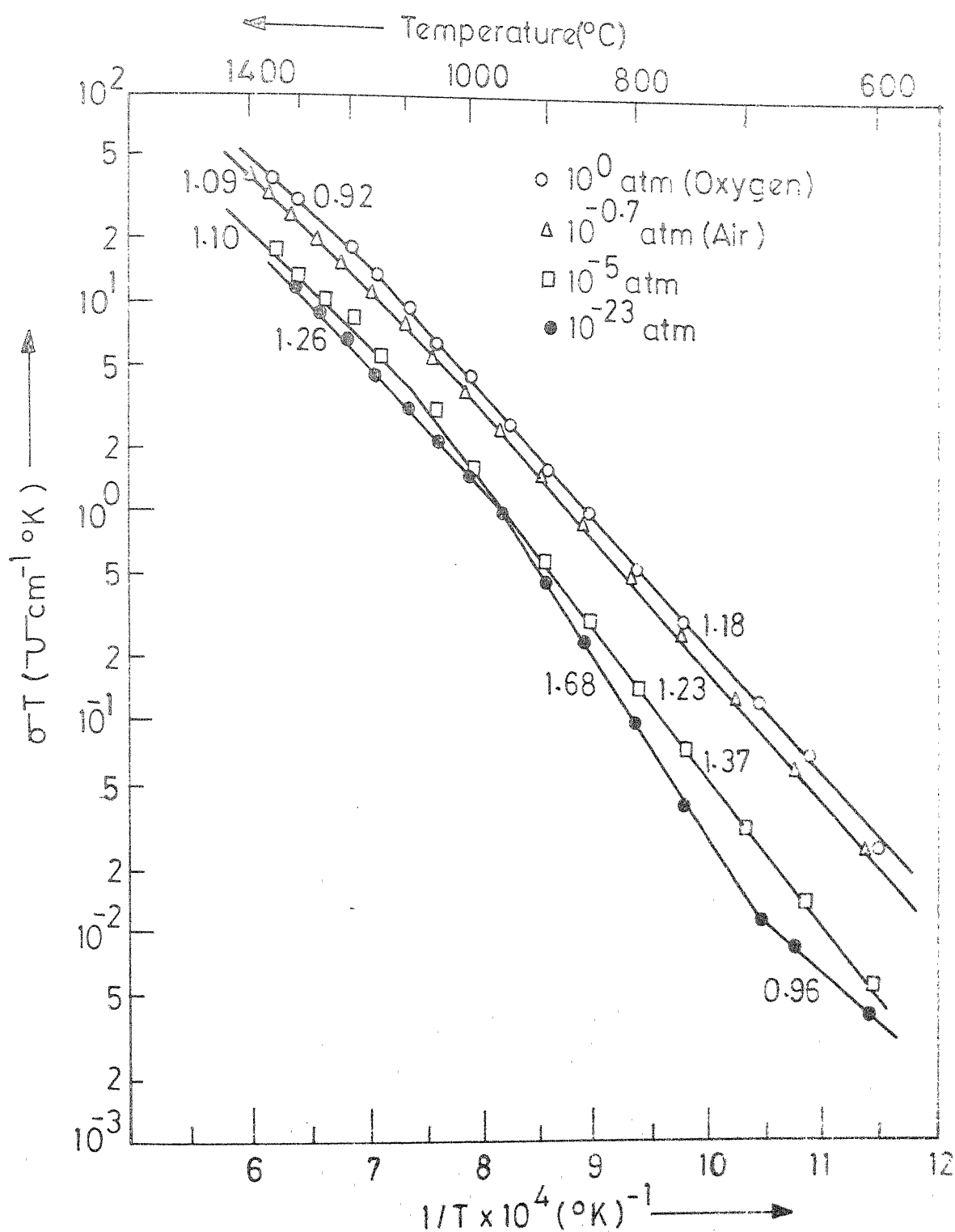
FIG. 5.24 ELECTRICAL CONDUCTIVITY OF ThO$_2$ -4 MOLE%
CaO SAMPLE AS A FUNCTION OF TEMPERATURE
AT DIFFERENT OXYGEN PARTIAL PRESSURES.
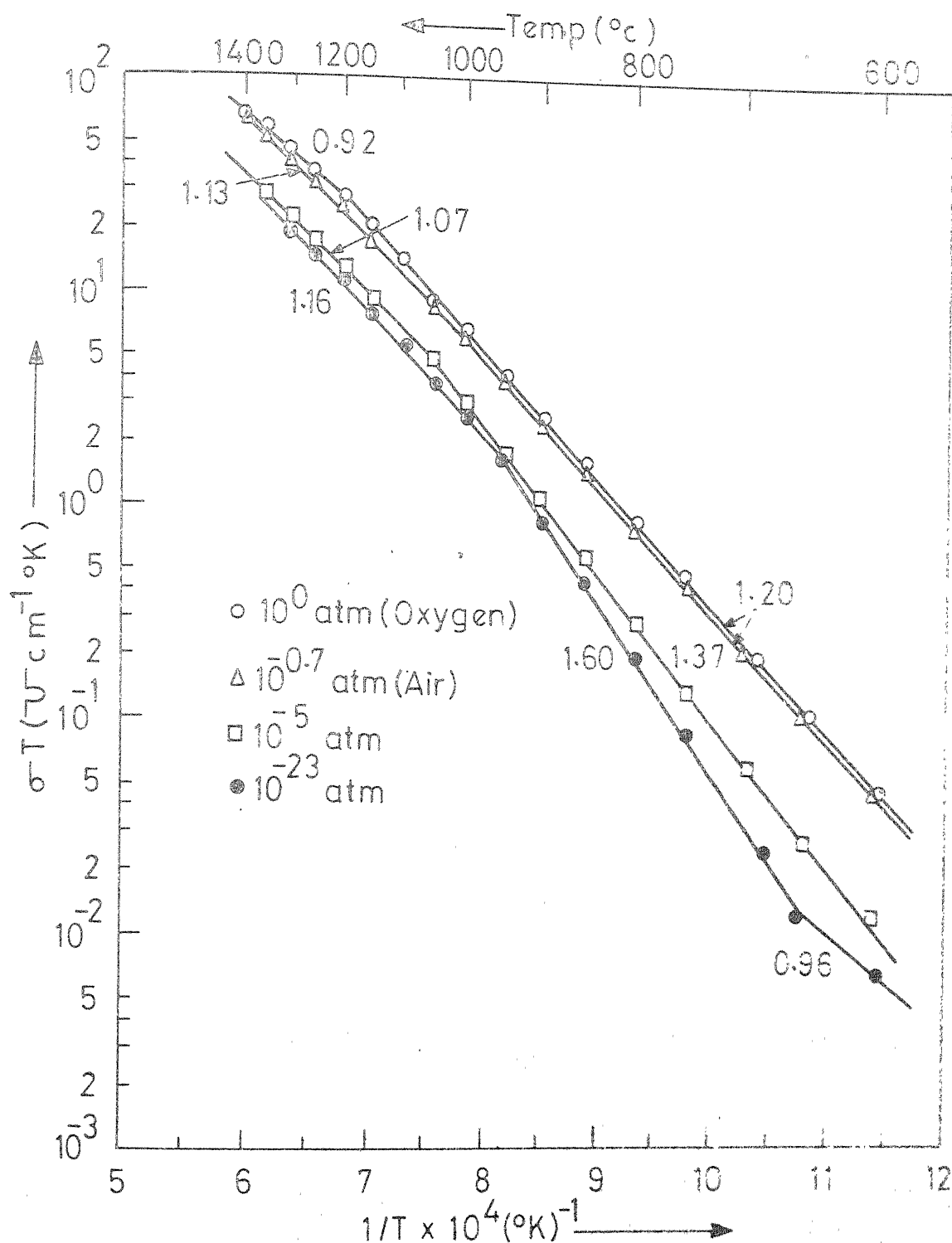
FIG.5.25 ELECTRICAL CONDUCTIVITY OF ThO₂ -7 mole % CaO
SAMPLE AS A FUNCTION OF TEMPERATURE AT
DIFFERENT OXYGEN PARTIAL PRESSURES.

partial pressures. The effect of P_{C_2} on the high temperature activation energy is insignificant compared to that in the intermediate and low temperature ranges. In the intermediate temperature range the activation energy in each of the specimens increases to a great extent with decreased oxygen partial pressure. While the high temperature break in the log σT vs $1/T$ plots for each of the specimens was observed at each of the oxygen partial pressures, the low temperature break was not present in the highly doped specimens (containing more than 2 m/o CaO) except at the partial pressure of 10^{-23} atm. On the other hand 'pure' thoria specimen shows the low temperature break at each oxygen partial pressure although it takes place at different temperatures. The activation energy in the low temperature range (whenever it is observed) is found to be strongly pressure dependent but contrary to that in the intermediate temperature range it decreases with decreasing P_{C_2}. It is interesting to note that the high temperature activation energy is always less than that in the intermediate temperature range while in the low temperature range it maintains a different relationship with that in the intermediate temperature range (Figs. 5.20 and 5.21). At high partial pressures, the low temperature activation energy is higher than that in the intermediate temperature range but with decreasing oxygen partial pressure the trend is reversed and the low temperature activation energy becomes less than that in the intermediate temperature range.

V-3. THERMOELECTRIC POWER

As a **supplement** to the electrical conductivity data, thermoelectric power measurements were carried out on a few of the samples. Seebeck coefficients of the lowest conducting 'pure' thoria and the highest conducting 7 m/o CaO specimens were measured in the temperature range of $600-1000^{\circ}C$ under fixed oxygen partial pressures. At each temperature and P_{O_2}, the EMFs across the specimens were measured with various temperature gradients and the Seebeck coefficient was calculated from the slope of the straight line obtained by plotting the EMF against temperature gradient. A set of such plots are shown in Fig. 5.26. The Seebeck coefficients obtained under various experimental conditions are presented in Fig. 5.27 in which Seebeck coefficient values have been plotted against temperature for two different compositions and partial pressures. It may be observed that the Seebeck coefficients in both the samples and partial pressures increase with increasing temperature especially in the low temperature range. However in most cases, a maximum value is obtained between $800-900^{\circ}C$. The drop at the high temperatures is not evident in all cases due to the limited data available. For each of the samples the Seebeck coefficient is smaller at lower oxygen partial pressures. At a fixed partial pressure, 7 m/o CaO specimen

133
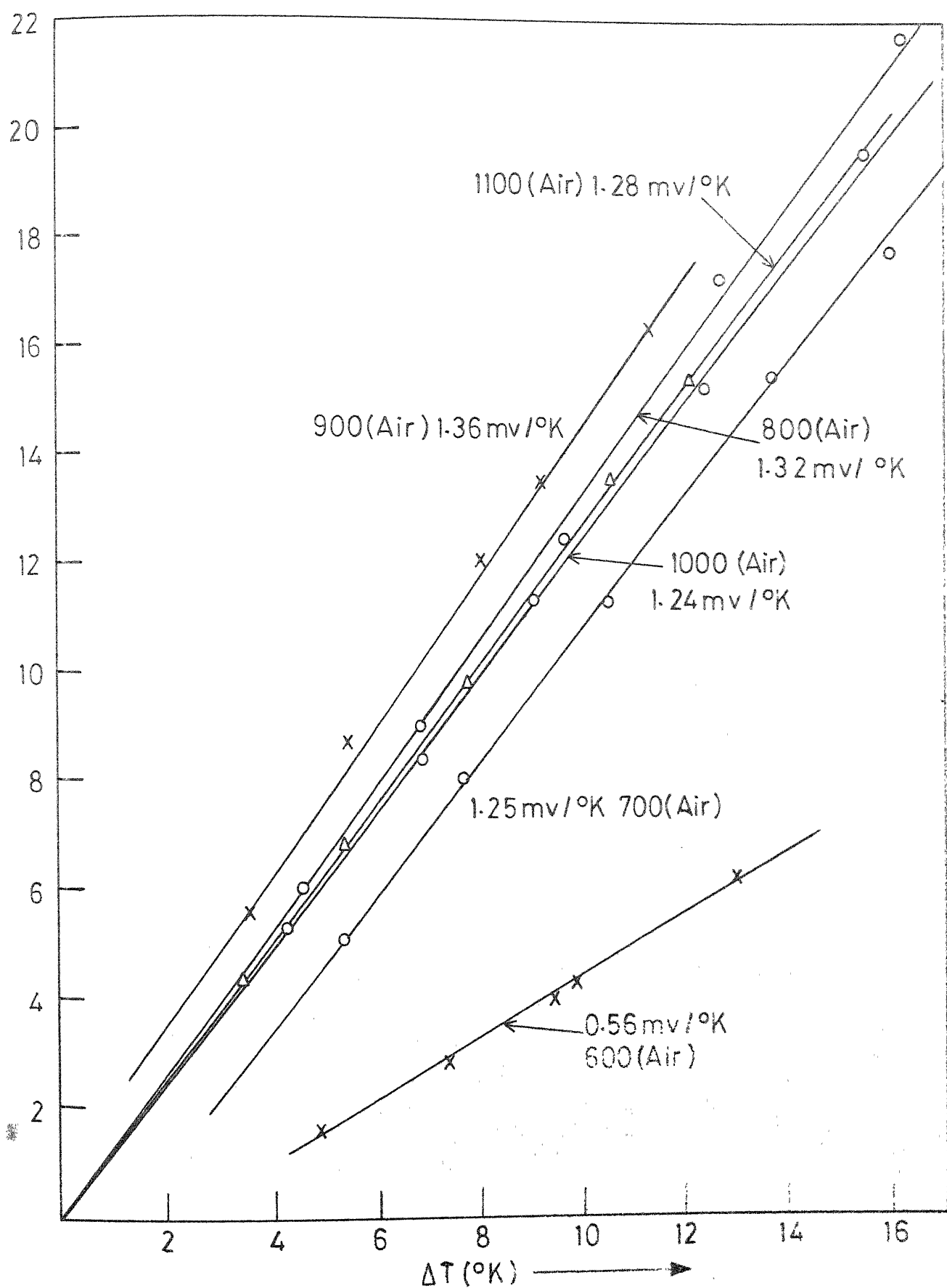
FIG.5.26 PLOT OF THERMAL EMF VS TEMPERATURE GRADIENT FOR 'PURE' ThO$_2$
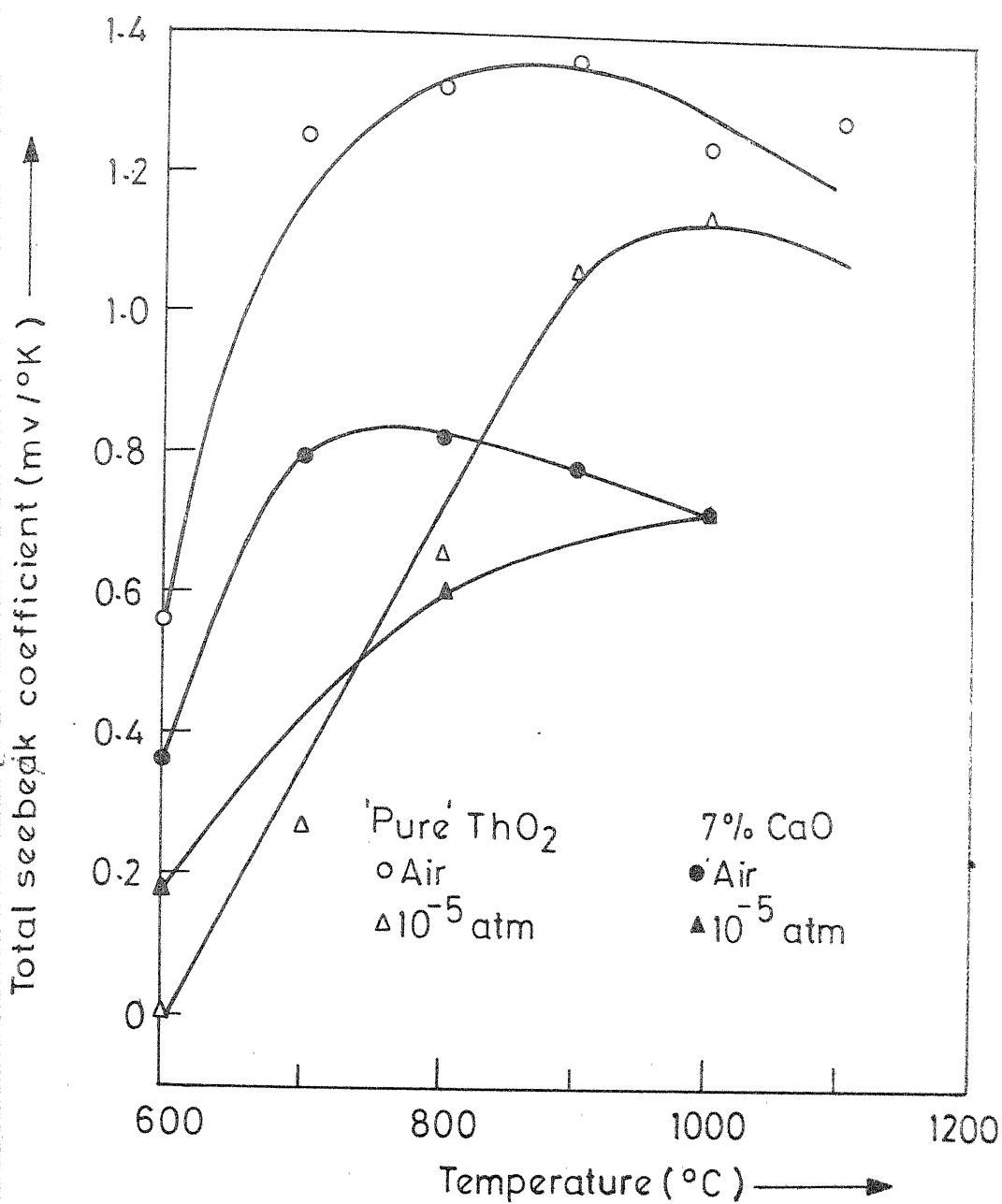
G.5.27 SEEBECK COEFFICIENT OF 'PURE' AND CaO-DOPED ThO₂ SPECIMENS

shows lower value than that of pure thoria. At a very low P_{O_2} (10^{-23} atm.) the Seebeck coefficient of 'pure' thoria was extremely small and therefore could not be measured with certainty. However, in the 7 m/o CaO specimen it was found to be 0.25 mV/^{O}K.

CHAPTER VI

DISCUSSION

VI-1. DEFECT STRUCTURE

To determine the defect structures from the conductivity data, it is customary to write the possible defect reactions under different experimental conditions, derive the P_{O_2} dependence of conductivity and compare the observed pressure dependence with the predicted variation. This has been done for 'pure' thoria and thoria doped with trivalent cation impurities by earlier investigators [52,87] and the probable defect structure has been postulated. Based on the principles described in Chapter I to derive the pressure dependence of defect concentrations in MO_2 type oxide having anti-Frenkel disorder, the defect concentration in ThO_2-CaO solid solutions in different P_{O_2} ranges may be calculated in the following way.

Substitution of Th^{4+} ions by Ca^{2+} ions results in an overall charge of -2 per each impurity cation site (Ca_{Th}'') and therefore assuming an anti-Frenkel type defect model, the neutrality condition may be written as

$$[h^\cdot] + 2[V_O^{\cdot\cdot}] = [e'] + 2[O_i''] + 2[Ca_{Th}''] \qquad (VI-1)$$

As in the case of $ThO_2-Y_2O_3$ solid solutions, the concentration of oxygen vacancies in a CaO doped ThO_2 lattice will be much greater than that of oxygen interstitials i.e. $[V_O^{..}] \gg [O_i'']$ and therefore the defect concentration is chiefly determined by the concentration of the impurity ions. In the intermediate oxygen partial pressure range, where ionic defect compensation takes place

$$[V_O^{..}] = [Ca_{Th}''] \tag{VI-2}$$

and in the high P_{O_2} range where the electron holes are the predominant defect

$$[h^.] = 2[Ca_{Th}''] \tag{VI-3}$$

However, in the low P_{O_2} range the neutrality condition remains as

$$[e'] = 2[V_O^{..}] \tag{VI-4}$$

Equations (I-6) to (I-13) are still valid for this system and therefore, applying the above mentioned neutrality conditions, the variation of the individual defect concentrations may be calculated as a function of oxygen partial pressure in the three different P_{O_2} ranges. It may be assumed that

$$[Ca_{Th}''] = [Ca]_T = [Ca] \tag{VI-5}$$

where $[Ca]_T$ is the total number of calcium ions.
At high P_{O_2} range:

$$[h^\cdot] = 2[Ca_{Th}''] = 2[Ca]_T \qquad (VI-6)$$

and

$$[e'] = K_2/2[Ca]_T \qquad (VI-7)$$

$$[V_O^{\cdot\cdot}] = \frac{4K_4[Ca]_T^2}{K_2^2} P_{O_2}^{-1/2} \qquad (VI-8)$$

and

$$[O_i] = \frac{K_3}{4[Ca]^2} P_{O_2}^{1/2} \qquad (VI-9)$$

At intermediate P_{O_2} range:

$$[V_O^{\cdot\cdot}] = [Ca]_T \qquad (VI-10)$$

$$[O_i''] = K_1/[Ca]_T \qquad (VI-11)$$

$$[h^\cdot] = \left(\frac{K_3[Ca]_T}{K_1}\right)^{1/2} P_{O_2}^{1/4} \qquad (VI-12)$$

and

$$[e'] = \left(\frac{K_4}{[Ca]_T}\right)^{1/2} P_{O_2}^{-1/4} \qquad (VI-13)$$

At low P_{O_2} range:

$$[e'] = 2[V_O^{\cdot\cdot}] \qquad (VI-14)$$

$$\therefore \quad [V_O^{\cdot\cdot}] = (K_4/4)^{1/3} P_{O_2}^{-1/6} \qquad (VI-15)$$

end
$$[e'] = 2(K_4/4)^{1/3} P_{O_2}^{-1/6} \qquad (VI-16)$$

$$[h^\cdot] = (K_2/2)(4/K_4)^{1/3} P_{O_2}^{1/6} \qquad (VI-17)$$

and
$$[O_i''] = K_1(4/K_4)^{1/3} P_{O_2}^{1/6} \qquad (VI-18)$$

The graphical representation of the above results
is shown in Fig. 6.1. It may be mentioned that unlike that
in pure oxides (Fig. 1.2a) the concentration of oxygen
vacancies and interstitials in the intermediate P_{O_2} range of
Fig. 6.1 are not equal. The concentration of oxygen
vacancies is much greater than that of interstitials and is
independent of P_{O_2}. At the high P_{O_2} range, the hole concen-
tration in a doped oxide is independent of P_{O_2} while
in the mixed conduction region it is proportional to $P_{O_2}^{1/4}$.
Therefore from the above analysis it is expected that in
the mixed conduction region on the high P_{O_2} side, the hole
conductivity will be proportional to $P_{O_2}^{1/4}$ and a plot of log σ
vs log P_{O_2} will yield a slope of 1/4. However, in the
present investigation the slope was found to be 1/5
for 'pure' thoria at all temperatures   (Fig. 5.3) and it
varied between 1/5 and 1/8 in Ca-doped ThO_2 specimens
depending upon the temperature and CaO content. Earlier,
Bransky and Tallan [87] also obtained the 1/5 pressure
dependence in 'pure' ThO_2 at 1000°C. These results might,
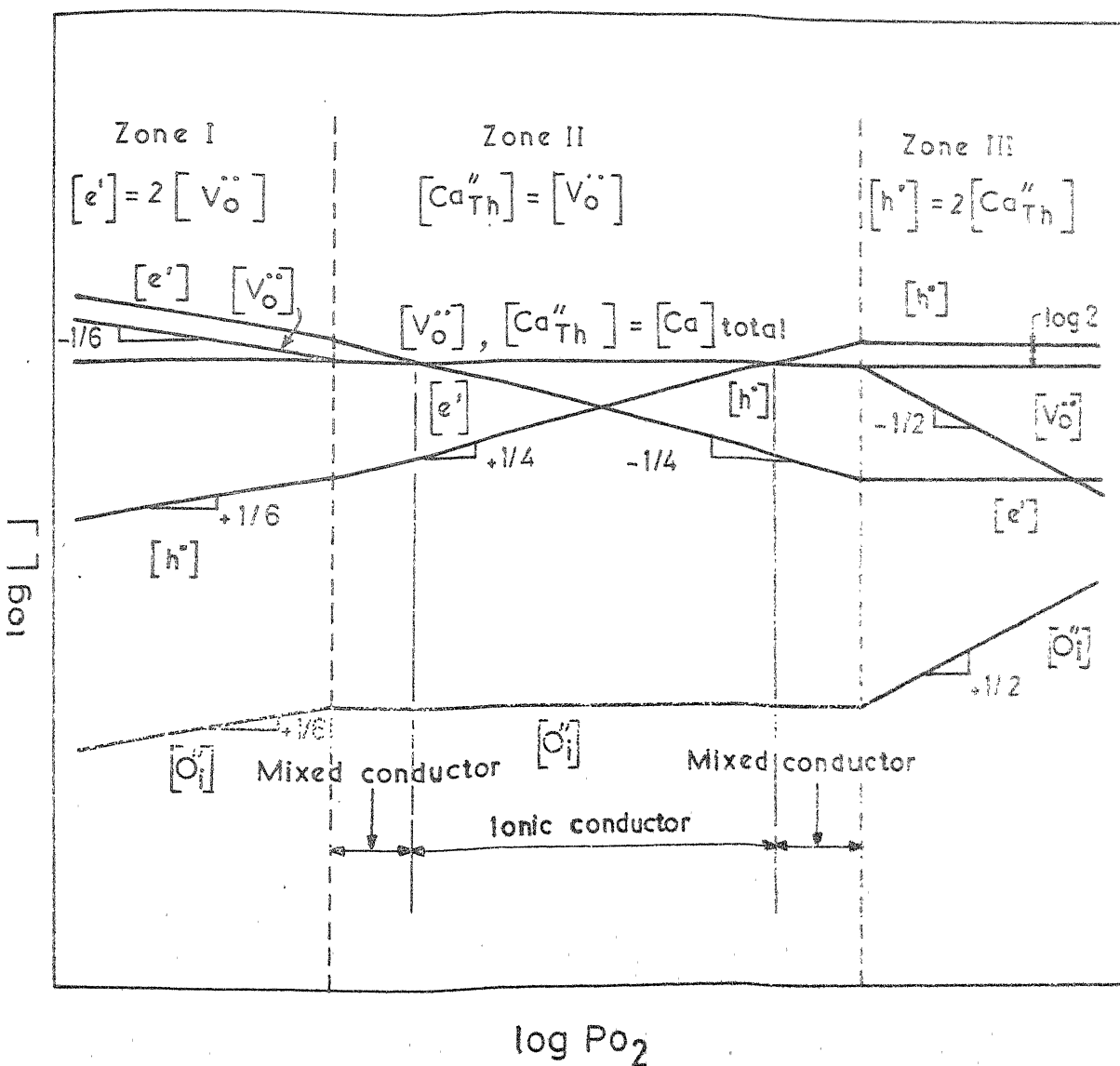
FIG. 6·1   DEFECT EQUILIBRIUM IN CaO DOPED ThO$_2$

therefore, suggest a defect model different from what has been discussed above.

It may be mentioned that the 1/5 pressure dependence may be expected on the basis of a defect reaction

$$O_2(g) \quad \rightleftharpoons \quad V_{Th}'''' + 4h^{\cdot} \qquad \text{(VI-19)}$$
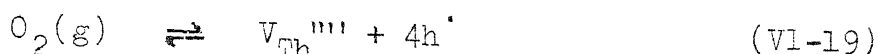
where predominant defects are fully ionized metal vacancies and electron holes and the charge neutrality condition is represented by

$$4[V_{Th}''''] \quad = \quad [h^{\cdot}] \qquad \text{(VI-20)}$$

The reaction constant of equation (VI-19) is given by

$$K_5 \quad = \quad [V_{Th}''''][h^{\cdot}]^4 \, P_{O_2}^{-1} \qquad \text{(VI-21)}$$

and the concentration of holes by

$$[h^{\cdot}] \quad = \quad (4K_5)^{1/5} \, P_{O_2}^{1/5} \qquad \text{(VI-22)}$$

While equation (VI-22) accounts for the observed pressure dependence in pure thoria, this model requires the presence of thorium vacancies for which there is no experimental evidence (e.g. density measurement). On the other hand, based on a detailed analysis of the experimental results obtained with 'pure' thoria, Bransky and Tallan [87] have pointed out that the observed 1/5 dependence may be expected from the defect model based on anti-Frenkel disorder as

proposed by earlier investigators. For this, they have
calculated the pressure dependence of total conductivity
instead of hole conductivity and assumed the presence of a
small amount of a trivalent cation impurity and also assumed
that the oxygen interstitials are the predominant defect in
the high oxygen partial pressure range. The charge neutrality
condition, therefore, is

$$[h^{\cdot}] + 2[V_O^{\cdot\cdot}] = [F_M'] + 2[O_i''] \qquad (VI-23)$$

where $[F_M']$ is the concentration of the impurity ion.
Based on this neutrality condition it may be shown [87] that

$$\frac{\sigma_T}{e[F_M']\mu_h} = x + \beta \left\{ (1-x) + [(1-x)^2 + \gamma]^{\frac{1}{2}} \right\} \qquad (VI-24)$$

where $\quad x = [h^{\cdot}]/[F_M'], \quad \beta = \mu_v/2\mu_h$

and $\quad \gamma = 16K_2/[F_M']^2 \qquad (VI-25)$

The pressure dependence of σ_T/σ_{ion} has been calculated as a
function of P_{O_2} taking arbitrary values of β and γ and it
has been found [87] that decreasing value of γ (i.e. increasing
impurity content) shifts the curve towards the higher partial
pressure range. To compare the experimental results, the
observed values of σ_T/σ_{ion} obtained in the present investigation
for 'pure' and CaO doped thoria specimens have been plotted
as a function of P_{O_2} (Fig. 6.2). The dashed curve in the
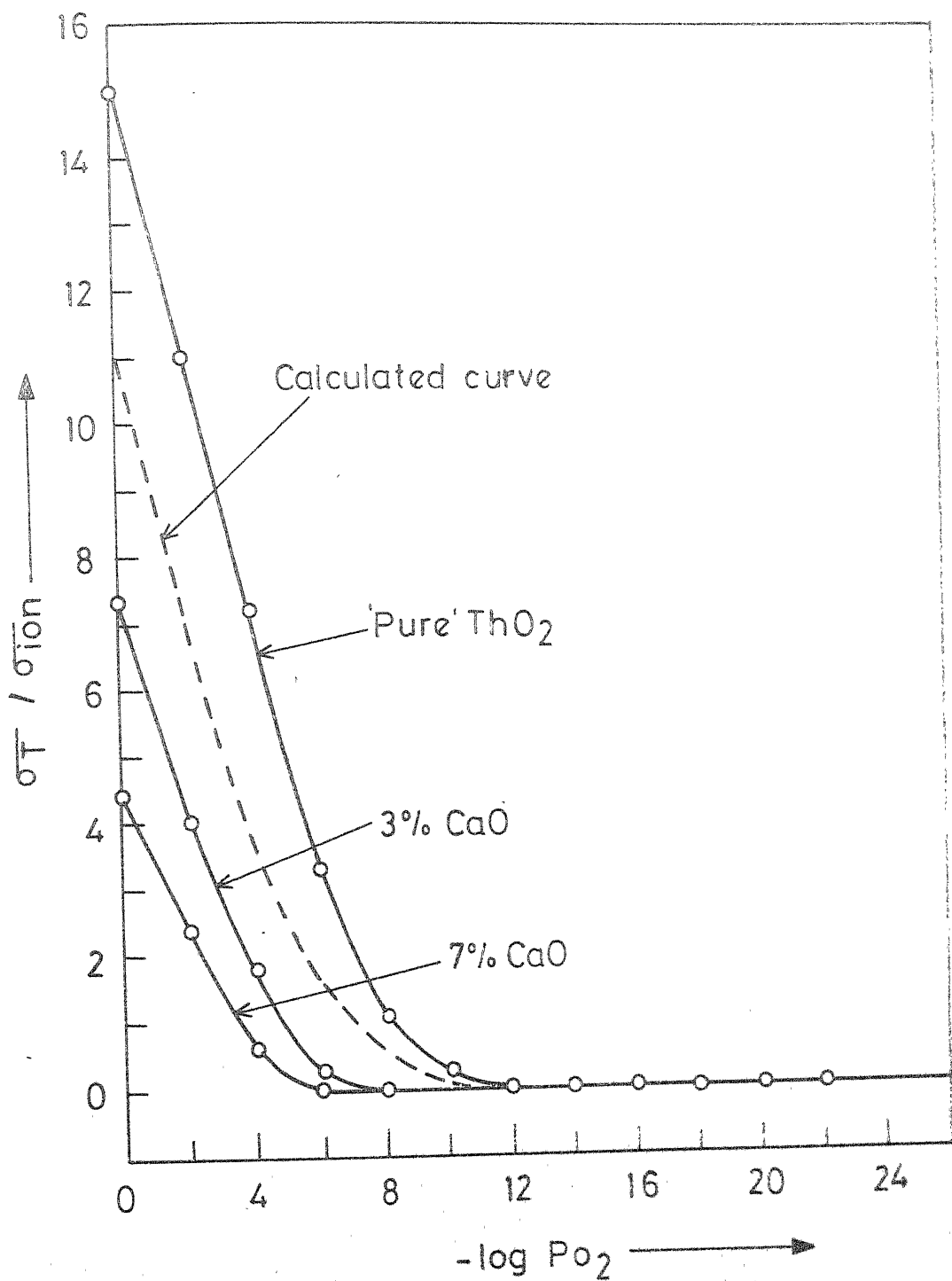
FIG. 6·2   COMPARISON OF THE OBSERVED PRESSURE
DEPENDENCE WITH THAT CALCULATED BY
ASSUMING $Po_2^{1/4}$ DEPENDENCE AT 1000°C.

figure is a reproduction of the theoretical pressure dependence calculated by Bransky and Tallan [87] for transition from pressure independent ionic conduction to $P_{O_2}^{1/4}$ dependent hole conduction, to which they fitted their experimental data on 'pure' thoria. It is interesting to note that the slopes of the experimental curves of the present investigation fit quite well with that of the calculated one. As expected, with increasing CaO content the curve is shifted to a higher partial pressure range because of the fact that with **increasing** impurity content the value of γ is decreased according the equation (VI-25). The experimental curve for 'pure' ThO_2 at each P_{O_2} is above the calculated one indicating higher hole conduction in the present sample than that of Bransky and Tallan [87]. This may be due to the presence of sufficient quantity of Fe ($\sim$ 90 ppm) in the starting thoria powders used in the present investigation and therefore increased the electronic conductivity of the specimen..

Based on their analysis, Bransky and Tallan have pointed out that the predicted 1/4 pressure dependence in the impurity controlled mixed conduction region may not be observed unless $\sigma_T/\sigma_{ion} \geqslant 10$. In the present investigation, the maximum values of σ_T/σ_{ion} obtained with 'pure' ThO_2 at different temperatures are between 10 and 30 (depending upon temperature). However, the number of experimental points

satisfying the condition $\sigma_T/\sigma_{ion} \geq 10$ are insufficient to observe the characteristic pressure dependence of 1/4. Similar arguments can be made for CaO-doped ThO$_2$ specimens for which the maximum values of σ_T/σ_{ion} are much less (between 3 and 10 depending upon composition and temperature) than that of 'pure' ThO$_2$, indicating that the experimental pressure range is very much within the transition zone and the observed linearity within a narrow P_{O_2} range does not correspond to the characteristic pressure dependence. The variation in the observed slopes are not due to the different defect structure but arises due to the differing experimental conditions.

VI-2. TRANSFERENCE NUMBER

The ionic transference number of ThO$_2$-CaO electrolytes in the mixed conduction region may be expressed as

$$t_{ion} = \frac{\sigma_{ion}}{\sigma_h + \sigma_{ion}}$$

$$= \frac{2\,|e|\,\mu_v[CaO]}{|e|\,\mu_h(K_3/K_1)^{\frac{1}{2}}[CaO]^{-\frac{1}{2}}\,P_{O_2}^{1/4} + 2\,|e|\,\mu_v[CaO]}$$

$$= \frac{1}{1 + \frac{1}{2}\beta_h(K_3/K_1)^{\frac{1}{2}}\,P_{O_2}^{1/4}\,[CaO]^{-\frac{1}{2}}} \qquad (VI-26)$$

In Figs. 5.14 and 5.15 it is evident that t_{ion} increases with decreasing P_{O_2}. 'Pure' thoria becomes fully ionic below an oxygen partial pressure of 10^{-12} atm. at $1000°C$ compared to 10^{-10} atm. obtained by earlier investigators. This is expected from the higher impurity concentration in the present material especially the presence of 90 ppm of Fe which is known to contribute to the electronic conductivity of the material.

As expected from equation (VI-26), addition of CaO increases the ionic transference number at each P_{O_2} and therefore improves the electrolytic behaviour of the solid solution. By addition of 7 m/o CaO, the conductivity of the solid solution becomes fully ionic below about 10^{-6} to 10^{-9} atm., depending on temperature and may be considered as a useful solid electrolyte below this partial pressure range. It may be pointed out that yttria doped thoria electrolytes are also useful in the same partial pressure range. The boundaries of the electrolytic domain on the high P_{O_2} side for pure and 7 m/o CaO doped thoria specimens as obtained in the present investigation, are shown in Fig. 6.3 along with those of yttria doped thoria electrolytes.

VI-3. IONIC CONDUCTIVITY

Assuming that the mobility of the defect is independent of its concentration, the ionic conductivity of
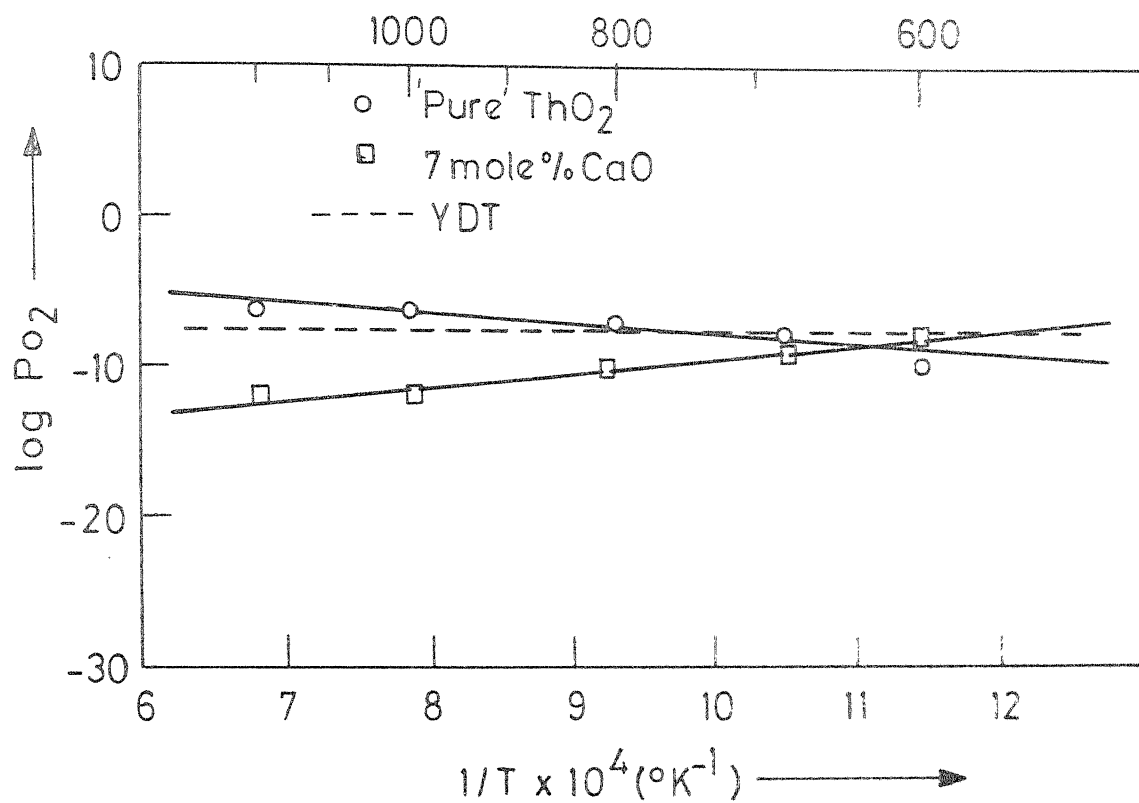
FIG.6·3   HIGH PRESSURE BOUNDARY OF THE ELECTROLYTIC
DOMAINS OF ThO$_2$ BASE ELECTROLYTES

ThO_2-CaO solid solution is expressed as

$$\sigma_{ion} = 2 |e| \mu_V [V_O^{\cdot\cdot}]$$

$$= 2 |e| \mu_V [CaO] \qquad\qquad (VI-27)$$

which shows that σ_{ion} is proportional to [CaO]. In Fig. 6.4, log ionic conductivity of ThO_2-CaO electrolytes has been plotted against percent anion vacancy as well as mole percent **impurity** concentration, along with that of ThO_2-$YO_{1.5}$ electrolytes obtained by different investigators. As expected, the conductivity increases with increasing CaO content. The conductivity of pure thoria obtained in the present investigation is lower than that obtained by the earlier investigators and is probably due to the lower density of the specimen used in the present investigation. A lower conductivity may be expected in a purer sample, but it is not the case in the present study. On the other hand, the conductivities of the ThO_2-CaO solid solutions are higher than the corresponding values obtained by Steele and Alcock [49] and are very close to that of ThO_2-$YO_{1.5}$ electrolytes measured by the same investigators. However the conductivity values of ThO_2-$YO_{1.5}$ electrolytes measured by Bauerle [54] are much higher than that measured by either Lasker and Rapp [52] or Steele and Alcock [49]. In the present investigation the ionic conductivities were not determined beyond 7 m/o CaO content. However, from the
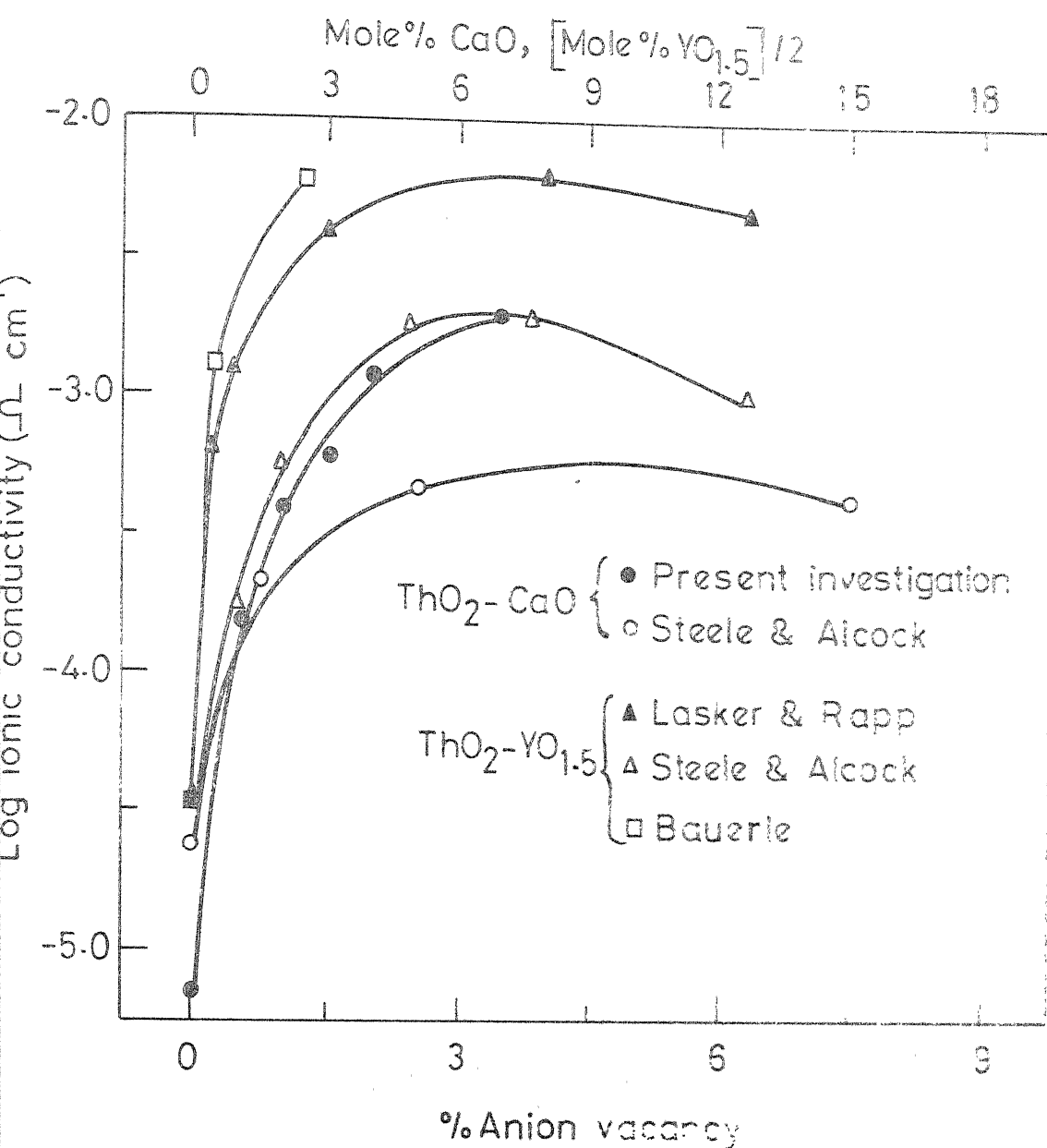
FIG.6·4 IONIC CONDUCTIVITY OF ThO$_2$ BASE ELECTROLYTES AS A FUNCTION OF % ANION VACANCY AT 1000°C.

conductivity values obtained in air (Fig. 5.2) it is expected that a slightly higher ionic conductivity may be obtained at around 10 m/o CaO. At higher concentrations the lowering of conductivity in both the systems may be attributed to the decreased mobility of the defects mainly due to impurity defect interactions.

It may be observed in Fig. 6.4 that the ionic conductivities of ThO_2-CaO electrolytes are in general slightly lower than the corresponding values in ThO_2-$YO_{1.5}$ electrolytes. The lower ionic conductivity in ThO_2-CaO electrolytes may be explained on the basis of impurity-vacancy interaction. In CaO doped samples, the impurity sites have an overall charge of -2 whereas in $YO_{1.5}$ doped specimens it has only one negative charge. However, oxygen vacancies have two positive charges and therefore in CaO doped lattice the impurity vacancy interaction is stronger than that in $YO_{1.5}$ doped lattice. Moreover, the defect pairs in ThO_2-CaO specimens are neutral and hence do not contribute to the electrical conductivity. Another probable reason for higher conductivity in ThO_2-$YO_{1.5}$ electrolytes could be the larger difference between the ionic radii of the impurity and the host cations (Y^{3+} = 1.07 A°, Th^{4+} = 1.15 A°). The Ca^{2+} ionic radius (1.10 A°) is relatively closer to that of Th^{4+} and therefore ThO_2-CaO lattice is more densely packed than that of ThO_2-$YO_{1.5}$ and the movement of ions becomes easier in the latter system. Such arguments have been earlier used by Tien and Subbarao [108] to explain the conductivity behaviour

of ZrO_2-CaO specimens.

To verify the dilute solution model in case of ThO_2-CaO solid solutions, log σ_{ion} has been plotted against logarithm of CaO concentration and is shown in Fig. 6.5. As expected, straight lines were obtained at different temperatures. At each temperature, the line is extrapolated to the ionic conductivity of 'pure' thoria and the corresponding CaO content has been determined. It has been found that the impurity content in the 'pure' thoria specimens is of the order of 0.1 to 0.2 m/o. This is in agreement with the chemical analysis (Table 3.1) which shows around 2000 ppm of Ca in the starting thorium oxide powder.

VI-4   GRAIN BOUNDARY CONDUCTION

It has been observed in the present investigation that the activation energy for ionic conduction in both 'pure' and CaO doped thoria specimens decreases in the low temperature region relative to that in the intermediate temperature region (Fig. 5.19). This lowering of activation energy may be attributed to the grain boundary effect.

In a polycrystalline material, grain boundaries are crystallographically disordered regions and have higher energies than the inside of the grains. The jump frequency of any atomic specie within the grain boundary region is an order of magnitude higher than that within the grain and as a result the diffusion through the grain boundaries is
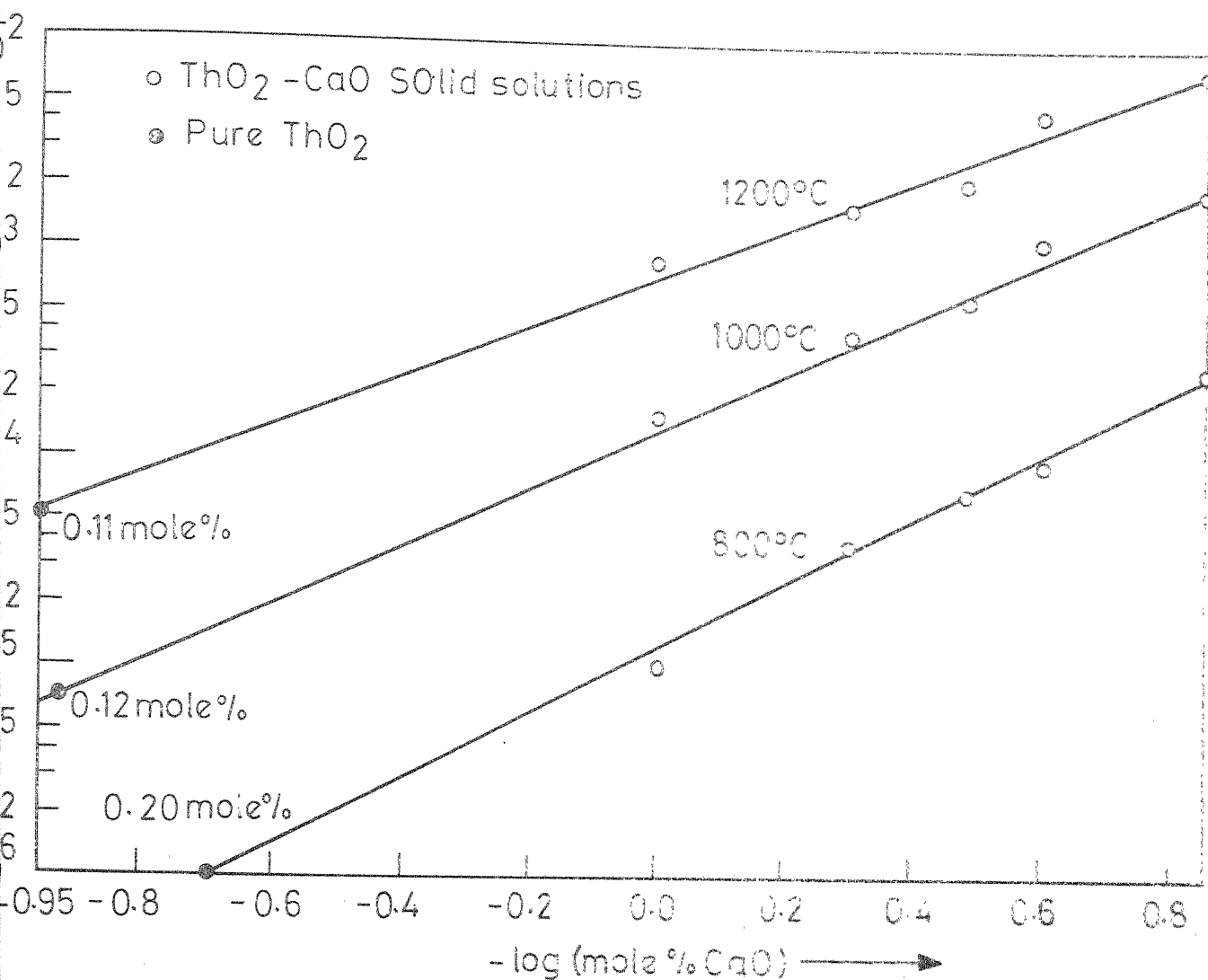
FIG. 6·5 LOG IONIC CONDUCTIVITY PLOTTED AGAINST LOG (————) AND EXTRAPOLATED TO THAT OF P·RE ————————— THE IMPURITY CONTENT OF 'PURE' ThO₂.

much easier than diffusion through the bulk. Enhanced
oxygen diffusion along grain boundaries or dislocations has
been observed in a number of oxide systems such as Al_2O_3
[123], MgO [124,125], Fe_2O_3 [126], CoO [127], $SrTiO_3$ [128] etc.
The activation energy for diffusion through the grain bounda-
ries is lower compared to that through the bulk. However,
since the volume of the grain boundary region is much smaller
than the bulk volume, the grain boundary contribution becomes
significant only at lower temperatures. Similar effects of
grain boundaries on the electrical conduction have been
observed in ionic conductors like alkali halides [129] and
CaO stabilized zirconia specimens [130]. The observed grain
boundary activation energy of 1.0 ± 0.05 ev in the present
investigation is very close to that of 0.96 ev obtained in
calcia stabilized zirconia specimens [130].

It may be noticed in Fig. 5.19 and Table 5.4 that
the effect of grain boundaries becomes observable at lower
temperatures as the CaO content of the specimen is increased,
indicating that the addition of impurities increases the con-
ductivity of the bulk more sharply than that of the grain
boundaries. This is in contrast to the fact that grain size
of the specimens decreases with increasing CaO content (Fig. 5.1).
However, it may be mentioned that the defect concentration at
the grain boundaries is much higher than that of the bulk
and the conductivity in this region does not follow the

dilute solution model i.e. the mobility of the defect is
lowered at high defect concentrations. Therefore the effect
of impurities is less prominent at the grain boundaries than
in the bulk. It may also be mentioned that either with
increasing CaO content or increasing P_{O_2} the total conductivity
of the specimens is increased and therefore the effect of
grain boundaries becomes prominent only at lower temperatures
(Figs. 5.19 and 5.20).

While the effect of grain boundary is quite distinct
at lower oxygen partial pressures where the samples are fully
ionic conductors and the conductivity values are relatively
lower, it is not so at higher pressures where the samples
are predominantly electron hole conductors. It may be observed
that between pure oxygen and 10^{-5} atm. of oxygen partial
pressure, the samples containing higher amount of CaO do
not show any change in activation energy in the low temperature
range (Figs. 5.16 to 5.18). On the other hand, pure ThO_2 and
1 m/o CaO sample show an increased activation energy compared
to that in the intermediate temperature range. A similar
behaviour has been observed in pure ZrO_2 by Kumar et al. [131]
who plotted electronic conductivity against $1/T$, and obtained
a higher activation energy of 86 Kcal/mole below $700^\circ C$
compared to 30.5 Kcal/mole above this temperature. It may
be mentioned that the activation energy for movement of
electron or electron holes through the grain boundaries is

expected to be higher than that through the bulk because
the grain boundaries can act as effective scattering centres
for the free electrons due to their highly disordered nature.
The effect of grain boundaries is predominant at low temper-
atures and therefore it increases the activation energy for
conduction in this temperature range. In case of samples
having higher percentages of CaO, not only the overall conduc-
tivity is higher but the ionic transference number is also more
and therefore it becomes difficult to observe such changes
in activation energy in these samples.

VI-5. ACTIVATION ENERGY IN THE HIGH AND INTERMEDIATE TEMPERATURE REGION

In the low temperature range the activation energy
for conduction was found to be either lower or higher than
that in the intermediate temperature range depending on the
partial pressure. On the other hand, the activation energy in
the high temperature region is observed to be lower than that
in the intermediate temperatures range for each of the oxygen
partial pressures and compositions studied (Figs. 5.16-5.19 and
Table 5.3). The change in activation energy is comparatively
more distinct at the lowest P_{O_2} value where the samples may
be considered as exclusive ionic conductors. Earlier studies
on 'pure' ThO_2 [87], pure HfO_2 [96] and yttria doped thoria
specimens [87] showed similar behaviour at high oxygen
partial pressures. However, Bransky and Tallan [87] have

observed that at low P_{O_2} (ionic conduction region) the activation energy at high temperature range is higher than that at intermediate temperatures.

In the intermediate and high temperature ranges, the activation energy for ionic transport in 'pure' ThO_2 observed in the present investigation is quite high compared to that obtained by earlier investigators, as shown below:

	High Temperature	Intermediate Temperature
High P_{O_2}	0.77 [87], 0.97 [P]	0.98 [87], 1.30 [P]
Low P_{O_2}	1.17 [87], 1.28 [P]	0.89 [87], 1.80 [P]

[P] represents present investigation.

In the ThO_2-CaO specimens, the activation energies in the high temperature range for different P_{O_2} and compositions vary between 1.0 and 1.4 ev while in the intermediate temperature range the values are 1.30 ± 0.1 ev in air and 1.75 ± 0.15 ev at a $P_{O_2} = 10^{-23}$ (Table 5.3). For the same system the activation energy values of 1.1 and 0.9 ev were obtained in air by Valchenkova and Palguev [116] and Ullmann [117] respectively. The results of the present investigation are thus in good agreement with the published results in air atmosphere. No earlier results are however available at lower partial pressures to compare with the present data.

The activation energies observed for the ThO_2-CaO compositions may also be compared with those reported in the ThO_2-$YO_{1.5}$ system. The activation energies observed are

1.12 to 1.38 [86], 1.2 [52] and 1.09 [49]. These values are close to those observed on CaO-doped ThO_2 specimens measured in air over a wide temperature range but are lower than the values observed in the ionic conduction region at intermediate temperature.

The high values of activation energy in the intermediate temperature region compared to those at high temperatures may be explained if one considers that the oxygen vacancies in this temperature range are associated with the impurity cations. As has been mentioned earlier (Section VI-4), the formation of such defect complexes is favoured in a ThO_2-CaO lattice due to a favourable charge distribution between the oxygen vacancies and the Ca^{2+} ions. Dielectric and mechanical relaxation experiments have earlier indicated the presence of such defect complexes in CaO doped ThO_2 specimens [115]. The high value of activation energy (1.80 ev) in the intermediate temperature range in pure thoria of the present investigation compared to that of Bransky and Tallan [87] may be attributed to the presence of a significant quantity of CaO (Table 3.1) in the starting material.

It may also be noticed in Table 5.3 that the activation energy for ionic conduction (i.e. at $P_{O_2} = 10^{-23}$ atm.) remains high and nearly constant (1.80-1.90 ev) in the intermediate temperature region upto 2 m/o CaO and decreases thereafter (Fig. 5.19). These results may be interpreted as

follows: The introduction of increasing amounts of CaO in ThO_2 lattice tends to increase the concentration of defect complexes referred to above which in turn lead to an increase in activation energy for defect migration. However, at higher CaO contents the lattice becomes more open with a larger number of vacancies and consequently the activation energy for conduction is reduced.

By increasing oxygen partial pressure the contribution from the hole conductivity is increased and therefore the observed activation energy is less representative of the motion of defect complexes.

In the high temperature region, the activation energies are much closer to those observed earlier in pure ThO_2 and $ThO_2-YO_{1.5}$ solid solutions and it may be expected that the defects are in the dissociated state at these high temperatures. The difference between the activation energies in the high and intermediate temperature ranges, in that case, gives the binding energy for the defect complex and is found to vary between 0.4 to 0.5 ev for different CaO-doped ThO_2 specimens. These values may be compared with those of 0.3-0.4 ev [132] obtained in alkali halides with divalent impurities. For oxide systems, a higher value of binding energy is expected due to the higher charges associated with the defects.

In Fig. 5.19 and Table 5.4, the transition temperature decreases with increasing CaO content. This is in contrast to the fact that with increasing CaO content the defect concentration increases and the transition should take place at higher temperatures. However, the observed lowering of transition temperature may be due to the relative changes of activation energy in the two temperature ranges.

VI-6. THERMOELECTRIC POWER

As has been mentioned earlier, the total Seebeck coefficient of a mixed conductor is given by

$$\alpha_T = t_{ion} \cdot \alpha_{ion} + t_h \alpha_h \tag{VI-28}$$

Assuming both t_{ion} and t_h to be independent of temperature, the temperature dependence of α_T may be given by

$$d(\alpha_T)/dT = t_{ion} \, d\alpha_{ion}/dT + t_h \, d\alpha_h/dT \tag{VI-29}$$

α_h in a p-type semiconductor is given by

$$\alpha_h = \frac{k}{e} [\ln \frac{p_o}{p} + A] \tag{VI-30}$$

where p_o is the effective density of states at the transport level and A is a term connected with the kinetic energy of the charge carrier and is generally small and independent of temperature. The temperature dependence of α_h may be expressed as

$$\frac{d(\alpha_h)}{dT} = -\frac{k}{e}\frac{d(\ell_n \, p)}{dT} \qquad (VI-31)$$

Therefore the value of α_h decreases with increasing temperature. On the other hand, α_{ion} is comparatively less dependent on temperature and its value is much smaller compared to that of α_h. At $1000^{\circ}C$ and 10^{-1} atm. of oxygen partial pressure, the estimated α_i for 'pure' ThO_2 is 0.45 mV/$^{\circ}$K compared to 1.4 mV/$^{\circ}$K for α_h [87]. However, Tallan and Bransky [70] have observed a slow increase of α_i as a function of temperature. In the present investigation, the value of α_i for 'pure' ThO_2 could not be measured due to its very low ionic conductivity at low temperatures. However, for 7 m/o CaO it was found to be 0.25 mV/$^{\circ}$K.

The observed temperature dependence of α_T in the present investigation may be explained if one considers the temperature dependence of t_{ion} under different experimental conditions. The variation of t_{ion} for 'pure' ThO_2 and 7 m/o CaO specimen as a function of temperature and P_{O_2} is shown in Fig. 6.6.

Lowering of α_T with increasing temperature, was observed in the temperature range (above $800^{\circ}C$) where both (Fig. 5.27) t_{ion} and t_h remains constant. This is consistent with the predicted temperature dependence of α_h, the value of α_{ion} to being small and comparatively insensitive/temperature in this
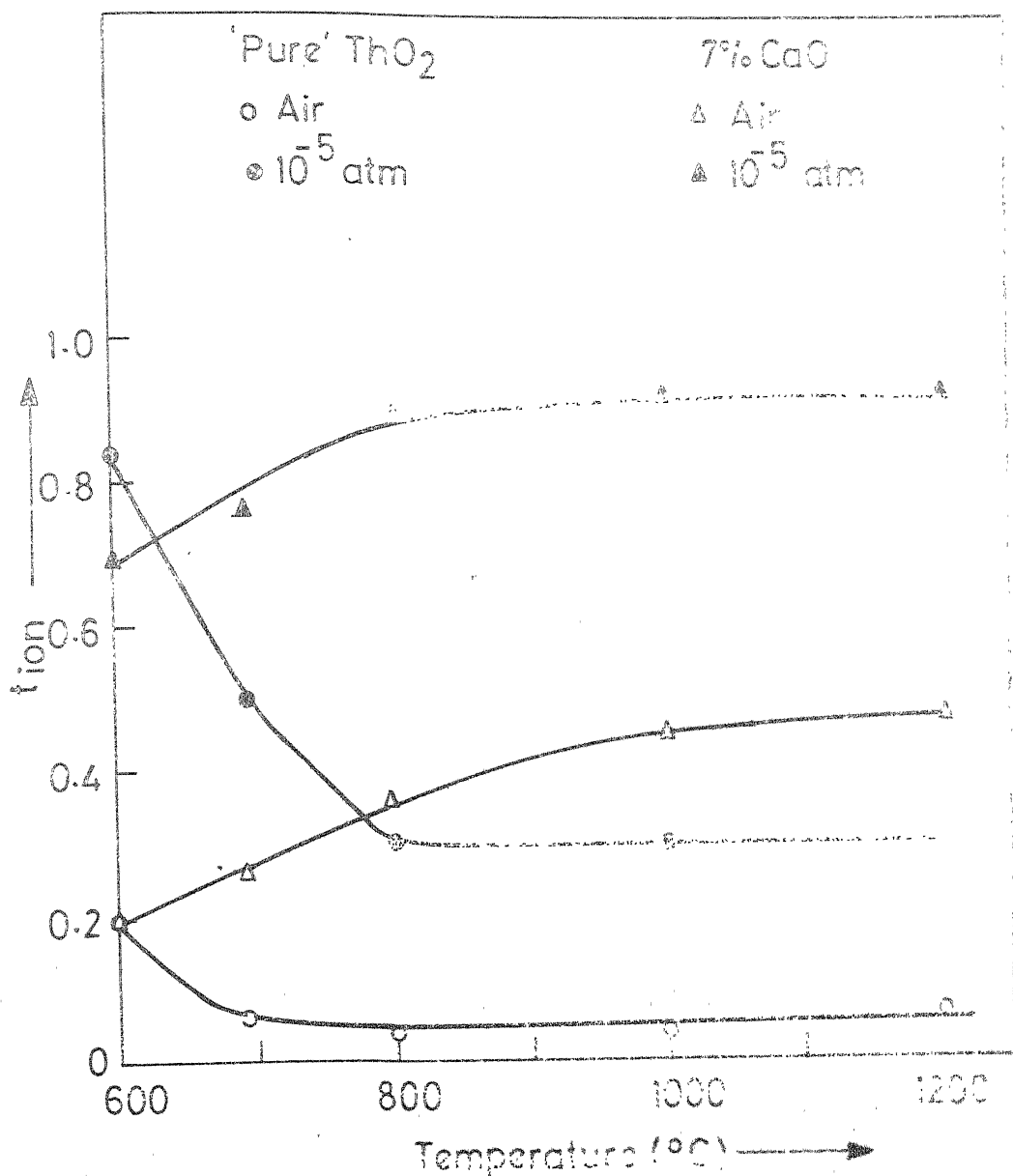
FIG.6·6   IONIC TRANSFERENCE NUMBERS AS A FUNCTION OF TEMPERATURE.

CHAPTER VII

CONCLUSIONS

The electrical conductivity as well as thermo-
electric power measurements on pure and CaO-doped thoria
ceramic electrolytes have been carried out under different
oxygen partial pressures and temperatures. The oxygen partial
pressure inside the specimen holder tube was maintained with
the help of a solid electrolyte oxygen pump and probe. As
a result of this investigation the following conclusions
may be arrived at:

1) Addition of CaO to ThO_2 results in a cubic
fluorite type solid solution. Based on X-ray and metallographic
examination, the solubility limit of CaO in ThO_2 is placed at
about 10 m/o.

2) At all temperatures and for all compositions
the total electrical conductivity decreases with decreasing
oxygen partial pressure down to $P_{O_2} = 10^{-6}$ to 10^{-10} atm. and
thereafter remains invariant with oxygen activity. This is
interpreted as indicating electron hole conduction in the oxygen
rich region and purely oxygen ion conduction through a vacancy
mechanism in the low oxygen pressure region. The slope of
the $\log\sigma$ vs $-\log P_{O_2}$ was utilized to arrive at the above
defect structure.

3) Ionic conductivity increases with increasing CaO content following the dilute solution model. At a given temperature and oxygen partial pressure, the ionic transference number increases with increasing CaO content.

4) The variation of conductivity with reciprocal temperature led to three different slopes in the different temperature regions. These slopes were also a function of composition and at low and intermediate temperatures also of P_{O_2}. The conductivity in the low temperature region is influenced by grain boundary effects while in the intermediate region a defect complex formation appears to be operative. The conductivity at the highest temperatures then represents the behaviour due to dissociated defects.

5) Thermoelectric power was found to increase with increasing temperature upto $800-900^{\circ}C$ and decreased slightly thereafter. The value of the Seebeck coefficient was also a function of composition and oxygen partial pressure. These results are consistent with the postulated defect structure and observed electrical conductivity.

6) An oxygen pump based on zirconia solid electrolyte may be used to maintain the required oxygen activity in a flowing inert gas-oxygen mixture. However, the control becomes difficult at some intermediate P_{O_2} range which depends upon the experimental parameters. These oxygen pumps are not useful above about $900^{\circ}C$ due to a significant oxygen leakage through the electrolyte tube.

REFERENCES

1. C. Wagner, Z. Physik. Chem., Abt. B 21, 25 (1933).

2. A.B. Lidiard in Handbuch der Physik, ed. S. Flügge, Springer-Verlag, Berlin, 20, 246 (1957).

3. L.W. Barr and A.B. Lidiard in Physical Chemistry: An Advanced Treatise, eds. H. Eyring, D. Henderson and W. Jost, Academic Press, New York, Vol. 10, p. 151 (1970).

4. P. Supitz and J. Teltow, Phys. Stat. Sol., 23, 9 (1967).

5. H. Dünwald and C. Wagner, Z. Physik. Chem., Abt. B 17, 467 (1932).

6. H. Dünwald and C. Wagner, Z. Physik. Chem., Abt. B 22, 212 (1933).

7. H.H.V. Baumbach and C. Wagner, Z. Physik. Chem., Abt. B 22, 199 (1933).

8. H.H.V. Baumbach, H. Dünwald and C. Wagner, Z. Physik. Chem., Abt. B 22, 226 (1933).

9. C. Wagner, Z. Physik. Chem., Abt. B 22, 181 (1933)

10. C. Wagner, Z. Elektrochem. angew. Physik. Chem., 39, 543 (1933).

11. H.H.V. Baumbach and C. Wagner, Z. Physik. Chem., Abt. B 24, 59 (1934).

12. K. Nagel and C. Wagner, Z. Physik. Chem., Abt. B 25, 71 (1934).

13. C. Wagner, Physik. Z., 36, 721 (1935).

14. C. Wagner and E. Koch, Z. Physik. Chem., Abt. B 32, 439 (1936).

15. J. Gundermann, K. Hauffe and C. Wagner, Z. Physik. Chem., Abt. B 37, 148 (1937).

16. J. Gundermann and C. Wagner, Z. Physik. Chem., Abt. B 37, 155, 157 (1937).

17. E. Koch and C. Wagner, Z. Physik. Chem., Abt. B 38, 295 (1937).

18. C. Wagner and H. Hammen, Z. Physik. Chem., Abt. B 40, 197 (1938).

19. K. Kiukkola and C. Wagner, J. Electrochem. Soc., 104, 379 (1957).

20. H. Peters and H. Möbius, Z. Physik. Chem., 209, 298 (1958).

21. H. Peters and G. Mann, Z. Elektrochem. Ber. Bunsenges. Physik. Chem., 63, 244 (1959).

22. H. Schmalzried, Z. Physik. Chem. N. F., 25, 178 (1960).

23. H. Schmalzried, Z. Elektrochem., 66, 572 (1962).

24. W.D. Kingery, J. Pappis, M.E. Doty and D.C. Hill, J. Amer. Ceram. Soc., 42, 393 (1959).

25. N.M. Tallan, R.W. Vest and H.C. Graham, in Material Science Research, ed. H. Otto and S. Locke, Vol. 2, p. 33, Plenum Press,(1965).

25a. B.C.H. Steele in Electromotive Force Measurements in High-temperature Systems, ed. C.B. Alcock, American Elsevier Publ. Co., p. 109, (1968).

25b. L. Heyne in Mass Transport in Oxides, eds. J.B. Wachtman Jr. and A.D. Franklin, N.B.S. Special Publication No. 296, p. 149 (1968).

26. R.A. Rapp in Thermodynamics of Nuclear Materials 1967, International Atomic Energy Agency, Vienna, p. 359, (1968).

27. T.H. Etsell and S.N. Flengas, Chem. Rev., 70, 339 (1970).

28. J. Weissbart and R. Ruka, J. Electrochem. Soc., 109, 723 (1962).

29. R.A. Rapp and D.A. Shores in Techniques of Metal Research, Vol. 4, Part 2, ed. R.A. Rapp, Interscience Publishers, New York, p. 123 (1970).

30.   J. Weissbart and R. Ruka, Rev. Sci. Instr., 32, 593 (1961).

30a.   R.J. Fruehan, L.J. Martonik and E.T. Turkdogan, Trans.
        AIME, 245, 1501 (1969).

31.   K. Goto and Y. Matsushita, J. Japan Iron and Steel Inst.,
        50, 1821 (1964); 51, 1825 (1965).

32.   H.H. Möbius, Z. Physik. Chem., 230, 396 (1965).

33.   R. Szwarc, K.E. Oberg and R.A. Rapp, High Temp. Sci.,
        4, 347 (1972).

33a.   T.A. Ramanarayanan and R.A. Rapp, Met. Trans., 3, 3239
        (1972).

34.   W. Pluschkell and H.J. Engell, Metallk., 56, 451 (1965).

35.   C.B. Alcock and T.N. Belford, Trans. Faraday Soc., 60,
        822 (1964).

36.   T.N. Belford and C.B. Alcock, Trans. Faraday Soc., 61,
        443 (1965).

37.   W.A. Fischer and W. Ackermann, Arch. Einsenhut-Henwesen,
        36, 643, 695 (1965); 37, 43, 697, 779 and 959 (1966).

38.   K.E. Oberg, L.M. Friedman, R. Szwarc, W.M.Boorstein and
        R.A. Rapp, J. Iron Steel Inst., 210, 359 (1972).

38a.   K.E. Oberg, L.M. Friedman, W.M.Boorstein and R.A. Rapp,
        Met. Trans., 4, 61 (1973).

39.   J. Osterwald, Z. Physik. Chem., 49, 138 (1966).

40.   H. Rickert, Electrochim. Acta., 11, 83 (1966).

41.   D. Yuan and F.A. Kröger, J. Electrochem. Soc., 116,
        594 (1969).

42.   C.J. Mogab, Rev. Sci. Instr., 43, 1605 (1972).

43.   C.J. Mogab, J. Vac. Sci. Tech., Sept. (1973).

44.   Y.K. Agrawal, D.W. Short, R. Gruenke and R.A. Rapp,
        J. Electrochem. Soc., 121, 357 (1974).

45.   C.B. Choudhary, H.S. Maiti and E.C. Subbarao, Proceedings
        of the Conference on Thermodynamic Measurements in
        Metallurgy, Kanpur, (1973).

46.   W.H. Davenport, S.S. Kistler, W.M. Wheildon and
        O.J. Whittemore, J. Amer. Ceram. Soc., 33, 333 (1950).

47. M.H. Leipold and J.L. Taylor in <u>Temperature, Its</u>
    <u>Measurement and Control in Science and Industry,</u>
    <u>3</u>, Pt. 2, Amer. Inst. of Physics, Reinhold, (1962).

48. W.T. Lindsay, Jr. and R.J. Ruka, Electrochimia Acta,
    <u>13</u>, 1867 (1968).

49. B.C.H. Steele and C.B. Alcock, Trans. Met. Soc.
    AIME, <u>233</u>, 1359 (1965).

50. J.D. Tretjakow and H. Schmalzried, Ber. Bunsenges
    Physik. Chem., <u>69</u>, 376 (1965).

51. J.W. Patterson, E.C. Bogren and R.A. Rapp, J.
    Electrochem. Soc., <u>114</u>, 752 (1967).

52. M.F. Lasker and R.A. Rapp, Z. Physik. Chem. N.F.,
    <u>49</u>, 198 (1966).

53. J. Rudolph, Z. Naturforsch., A <u>14</u>, 727 (1959).

54. J.E. Bauerle, J. Chem. Phys., <u>45</u>, 4162 (1966).

55. S.R. deGroot <u>in</u> <u>Thermodynamics of Irreversible</u>
    <u>Processes</u>, North Holland Publ. Co., Amsterdam, (1951).

56. H. Holtan Jr., Proc. K. Akad. Wetensch., <u>56B</u>, 490,
    510 (1953).

57. H. Holtan Jr., P. Mazur and S.R. deGroot, Physica,
    <u>19</u>, 1109 (1953).

58. L. Patrick and A.W. Lawson, J. Chem. Phys., <u>22</u>,
    1492 (1954).

59. Y. Suzuki, S. Endo and E. Haga, J. Phys. Soc. Japan,
    <u>14</u>, 729 (1959).

60. R.W. Christy, E. Fukushima and H.J. Li, J. Chem.
    Phys., <u>30</u>, 136 (1959).

61. R.W. Christy, J. Chem. Phys., <u>34</u>, 1148 (1961).

62. A. Kvist, Z. Naturforsch., <u>19a</u>, 1159 (1964).

63. A. Kvist and A. Randasalu, Z. Naturforsch., <u>21a</u>,
    278 (1966).

64. K. Wagner, Z. Physik. Chem., 21, 74 (1959).

65. H. Hoshino and M. Shimoji, J. Phys. Chem. Solids, 31, 1533 (1970).

66. A.W. Lawson, J. Appl. Phys. Suppl., 33, 466 (1962).

67. C. Wagner in Progress in Solid State Chemistry, ed. H. Reiss and J.O. McCaldin, Pergamon Press, Vol. 7, p. 1, (1972).

68. R.J. Ruka, J.E. Bauerle and L. Dykstra, J. Electrochem. Soc., 115, 497 (1966).

69. S. Pizzini, C. Riccordi and V. Wagner, Z. Naturforsch., 25a, 559 (1970).

69a. W. Fischer, Z. Naturforsch., 22a, 1557 (1967).

69b. K. Goto, T. Ito and M. Someno, Trans. AIME, 245, 1662 (1969).

70. N.M. Tallan and I. Bransky, J. Electrochem. Soc., 118, 345 (1971).

71. H.H. Möbius, Z. Chemie, 2, 100 (1962).

72. H.H. Möbius, Z. Chemie, 4, 81 (1964).

73. F.A. Kröger, The Chemistry of Imperfect Crystals, North Holland Publ. Co., Amsterdam, (1964).

74. L.E.J. Roberts in Non-stoichiometric Compounds, ed. L. Mandelcorn, Academic Press, New York, p. (1964).

75. D.M. Roy and R. Roy, J. Electrochem. Soc., 111, 421 (1964).

76. F. Hund, Ber. deut. Keram. Ges., 42, 251 (1965).

77. F.A. Kröger and H.J. Vink in Solid State Physics, eds. F. Seitz and D. Turnbull, Academic Press, New York, 3, 307 (1956).

78. R.W. Vest, N.M. Tallan and W.C. Tripp, J. Amer. Ceram. Soc., 47, 635 (1964).

79. R.J. Brook in <u>Electrical Conductivity in Ceramics and Glass</u>, ed. N.M. Tallan, Marcel Dekker Inc., New York, p. 179 (1974).

80. R.E. Howard and A.B. Lidiard, Phil. Mag., 2, 1462 (1957).

81. R.E. Howard and A.B. Lidiard, <u>Rept. on Prog. in Phys.</u>, ed. B.C. Stickland, 27, 161 (1964).

82. A.R. Allnatt and P.W.M. Jacobs, Proc. Roy. Soc. (London), A260, 350 (1961); A267, 31 (1962).

83. M. Shimoji and H. Hoshino, J. Phys. Chem. Solids, 28, 1155 (1967).

84. D.S. Tannhauser, J. Electrochem. Soc., 112, 793 (1972).

85. F. Hund and R. Mezger, Z. Physik. Chem., 201, 268 (1952).

86. E.C. Subbarao, P.H. Sutter and J. Hrizo, J. Amer. Ceram. Soc., 48., 443 (1965).

87. I. Bransky and N.M. Tallan, J. Amer. Ceram. Soc., 53, 625 (1970).

88. A.K. Mehrotra, H.S. Maiti and E.C. Subbarao, Mat. Res. Bull., 8, 899 (1973).

89. N.S. Choudhury and J.W. Patterson, J. Amer. Ceram. Soc., 57, 90 (1974).

90. J.M. Wimmer, L.R. Bidwell and N.M. Tallan, J. Amer. Ceram. Soc., 50, 198 (1967).

91. L. Primas and R.A. Rapp, Reported in Ref. 26.

92. W.E. Danforth, J. Franklin Inst., 266, 483 (1955).

93. W.E. Danforth and J.H. Bodine, J. Franklin Inst., 260, 467 (1955).

94. R.W. Vest and N.M. Tallan, J. Appl. Phys., 36, 543 (1965).

95. T.L. Markin, R.J. Bones and V.J. Wheeler, Proc. Brit. Ceram. Soc., 8, 51 (1967).

96. N.M. Tallan, W.C. Tripp and R.W. Vest, J. Amer. Ceram. Soc., 50, 279 (1967).

97. F. Hund and W. Dürrwächter, Z. Anorg. Allgem. Chem., 265, 67 (1951).

98. H.H. Möbius, H. Witzmann and F. Zimmer, Z. Chem., 4, 194 (1964).

99. G. Brauer and H. Gradinger, Z. Anorg. Allgem. Chem., 276, 209 (1954).

100. A.M. Diness and R. Roy, J. Mater. Soc., 4, 613 (1969).

101. A.M. Diness and R. Roy, Bull. Amer. Ceram. Soc., 43, 263 (1964).

102. R. Radzewitz, U.S. At. Energy Comn., KFK-433, 53 (1966).

103. K.A. Gingerich, U.S. At. Energy Comn., TID-14803, 7 (1961)

104. K.A. Gingerich and G. Brauer, Z. Anorg. Allgem. Chem., 324, 48 (1963).

105. J.R. Johnson and C.E. Curtis, J. Amer. Ceram. Soc., 37, 611 (1954).

106. H.H. Möbius, H. Witzmann and W. Witte, Z. Chem., 4, 152 (1964).

107. C.E. Curtis and J.R. Johnson, J. Amer. Ceram. Soc., 40, 63 (1957).

108. T.Y. Tien and E.C. Subbarao, J. Chem. Phys., 37, 1041 (1963).

109. D.W. Strickler and W.G. Carlson, J. Amer. Ceram. Soc., 48, 286 (1965).

110. C. Wagner in Proc. 7th Meeting Int. Comm. on Electrochem. Therm. and Kinetics, Lindau (1955), Butterworth Publ., London, p. 361 (1957).

129. J.F. Laurent and J. Banard, J. Phys. Chem. Solids, 7, 218 (1958).

130. T.Y. Tien, J. Appl. Phys., 35, 122 (1964).

131. A. Kumar. D. Rajdev and D.L. Douglass, J. Amer. Ceram. Soc., 55, 439 (1972).

132. A.J. Dekker, Solid State Physics, Prentice-Hall Publ. Co., p. 175 (1957).

APPENDIX

Table A1.1.1

Conductivity in Air

Temperature	Conductivity (moh. cm^{-1})		
($^{\circ}$C)	'Pure' ThO$_2$	1 m/o CaO	2 m/o CaO
607.0	0.957μ	3.831μ	18.95μ
655.0	2.408μ	12.75μ	48.82μ
703.0	5.690μ	31.46μ	95.87μ
753.0	12.789μ	75.59μ	197.02μ
807.0	26.588μ	158.0μ	371.24μ
852.5	44.947μ	266.8μ	598.7μ
905.5	78.07μ	453.3μ	966.1μ
955.0	121.87μ	715.6μ	1.451m
1004.0	176.4μ	1.265m	2.296m
1051.5	247.4μ	1.618m	3.019m
1097.5	428.9μ	2.369m	4.278m
1150.0	651.0μ	3.256m	5.608m
1203.0	659.3μ	4.455m	7.318m
1253.5	809.7μ	5.862m	9.167m
1303.5	957.4μ	7.405m	11.428m
1355.0	1.162m	9.713m	14.301m
1400.0	1.455m	11.865m	16.797m

Table A1.1.2

Conductivity in Air

Temperature (°C)	Conductivity (moh. cm^{-1})	
	3 m/o CaO	4 m/o CaO
609.0	26.22μ	35.28μ
655.0	54.35μ	71.98μ
703.0	113.2μ	146.1μ
750.0	208.7μ	270.5μ
804.0	389.3μ	509.4μ
852.0	645.4μ	850.5μ
902.0	1.038m	1.379m
954.0	1.635m	2.182m
1004.0	2.426m	3.253m
1052.0	3.410m	4.583m
1097.5	4.573m	6.104m
1146.0	6.121m	8.211m
1201.0	8.120m	10.778m
1251.0	10.361m	14.020m
1300.0	12.834m	17.245m
1348.0	15.303m	20.903m
1394.0	18.506m	24.992m

Table A1.1.3

Conductivity in Air

Temperature (°C)	Conductivity (moh. cm⁻¹)	
	5 m/o CaO	6 m/o CaO
608.0	41.272μ	44.89μ
658.0	83.00μ	92.74μ
706.0	166.17μ	185.26μ
752.0	303.81μ	338.82μ
801.0	544.0μ	607.4μ
852.0	942.0μ	1.049m
906.0	1.566m	1.745m
955.0	2.393m	2.661m
1005.0	3.495m	3.882m
1052.0	4.850m	5.373m
1098.0	6.447m	7.150m
1147.0	8.542m	9.415m
1202.0	11.17m	12.333m
1251.0	13.91m	15.294m
1301.0	19.28m	21.24m
1352.0	24.20m	26.75m
1409.0	30.51m	34.39m

Table A1.1.4

Conductivity in Air

Temperature (°C)	Conductivity (moh. cm⁻¹) 7 m/o CaO
607.0	49.77μ
655.0	110.6μ
703.0	216.25μ
751.0	399.3μ
801.0	717.2μ
853.0	1.248m
903.0	2.001m
955.0	3.200m
1004.0	4.631m
1052.0	6.600m
1099.0	9.978m
1152.0	12.095m
1205.0	16.060m
1256.0	20.438m
1304.0	25.509m
1353.0	31.414m
1399.0	37.283m

Table A1.1.5

Conductivity in Air

Temperature (°C)	Conductivity (moh. cm^{-1})	
	10 m/o CaO	15 m/o CaO
604.0	53.80μ	39.94μ
652.0	120.2μ	91.42μ
698.0	234.1μ	182.6μ
747.0	452.8μ	354.9μ
808.0	932.8μ	755.6μ
856.0	1.581m	1.305m
904.0	2.494m	2.08m
951.0	3.77m	3.16m
1000.0	5.98m	4.78m
1049.0	7.88m	6.73m
1095.0	11.00m	9.36m
1151.0	15.15m	13.38m
1198.0	21.20m	18.25m
1247.0	25.35m	22.43m
1300.0	32.62m	29.25m
1348.0	39.2m	35.89m
1396.0	48.59m	43.95m

Table A1.2.1

Conductivity Values in Oxygen Atmosphere

Temperature	Conductivity of 'pure' ThO_2 (moh. cm^{-1})	Temperature	Conductivity (moh. cm^{-1})	
			4 m/o CaO	7 m/o CaO
607	0.765μ	600	29.59μ	54.03μ
650	1.718μ	648.5	75.08μ	122.3μ
700	4.430μ	685	132.4μ	211.9μ
750	10.81μ	751	320.8μ	502.0μ
798	22.35μ	800	571.9μ	880.0μ
850	45.13μ	850	919.6μ	1.476m
902	81.99μ	900	1.473m	2.533m
		950	2.263m	3.564m
1001	205.1μ	999	3.738m	5.468m
		1050	4.689m	7.107m
1092	389.7μ	1099	7.251m	11.19m
		1150	9.99m	15.11m
1199	707.9μ	1200	12.90m	19.47m
		1250	16.06m	24.47m
1301	1.119m	1300	20.30m	29.79m
		1350	24.42m	36.05m
1405	1.637m	1401	–	40.30m

Table A1.2.2

Conductivity in Oxygen Atmosphere

Temperature (°C)	Conductivity (moh. cm⁻¹)		
	1 m/o CaO	2 m/o CaO	3 m/o CaO
605	3.824μ	20.32μ	32.24μ
652	14.82μ	58.84μ	72.67μ
697	40.90μ	127.99μ	144.9μ
750	101.08μ	263.3μ	289.9μ
800	197.12μ	468.7μ	514.3μ
800	210.3μ	494.0μ	519.5μ
854	365.45μ	819.3μ	896.9μ
899	666.5μ	1.378m	1.486m
950	1030.1μ	2.049m	2.211m
1000	1.523m	2.915m	3.186m
1051	2.467m	4.385m	4.745m
1150	4.496m	7.61m	8.193m
1200	5.964m	9.801m	10.70m
1299	9.836m	15.02m	16.38m
1348	12.42m	18.28m	20.07m
1400	15.74m	22.24m	23.89m

Table A1.3.1

Conductivity Values at $P_{O_2} = 10^{-5}$ atm.

Temperature ($^{\circ}$C)	Conductivity (moh. cm^{-1})		
	'Pure' ThO$_2$	4 m/o CaO	7 m/o CaO
604	0.185μ	6.544μ	13.53μ
652	0.330μ	15.78μ	29.89μ
698	0.5926μ	33.67μ	62.15μ
750	1.098μ	70.17μ	133.0μ
800	2.080μ	140.5μ	268.6μ
850	4.045μ	268.7μ	505.2μ
902	7.459μ	487.2μ	896.2μ
951	12.34μ	798.0μ	1.432m
1000	19.70μ	1.365m	2.386m
1049	30.10μ	2.420m	3.704m
1096	41.74μ	-	-
1149	63.56μ	3.930m	6.408m
1200	91.12μ	5.836m	8.873m
1250	118.4μ	6.828m	10.98m
1298	162.7μ	8.719m	13.98m
1349	203.8μ	11.02m	17.09m

Table Al.3.2

Conductivity Values at $P_{O_2} = 10^{-5}$ atm.

Temperature ($^\circ$C)	Conductivity (moh. cm^{-1})		
	1 m/o CaO	2 m/o CaO	3 m/o CaO
605	0.929μ	3.922μ	5.10μ
653	2.425μ	9.789μ	12.22μ
750	12.91μ	42.88μ	33.60μ
700	5.76μ	20.90μ	25.84μ
800	27.61μ	83.66μ	103.8μ
851	53.23μ	155.4μ	199.7μ
900	95.33μ	268.6μ	347.5μ
950	172.39μ	455.1μ	550.6μ
1000	291.8μ	824.7μ	1070.1μ
1049	609.2μ	1.3152m	1.606m
1100	843.1μ	1.756m	2.141m
1150	1.180m	2.364m	2.868m
1200	1.666m	3.116m	3.769m
1252	2.463m	4.140m	5.081m
1301	3.219m	5.304m	6.176m
1350	4.197m	6.663m	7.539m

Table A1.4.1

Conductivity Values at $P_{O_2} = 10^{-23}$ atm.

Temperature ($^{\circ}$C)	Conductivity (moh. cm^{-1})		
	'Pure' ThO$_2$	4 m/o CaO	7 m/o CaO
602	0.134μ	4.595μ	7.959μ
657	0.179μ	9.369μ	16.10μ
685	0.226μ	13.68μ	26.98μ
750	0.497μ	39.27μ	87.48μ
800	0.781μ	91.66μ	192.7μ
854	1.183μ	203.3μ	410.0μ
902	1.806μ	380.9μ	742.2μ
955	3.400μ	811.5μ	1.427m
1001	6.450μ	1.197m	2.097m
1047	11.500μ	1.691m	2.945m
1099	20.24μ	2.307m	4.219m
1149	32.33μ	3.234m	5.649m
1200	48.81μ	4.553m	7.689m
1250	68.59μ	5.815m	9.747m
1300	92.78μ	7.482m	12.18m

Table Al.4.2

Conductivity Values at $P_{O_2} = 10^{-23}$ atm.

Temperature ($^\circ$C)	Conductivity (moh. cm^{-1})		
	1 m/o CaO	2 m/o CaO	3 m/o CaO
610	0.602μ	2.02μ	3.161μ
651	1.284μ	4.275μ	6.076μ
698	2.356μ	7.64μ	11.32μ
754	3.947μ	12.63μ	24.91μ
800	6.74μ	20.91μ	48.14μ
852	16.62μ	51.00μ	103.5μ
898	44.84μ	124.6μ	225.3μ
950	855.2μ	232.6μ	362.7μ
1000	168.7μ	426.0μ	601.6μ
1050	291.1μ	681.6μ	924.3μ
1097	461.1μ	951.9μ	1.253m
1152	696.1μ	1.304m	1.715m
1200	946.0μ	1.666m	2.171m
1249	1.338m	2.181m	2.827m
1299	1.942m	3.036m	3.673m

Table A2.1.1

Conductivity at 600°C

$-\log P_{C_2}$	Conductivity (μ moh. cm^{-1})		
	'Pure' ThO$_2$	4 m/o CaO	7 m/o Ca.
3.28	0.256	8.23	18.53
4.15	0.209	6.34	15.18
4.65	0.198	5.56	13.57
5.35	0.190	4.76	12.08
6.22	0.180	4.32	11.22
7.94	0.171	4.157	10.9
8.62	0.132	3.922	10.39
13.17	0.170	4.186	10.93
17.82	0.158	3.61	9.34
20.20	0.145	3.39	8.77
21.34	0.137	3.30	8.60
23.84	0.132	3.27	8.54

Table A2.1.2

Conductivity at $600\,^{\circ}C$

-log P_2	Conductivity (μ moh. cm^{-1})		
	1 m/o CaO	2 m/o CaO	3 m/o CaO
3.35	0.657	3.679	6.18
4.52	0.637	3.007	...2
4.93	0.626	2.70	3.85
5.38	0.620	2.651	3.53
4.09	0.601	2.475	2.81
14.37	0.60	2.458	2.8
16.52	0.606	2.487	2.82
18.44	0.603	2.481	2.81
20.37	0.604	2.489	2.82
22.85	0.603	2.48	2.79
24.89	0.601	2.46	2.78

Table A2.2.1

Conductivity at 685°C

$-\log P_{O_2}$	Conductivity (μ moh. cm^{-1})		
	'Pure' ThO_2	4 m/o CaO	7 m/o CaO
3.16	1.230	35.98	73.68
4.07	0.838	28.65	62.61
4.61	0.730	25.33	57.57
5.89	0.536	20.51	50.58
7.71	0.334	14.85	42.97
11.34	0.286	14.78	43.38
15.17	0.301	14.73	42.94
16.72	0.287	14.73	42.97
17.34	0.282	14.56	42.76
18.58	0.278	15.26	43.18
19.30	0.285	15.09	43.76
21.37	0.290	14.68	44.04

Table A2.2.2

Conductivity at 685°C

-log P_{O_2}	Conductivity (μ noh. cm^{-1})		
	1 m/o CaO	2 m/o CaO	3 m/o CaO
4.0	7.588	21.453	23.612
4.25	6.621	19.616	21.676
5.1	5.422	16.528	18.562
5.43	4.865	15.232	17.265
14.85	3.250	11.162	12.453
15.78	2.732	10.517	11.377
17.42	2.774	10.751	11.616
17.83	2.718	10.634	11.357
18.14	2.682	10.601	11.297
19.08	2.623	10.501	11.197
19.92	2.62	10.517	11.201
20.74	2.578	10.417	11.257
21.45	2.598	10.457	11.217

Table A2.3.1

Conductivity at 8..°C

−log P_{O_2}	Conductivity (μ m. ch. cm^{-1})		
	'Pure' Th$_2$	4 m/o Ca.	7 m/o Ca.
3.15	6.80	178.6	366.7
3.84	4.96	154.4	339.1
4.19	4.24	144.38	314..
4.82	3.29	132.1	3...6
5.74	2.31	116.98	264.9
7.15	1.48	97.64	261.3
13.24	0.924	98.54	263.6
14.17	0.915	98.83	264.2
14.35	0.970	98.90	264.2
15.83	1.092	99.25	264.2
16.38	0.951	101.22	266.-
17.30	1.021	101.72	268.19

Table A2.3.2

Conductivity at 800°C

-log P_{O_2}	Conductivity (μ moh. cm^{-1})		
	1 m/o CaO	2 m/o CaO	3 m/o CaO
4.07	36.02	99.73	116.08
4.37	31.20	89.22	104.59
4.68	29.64	86.01	101.8
5.7	22.44	7.05	66.02
14.80	10.56	40.07	53.0
15.64	10.68	40.23	60.12
16.84	10.59	40.06	6.71
17.58	10.70	40.06	61.03
17.76	10.59	39.60	61.35
4.22	33.79	95.69	112.57
3.72	39.37	107.88	124.55
3.48	42.88	115.66	139.53
3.45	43.24	116.23	132.33
3.45	44.05	117.6	134.57
12.77	10.98	39.6	58.80
10.84	10.65	39.4	55.66
8.99	10.70	4.3	79.20
7.60	11.35	44.27	63.30

Table A2.4.1

Conductivity at 1...°C

-log P_{C_2}	Conductivity (μ moh. cm^{-1})		
	'Pure' Th$_2$	4 m/o Ca	7 m/o Ca
3.23	49.05	1.743	2.62
4.09	34.13	1.652	2.517
5.08	24.61	1.372	2.146
5.92	18.81	1.241	2..5.
6.31	18.98	1.232	2..
7.23	17.04	1.212	2. 5
10.62	16.86	1.276	2. 5)
15.97	15.12	1.224	2.. 5
18.38	14.98	1.212	2...5
22.09	6.784	1.196	1.959
24.28	6.94	1.192	1.989

Table A2.4.2

Conductivity at 1..°C

-log P$_{O_2}$	Conductivity (μ moh. cm^{-1})		
	1 m/o CaO	2 m/o Ca.	3 m/o Ca.
3.25	393.1	833.1	1.73.7
3.95	326.3	722.7	939.5
4.83	271.3	624.9	823.3
5.92	240.6	567.9	756.1
7.56	230.6	551.4	734.2
17.50	230.6	551.4	734.2
20.34	223.6	535.5	715.0
21.65	166.3	426.1	603.9
22.53	168.6	429.1	601.0
24.71	169.0	407.4	601.3

Table A2.5.1

Conductivity at $120\,^{\circ}$C

-log P$_{O_2}$	Conductivity (moh. cm^{-1})		
	'Pure' ThO$_2$	4 m/o CaO	7 m/o CaO
3.21	185.0 μ	6.36 m	9.48 m
4.22	128.5 μ	5.75 m	8.65 m
5.18	95.68 μ	5.19 m	8.05 m
6.05	77.94 μ	5.22 m	7.95 m
8.10	68.62 μ	5.11 m	7.91 m
9.75	68.43 μ	4.99 m	7.78 m
13.25	68.13 μ	4.97 m	7.78 m
16.41	67.87 μ	5.11 m	7.86 m
17.28	63.43 μ	4.94 m	7.86 m
17.94	52.00 μ	4.83 m	7.69 m
20.34	50.07 μ	4.91 m	7.78 m
22.75	49.18 μ	4.78 m	7.69 m
25.80	50.26 μ	4.78 m	7.69 m

Table A2.5.2

Conductivity at 12.°C

-log P_{O_2}	Conductivity (m moh. cm^{-1})		
	1 m/o Ca	2 m/o Ca	3 m/o Ca
3.2	1.895	3.488	4.16
3.95	1.59	3.0	3.0312
4.98	1.343	2.458	3.072
6.07	1.216	2.238	2.853
7.67	1.203	2.238	2.013
17.61	1.15	2.142	2.735
20.12	0.971	1.807	2.377
21.44	0.93	1.688	2.29
22.52	0.907	1.648	2.243
24.93	0.907	1.665	2.243

ME-1975-D-MAI-ELE